**Eberhard Karls Universität Tübingen**
Mathematisch-Naturwissenschaftliche Fakultät
Fachbereich Geowissenschaften
**Institut für Geographie**

# Simulated climate change and its effects on the hydrology of the Saale River catchment

**Diploma thesis**

by

**David Schäfer**

**Supervisors:**

**Prof. Dr. Volker Hochschild**
Universität Tübingen

**Dr. Andreas Marx**
Helmholtz Zentrum für Umweltforschung UFZ

# Contents

# Statement of Authorship

Except where reference is made in the text of this thesis, the entire work contains no material published elsewhere or already submitted for the award of any other degree in a tertiary institution.

# Acknowledgments

In first place a want to thank my supervisors, Prof. Dr. Volker Hoschschild and Dr. Andreas Marx for making this cross-institutional diploma thesis possible. In particular, I wish to thank Dr. Andreas Marx for providing the topic, every day guidance, constructive feedback and the large amount of patience with a not always purposefully working student.

I want to thank further all members of the Stochastic Hydrology and Water Resources Management working group of the Department Computational Hydrosystems at the Helmholtz Centre for Environmental Research - UFZ. Special thank to the group leader, Dr. Luis E. Samaniego-Eguiguren for sharing the hydrological model and all necessary data and to Matthias Zink for the detailed introduction to the modelling procedure.

I am grateful to all people who guided me throughout the last year and are directly or indirectly part in this work's development process. Particular thank to my friend Marie Felicitas Busch for proofreading and day-in, day-out love and support. I am further indebted to my mother and grand-mother for providing the solid and secure background, that I experienced during my entire life.

Last but not least I want to thank my office colleague Greta Jäckel for the relaxed, in times serious-constructive or just humorous working atmosphere.

The data used in this work was gathered from a number of different agencies and authorities: The Regional Climate Model data was provided by the EU-Project ENSEMBLES, input data to the hydrological model by the Bundesanstalt für Geowissenschaften und Rohstoffe (geological and soil map), Bundesamt für Kartographie und Geodäsie (Digital Elevation Model), Landesbetrieb für Hochwasserschutz und Wasserwirtschaft Sachsen-Anhalt (gauging data), Thüringer Landesanstalt für Umwelt und Geologie (gauging data), Deutscher Wetterdienst (meteorological data) and the National Aeronautics and Space Administration (Landsat TM5 land cover data).

# Summary

Longterm weather observations clearly indicate changing climatic conditions in Germany. Available measurement data indicates an increase of annual average temperature of 1° K and a moderate increase of annual precipitation (9%) during the last century (Schönwiese et al. (2006)). Both, increases of temperature and precipitation are mainly based on higher surpluses during the winter seasons until now. Available computer-based climate simulations project an ongoing warming trend and further changes in the seasonal distribution of precipitation. These changes in atmospheric conditions had and will have consequences on water resources IPCC (2007). As extreme changes in water availability may have severe consequences, such as an higher number or intensity of floods during winter and/or water shortage in summer, knowledge about possible impacts of climate change on river hydrology is of great socio-economical relevance.

In this study the output from four methodological similar climate model combinations is compared and evaluated against observation. Differences in simulated future changes in the climatology of the Saale River basin, situated in central Germany, and their translation into river hydrology are quantified. A bias correction is applied and its effects on RCM simulated meteorology in present and future, as well as consequences for results from the hydrological modelling are reviewed. In order to estimate regional variations of climate change impact and performance differences due to catchments size, the study area is further divided into five sub-catchments covering areas between less than 900 km$^2$ to more than 23700 km$^2$. Four Regional Climate Models (RCM) from the ENSEMBLES-Project (van der Linden and Mitchell (2009)), downscaling A1B boundary conditions from two different Global Circulation Models (GCM), are used to force the hydrological model mHM. A bias correction is applied and evaluated for the 1961-1990 reference, a 1980-2009 control and two scenario periods (2011-2040 and 2061-2090). Subsequently both datasets for any RCM are used to generate in overall eight synthetic discharge timeseries at five different gauging stations. Modelled discharge is evaluated against observation in the reference and for changes in mean discharge in both scenario periods.

All RCM significantly overestimate past annual precipitation (+24% to + 57%). The bias correction applied is suitable to reduce these deviations from observational data for the 1961-1990 correction period considerably (3% and 6%), without substantial side-effects on RCM dynamics. Forcing the hydrological model with uncorrected RCM data reproduces the inherent input data biases, certain regional performance differences can

be stated but non of the simulation results is in a reasonable range. Corrected RCM data performed rather well, modelled streamflow is in most cases close to observation. Catchment size does influence model performance, biases are considerably higher at the two gauging stations covering areas less than about 6000 $km^2$. An increase of annual mean temperature, ranging from 0.8° K to 1.8° K in the first and from 2.5° K to 3.9° K in the second scenario period, is simulated by all models. Changes in yearly precipitation range from 0% to 4% in the 2011-2040 and from 4% to 9% in the 2061-2090 period. These differences are mainly based on upward trends in autumn and winter during the first, and additionally increasing spring precipitation totals in the second scenario period. Climate dynamics translates into higher discharge during winter and lower during spring, with a positive trend in annual mean streamflow in the first but without clear signal in the second scenario period. Differences in the sub-catchments are rather small. The bias correction applied is hardly altering climate change impact on hydrology in the first scenario period but, depending on RCM, more substantially in the second. It could be shown that simulated impact of climate change is quite sensitive to forcing RCM, whereas the general tendency of changes, positive or negative in arithmetic sign, is basically controlled by driving GCM.

# 1 Introduction

### Problem Formulation

Climate change, a topic gaining much attention during the recent years, is now well supported by all available longterm weather records. The Fourth Assessment Report (AR4) of the Intergovernmental Panel on Climate Change (IPCC (2007)) reported an increase of average surface temperatures over Europe of 0.9° K for the 20th century and an even higher upward trend during the last two decades. The warming is not uniformly distributed, temperature increases are in general more pronounced in winter and more substantial in central and north-eastern Europe than in the Mediterranean. Precipitation measurements indicate even stronger regional differences. Winter rainfall amounts are increasing in northern and atlantic Europe, whereas total yearly precipitation is decreasing in the southern part of the continent (IPCC (2007)). Temperature trends in Germany are slightly higher than in continental average. Within the period from 1901 to 2000 mean surface temperatures increased about 1° K in all seasons. A higher inter-annual variability is reported for the 1981-2000 time-slice, temperatures increased disproportionally during winter and are stagnating in autumn (Schönwiese et al. (2006)). Averaged total yearly precipitation amounts rose about 9% during the 20th century, highest gains are observed for winter (19%), while in summer a slight but statistically not significant decrease (-3%) is reported.

The altered meteorology is very likely to be reflected in river discharge. Petrow and Merz (2009) proved upward flood trends, especially during winter for a large number of gauging stations all over Germany. For the study area, the basin of the Saale River, there is no clear evidence for generally increasing yearly maximum discharge. The authors found an increase of maximum winter and a decrease of maximum summer streamflow volume at five gauging stations within the study area. The catchment, situated in central Germany, is already characterised by a distinct hydrological dichotomy between high discharge conditions during the first and a pronounced low flood period during the second half of the hydrological year. Changes in water supply, as sketched in Petrow and Merz (2009), and according to the AR4 most likely to aggravate for central Europe, have the potential to provoke future summer water shortage and winter flood damage. It is therefore of general importance to estimate possible changes of the climatological conditions and the impacts on hydrology with the tools available, in order to assess coping capacities and adaption strategies in time.

Climate models, computer-based simulations of the climate systems have become an important tool for assessing possible future atmospheric trends. Until recently however all of them lacked a number of shortcomings. Long computational run-time hindered large ensemble studies (van der Linden and Mitchell (2009)), horizontal resolutions were usually too coarse to fit the requirements of impact models (Fowler and Kilsby (2007)) and climate models had problems to reproduce observed past climate (e.g. Jacob et al. (2007), Christensen et al. (2008)). Continuous research effort now provides a reasonable set of techniques to deal with these methodological challenges. Continuous research effort is spend to steadily inprove these models and reasonable set of techniques to deal with methodological challenges is now available.

Model resolutions and consequently the gap between atmospheric and hydrological models generally decrease (Fowler and Kilsby (2007)), the EU-project ENSEMBLES provides a large database of output from different dynamical regional climate models, all available in comparable temporal and spatial scales and therefore qualified for comprehensive multi model studies (van der Linden and Mitchell (2009)). State of the art mesoscale hydrological models allow to appropriately simulate streamflow on modelling scales covering several km (Kumar (2010)) and a number of bias correction techniques have been proposed to deal with biased climate model output (e.g. Hay et al. (2000), Kunstmann et al. (2004), Haerter et al. (2011)).

### Literature Review

A number of studies assessing hydrological impacts of climate change in Germany have been carried out during the last decade. While early publications with a similar setup to the present study, forcing a hydrological model with climate model data, were mainly scientifically motivated, public commissioned research efforts gained importance during the recent years. Examining related scientific literature chronically, advancing computer hardware technology is tracing on study design. During the years modelling areas increased and temporal and/or spatial resolution generally decreased. Beside these general tendencies a variety of SRES emission scenarios (IPCC (2000)), downscaling techniques and hydrological models have been used in order to simulate climate change impact on river discharge.

Menzel and Bürger (2002) evaluated climate change impact on the hydrology of the Mulde River, as the Saale a tributary of the Elbe. The hydrological model HBV-D was driven with statistically downscaled output from the Global Circulation Model (GCM) ECHAM4/OPYC3, a previous version of ECHAM5/MPI-OM, under the IS92a emission scenario (see 2.2.1). The authors reported a distinct decrease of monthly mean discharge for the entire year, but especially during winter and summer, resulting in a more pronounced yearly cycle for the period 2061-2090.

Shabalova et al. (2003) used output from the HadRM2 Regional Climate Model (RCM), a former version of the HadRM3Q0 RCM, to evaluate the climate change signal for the period 2080-2099 under the emission scenario IS92a. Two different bias correction methods have been applied to account for the deviation between simulated and observed climatology. Hydrological modelling with RhineFlow suggested only a slight decrease of the annual mean, but considerably increased winter and reduced summer discharge. The effect of bias correction were rather low when examining changes between scenario and reference period but distinctive with respect to discharge variability.

Kunstmann et al. (2004) used dynamically downscaled IS92a ECHAM4 circulation fields for streamflow prediction with the hydrological model WaSiM in the small alpine catchment of the river Ammer. The results indicated a decrease of summer and enhanced winter discharge for the years 2032-2039. Great differences were reported between the sub-catchments. It was reported that especially the mountainous basins are likely to see more pronounced impact of changing climatic conditions than the sub-catchments with lower elevation differences.

Menzel et al. (2006) used a statistical downscaling approach on ECHAM4/OPYC3 and HadCM model output simulated with IS92a scenario boundary conditions. Assessing climate change impacts on the hydrology of the Rhine catchment with the HBV-D model, the authors explicitly determined the differences between two different GCM, results are however only evaluated on the basis of yearly averages. During the control period (1961-1995), model runs with downscaled GCM data clearly overestimated the results of a control run driven with measured meteorological input. The ECHAM4/OPYC3 model usually showed higher biases in the different sub-catchments considering annual mean discharge, a less clear error signal was found with respect to mean flood conditions. Depending on the sub-catchment, modelling results either over- or underestimated observation, with highest biases changing between the models. For a future scenario (2061-2095) a clear increase in both evaluated hydrological parameters was reported, higher even in the ECHAM4/OPYC3 than the HadCM forced model chain.

A study focused on flood hazards in the upper Danube basin was carried out by Dankers et al. (2007). The authors explicitly addressed the influence of horizontal resolution when driving the hydrological model LISFLOOD with RCM data. Two different resolutions of the HIRHAM RCM were used (12 and 50 km), the former using the A2 scenario, the latter A2 and B2. The RCM overestimated yearly precipitation amounts, with a slightly higher bias in the high resolution realisation. The 12 km model run could match the observational areal precipitation pattern much better then the 50 km one. Differences resulting from resolution have been quite small in the hydrological simulations, modelling did only in a few sub-catchments improve substantially. Simulation of future discharge indicated an altered hydrological regime. Higher mean discharge in winter and lower in summer accompanied by an increase of flood frequency and/or intensity at most evaluated

gauging stations.

Hattermann et al. (2008) presented a study conducted within the framework of GLOWA-Elbe. The project aimed to assess impacts of climate change on the water balance of the Elbe catchment, possible feedback and interactions to and with socio-economical changes and suitable adaption strategies and was founded by the German Ministry of Education and Research 'Bundesministerium für Bildung und Forschung (BMBF)'. Using the statistical model STAR to downscale ECHAM4/OPYC3 A1 scenario circulation fields, the eco-hydrological model SWIM was forced to simulate discharge timeseries for the five years from 2051-2055. On the back of the project aims, going beyond pure hydrological processes, the model chain was enlarged. Agro-economical modelling on the global and the regional scale was included, providing boundary conditions for the hydrological model. Results indicated a high uncertainty within the modelling chain, the authors did anyhow propagate two robust trends: reduced water availability in summer and an earlier high flow period.

In the year 2009 a comprehensive study founded by the Ministry of Agriculture and Environment of the federal state of Sachsen-Anhalt was published (Kropp et al. (2009)). This study covers two of the gauges, Hadmersleben (Bode) and Calbe-Grizehene (Saale) and one of the climate model setups, MPI-M-REMO with ECHAM5/MPI-OM boundary conditions in the A1B scenario, also used in the work on hand. A bias correction of the dynamical RCM was done, although the effects on hydrological modelling results were not explicitly addressed. The statistical RCM WETTREG and the emission scenario A2 and B1 where further included, and a detailed analysis of projected climate change in Sachsen-Anhalt was conducted. Both RCM, the statistical WETTREG and the dynamical REMO projected in all driving scenarios a significant trend of increasing temperatures, whereby REMO temperature anomalies exceeded the WETTREG projections. With respect to precipitation the models showed diverging result, a decreasing tendency in WETTREG and an increasing one in REMO with higher inter-annual variabilities in the latter. Wettest conditions result from the B1 scenario in both RCM simulations, even though uncertainty introduced by emission scenario was relatively small. Both RCM indicated a more balanced future distribution of precipitation throughout the year, lower amounts during the summer months and higher during winter. WETTREG forcing of the hydrological model SWIM, indicated a shift of the spring discharge peak into winter and lower summer discharge for the Saale. The decline of summer water supply was less distinct and limited to late summer/early autumn in the Bode River catchment. The REMO driven model runs indicated in turn raising discharge for both catchments, all emission scenarios and almost throughout the entire year. The increase was more pronounced during the winter months and tended towards zero during summer. The small differences between the emission scenarios considering the meteorological parameters are mirrored in the synthetic discharge timeseries produced with both RCM. The differences

remained pretty small, with B1 RCM scenarios translating into highest, A2 into lowest discharge.

A study using the statistical RCM STAR to downscale ECHAM5/MPI-OM A1B scenario output was published by Huang et al. (2010). Using the eco-hydrological model SWIM streamflow of the largest german rivers Elbe, Ems, upper Danube, Rhine and Weser was simulated for the periods 2009-2018 and 2051-2060. Two gauging station within the Saale catchment where included, the basin outlet Calbe-Grizehne and Laucha at the Saale tributary Unstrut, whereas only the former one was explicitly evaluated. Decreasing summer and increasing winter precipitation, the with STAR projected climatological trend for the century, were reflected in river discharge. For the 2009-2018 scenario period an increase of the winter discharge volume was reported, but changes have been relatively small. In the mid-century scenario period more significant changes were simulated, the authors reported changes in mean seasonal discharge of 13%, -15.5%, -24.4%, -30.1% for winter, spring, summer and autumn respectively at the gauging station Calbe-Grizehne.

Summarising the recent literature on hydrological impacts of climate change in Germany a number of conclusions can be drawn:

1. The hydrological impact of climate change does most likely imply a shift of the high discharge regime from spring into winter and more pronounced low flow conditions in summer.

2. The uncertainty introduced by different emission scenarios seems to be rather small, the variability in hydrological results due to driving GCM is usually not addressed in the available studies for Germany.

3. Most of the recent studies are focused on the comparison of statistical and dynamical downscaling approaches, an evaluation of different RCM in hydrological studies is missing.

### Objectives

From the gaps unfilled in dominating climate change impact study design and the previously sketched problems, how will observed climate dynamics evolve in future, what are the impacts on river hydrology, how to deal the methodological challenges and uncertainties accumulating in a large modelling chain, the main objectives of this work arise:

1. To analyse the differences in an ensemble of methodological similar GCM-RCM simulations with identical emission scenario boundary conditions and their translation into modelled river hydrology.

2. To quantify uncertainty introduced into hydrological simulations through the links of the climate model chain, data preprocessing and size of the modelling domain.

3. To estimate robust trends in regional climate projections and hydrological simulations for the mesoscale watershed of the Saale River, central Germany, for the first and the second half of the century.

### Methodology

The output from four dynamical RCM, ETHZ-CLM, HadRM3Q0, ICTP-REGCM and MPI-M-REMO, the former two downscaling HadCM, the latter ECHAM5/MPI-OM global A1B emission scenario circulation patterns, is processed. All RCM are provided by the ENSEMBLES-Project (van der Linden and Mitchell (2009)) in comparable horizontal and temporal resolutions. Climate model ability to reproduce observed climatological conditions is evaluated against gridded weather station data. Model biases and climatological dynamics are quantified with respect to monthly and seasonal mean temperatures, precipitation sums and, as a measure of extreme events, corresponding 95-percentiles, for a 1961-1990 control and two scenario periods (2011-2040 and 2061-2090).

The bias correction method proposed by Kunstmann et al. (2004) is applied, therefore observational meteorological data is interpolated to RCM grid resolution using Inverse Distance Weighting. Monthly correction factors are calculated as the quotient of longterm monthly precipitation sums (1961-1990) from observed and modelled rainfall data and subsequently multiplied to the respective daily values. The numerical effects of bias correction and its temporal stability is assessed by evaluating the bias corrected datasets against observation within a time-slice (1981-2009) not entirely covered by the correction period and both scenario periods.

The mesoscale hydrological model mHM is, after calibration to observation, forced by all available data. Synthetic discharge timeseries are generated at five different gauging stations all over the Saale basin, covering sub-catchments with areas between 888 $km^2$ and 23719 $km^2$. Two of three main tributaries are modelled explicitly, the Unstrut, the Bode and the Saale in the upper and middle reaches and at the basin outlet. General performance of all modelling runs is determined at every gauging station for the 1961-1990 period. Climate change impact on hydrology, differences and common trends between models and preprocessing (i.e. bias corrections) are examined for both scenario periods.

# 2 Methods

## 2.1 The Saale Catchment

The river Saale is, with a drainage area of 24 079 $km^2$ and a mean annual discharge of 117 $m^3/s$, the second largest tributary of the river Elbe. The catchment lies almost entirely within the boarders of the Federal Republic of Germany, although small feeders of the Weiße Elster and the Upper Saale, with an overall area of about 100 $km^2$, origin on the territory of the Czech republic. The watershed partly covers the five federal states of Sachsen, Niedersachsen, Bayern, Thüringen and Sachsen-Anhalt. Apart from this administrative breakdown, the catchment is divided into four subcatchments, the drainage areas of the Saale itself and of its three main tributaries, Unstrut (6343 $km^2$), Weiße Elster (5154 $km^2$) and Bode (3297$km^2$) (Internationale Kommission zum Schutz der Elbe (2005)). Figure 2.1 depicts topography, selected cities, rivers and the locations of gauging stations of interested for this work.

### 2.1.1 Hydrography

Short descriptions of the hydrography of the Saale and its three main tributaries, Unstrut, Weiße Elster and Bode, are given in the following subsections. The figures 2.2 to 2.6 depict the respective hydrological characteristics, longterm averages of monthly mean discharge and corresponding variability on the left hand side, yearly cycles, as the quotient of monthly and yearly mean flow volumes, on the right hand side.

#### The Saale

The Saale originates on the northern slope of the Fichtelgebirge and flows into the Elbe near Barby after a total distance of 433,9 km and a difference in elevation of 657,5 m (Internationale Kommission zum Schutz der Elbe (2005)). In the upper reaches the river passes the Fränkischen Wald in a narrow winding valley before braking through the Thüringer Schiefergebirge in a deeply incised one. In the middle reaches the river crosses the mesozoic mountainous forelands (see Section 2.1.3), where the valley first widens after Rudolstadt before narrowing again while passing the city of Jena. After taking the Unstrut near Naumburg and with the transition to the lower reaches, the morphology changes significantly. Meandering through a wide, shallow valley the Saale unites with the Weiße Elster

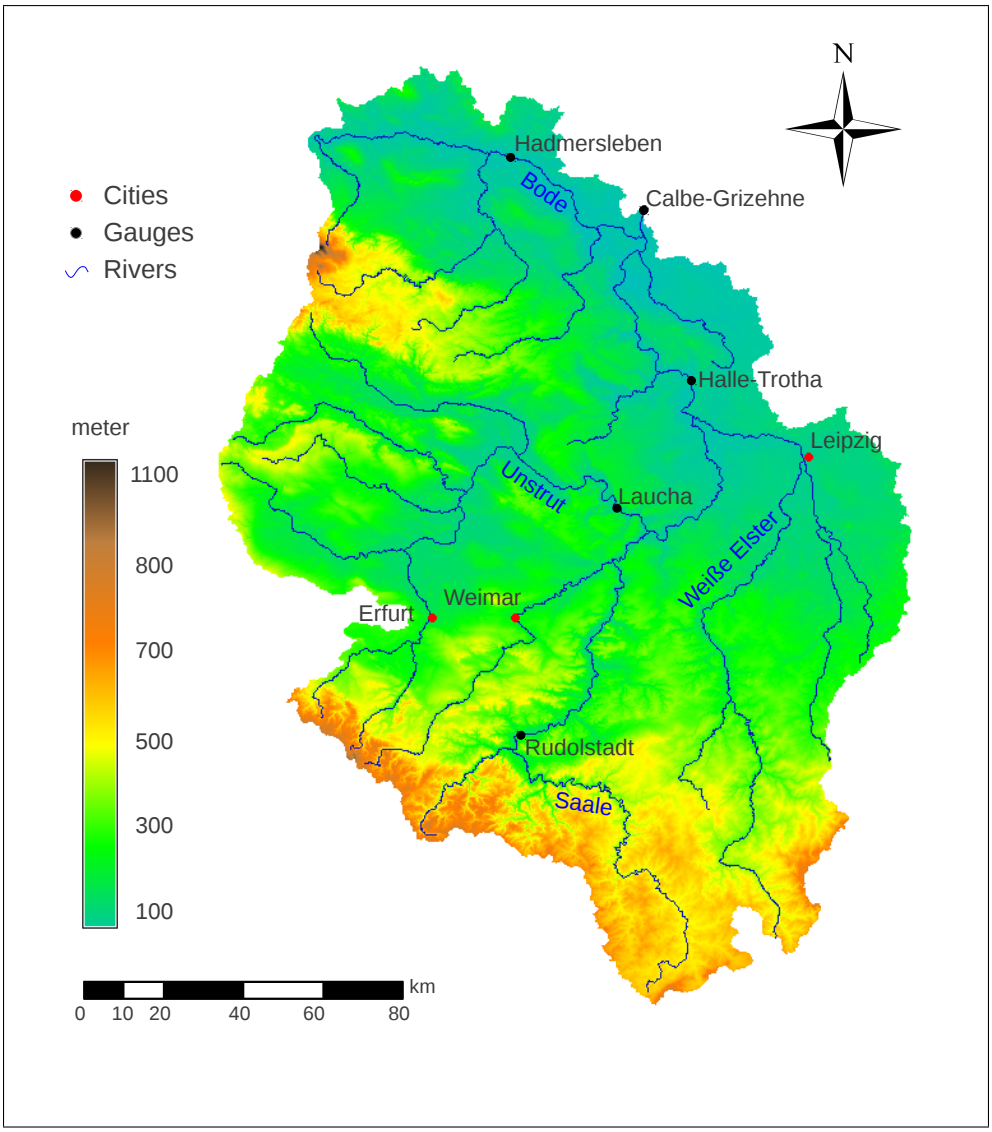


Figure 2.1: Map of the Saale River catchment. Source of the digital elevation model (DEM): Bundesamt für Kartographie und Geodäsie (BKG).

in the Leipziger Tieflandsbucht and takes it last large influx, the Bode, in the Elbe glacial valley near Bernburg, before the stream itself discharges into the Elbe (Internationale Kommission zum Schutz der Elbe (2005)). The hydrological regimes of the Saale and of all its major tributaries is heavily altered by a vast number of transverse structures, dams and retention areas. The discharge of the Saale itself is primary controlled by the Saale-Damsystem, damming the river in the upper reaches on a stretch of nearly 80 km. With an overall storage volume of more then 411 million $m^3$, the management of the system affects the river flow sustainably, the effects of regulation become apparent in the figures 2.2 and 2.3.

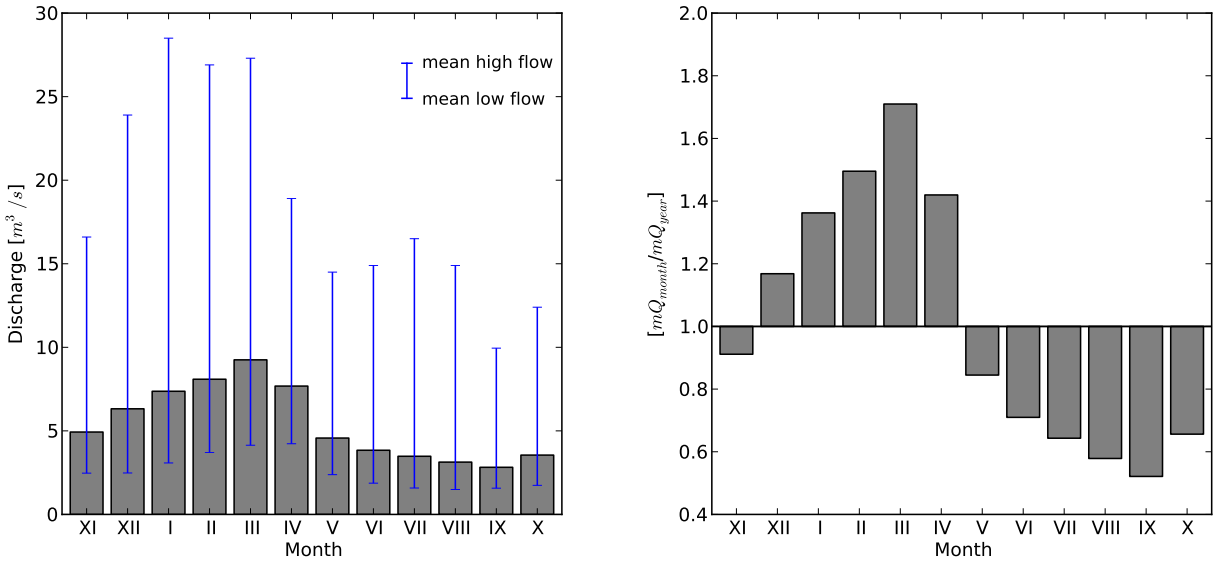


Figure 2.2: Gauge Hof, Saale. Timeseries: 1921-2007, source: Landesbetrieb für Hochwasserschutz und Wasserwirtschaft Sachsen-Anhalt (2010).

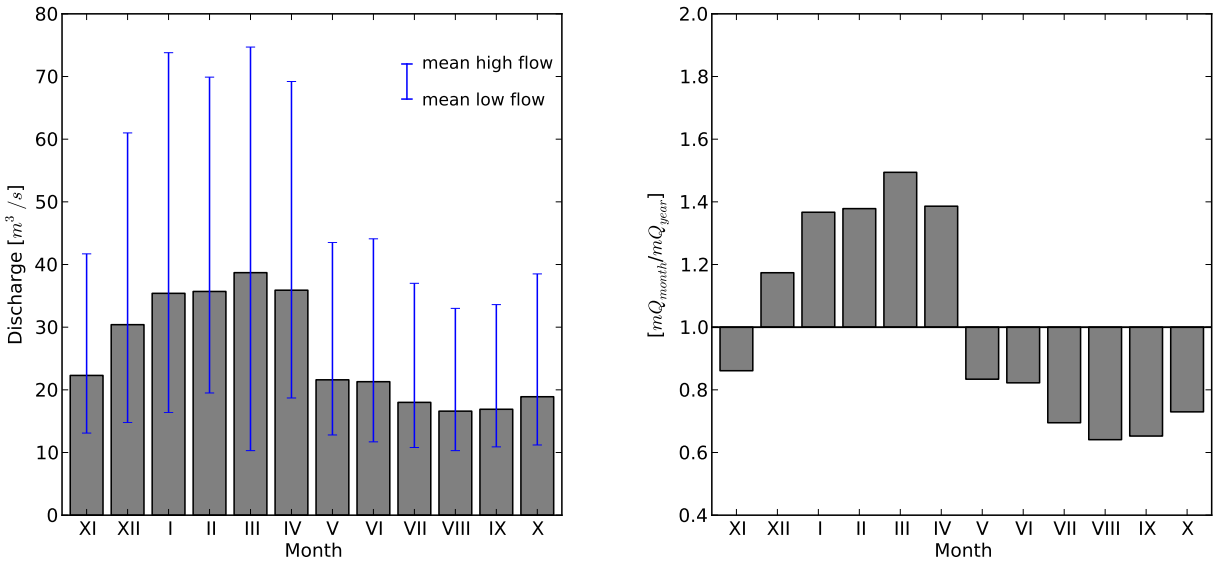


Figure 2.3: Gauge Rudolstadt, Saale. Timeseries: 1947-2007, source: Landesbetrieb für Hochwasserschutz und Wasserwirtschaft Sachsen-Anhalt (2010).

The annual course of discharge at the gauge Hof, upstream the Saale dams, shows a pronounced annual variation with high differences between mean monthly low and high flood conditions. At the downstream gauge of Rudolstadt the cushioning effect of river management is clearly visible. Peak and trough discharge are flattened, inter- and intra-month variability is reduced.

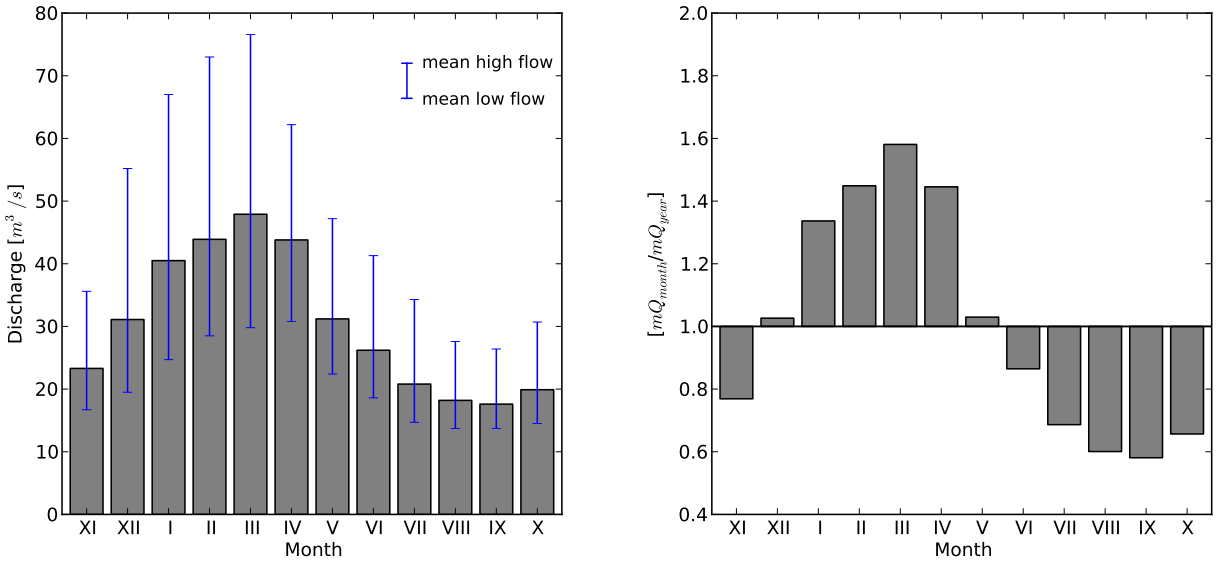


Figure 2.4: Gauge Laucha, Unstrut. Timeseries: 1946-2007, source: Landesbetrieb für Hochwasserschutz und Wasserwirtschaft Sachsen-Anhalt (2010).

### The Unstrut

The Unstrut, the largest of the three feeders drains the southern Harz, the western Thüringer Wald and, the central Thüringer Becken. The mean annual discharge rate of 30,3 $m^3/s$ is highly variable, due to great differences in altitude and precipitation (Landesbetrieb für Hochwasserschutz und Wasserwirtschaft Sachsen-Anhalt (2010)). A number of dams and retention areas with an overall storage volume of nearly 370 million $m^3$ (Internationale Kommission zum Schutz der Elbe (2005)) compensate these differences, giving the annual variability shown in Figure 2.4, highest discharge rates in spring and pronounced low flow conditions in autumn.

### The Weiße Elster

The comparable narrow watershed of the Weiße Elster covers the easterly Thüringer Schiefergebirge and the westerly part of the Leipziger Tieflandsbucht with a mean annual discharge of 17,5 $m^3/s$ (Landesbetrieb für Hochwasserschutz und Wasserwirtschaft Sachsen-Anhalt (2010)). The river origins in 723 m above sea level within the territory of the Czech Republic and flows into the Saale on the southerly outskirts of the city of Halle (78 m above sea level). The mountain stream morphology of the upper Weiße Elster and its feeders Trieb, Göltzsch, Weida and the lack of sufficient natural retention areas causes an exceptional high flood risk in the upper reaches. River discharge (see figure 2.5) is influenced by a number of reservoirs for drinking and industrial water purposes, in total 18 dams with an overall storage volume of 244 million $m^3$ (Internationale Kommission zum Schutz der Elbe (2005)) and by the lignite strip mining activities in the Leipziger Tieflandsbucht (Landesbetrieb für Hochwasserschutz und Wasserwirtschaft

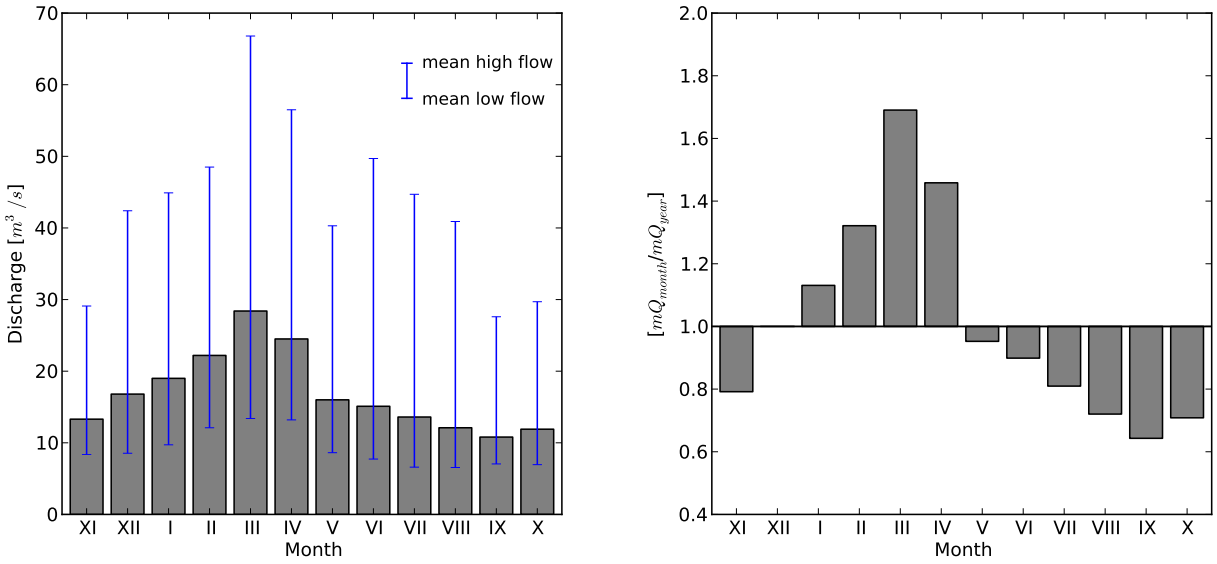


Figure 2.5: Gauge Zeitz, Weiße Elster. Timeseries: 1941-2007, source: Landesbetrieb für Hochwasserschutz und Wasserwirtschaft Sachsen-Anhalt (2010).

Sachsen-Anhalt (2010)).

### The Bode

The Bode and its tributaries drain large parts of the high precipitation Harz mountains. The river, more precise the two headwaters Cold and Warm Bode originate at a height of 873 m and 843 m above sea level, respectively. The fall descents quickly from source to outlet. Passing the town of Thale (156 m above see level) on the fringe of the Harz mountains after 64 km flow length, most of the total altitude difference of 787 m is overcome. The annual course of discharge with a characteristic peak in spring and distinct low water conditions in autumn (Figure 2.6) is significantly influenced by the dam buildings of the Rappbode-Talsperren with a storage capacity of roughly 126 million $m^3$ and a number of minor ponds, relics of the former mining activities still in use (Internationale Kommission zum Schutz der Elbe (2005)).

## 2.1.2 Climatology

The climate of the Saale Catchment, as of the Federal Republic of Germany in general, is described as warm temperate, fully humid and summer warm, Cfb according to the Köppen-Geiger climate classification (Kottek et al. (2006)). The weather is in general strongly influenced by the westerly drift bringing moist air and cyclonic precipitation from the Atlantic Ocean. Different circulation patterns may occur. Of certain importance for central European weather conditions, especially during spring, are low-precipitation easterly and frequently cyclonic northerly drifts (Liedtke and Marcinek (2002)). German

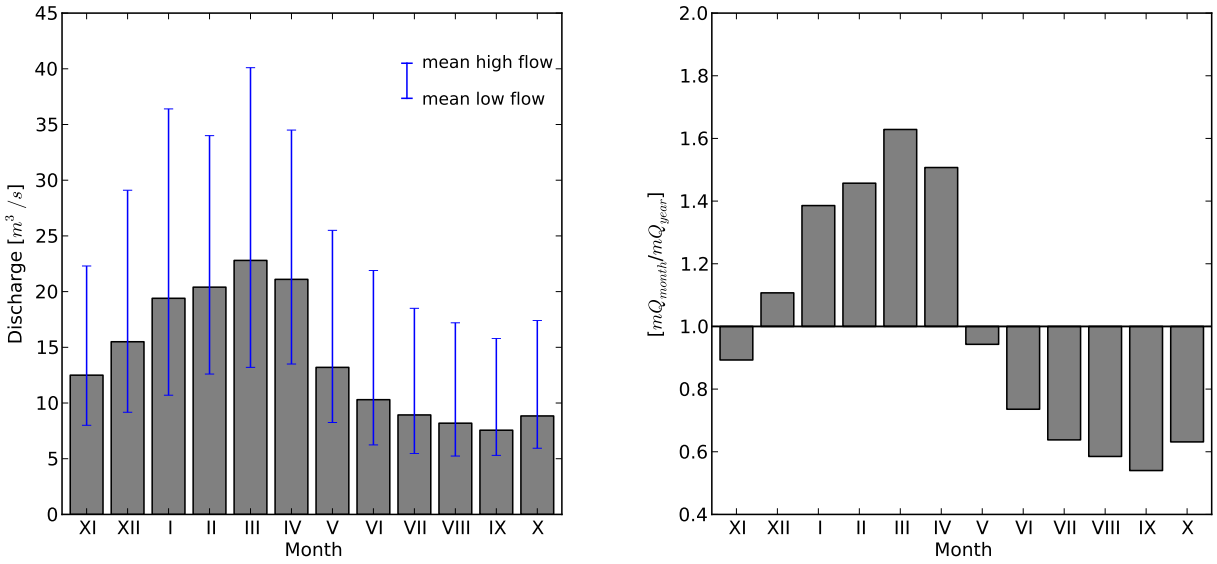


Figure 2.6: Gauge Hadmersleben, Bode. Timeseries: 1931-2007, Landesbetrieb für Hochwasserschutz und Wasserwirtschaft Sachsen-Anhalt (2010).

climate is therefore characterized by a smooth transition from the oceanic affected westerly to the more continental influenced easterly part of the country.

The National Atlas of the Federal Republic of Germany (Leibniz-Institut für Länderkunde (2003)) shows the transition from submaritime to subcontinental conditions going right through the watershed, roughly matching the boundary line between the Leipziger Tieflandsbucht and the Thüringer Becken. Beside this thermoclimatic classification, the pluvioclimatic one is of greater hydrological importance. A clear contrast has to be stated between the precipitation favoured mountainous climates, especially on the westerly exposed slopes of the Harz and the Thüringer Wald and the lowlands. Annual precipitation over the entire watershed sums up to 615 mm (Internationale Kommission zum Schutz der Elbe (2005)), but local rates range from about 1800 mm in the Brocken region to 450 mm in the city of Halle. Figure 2.7 depicts the climatology of the catchment.

### 2.1.3 Geology and Geomorphology

Surface characteristics and geology are important factors in the hydrological cycle, the complex nature of both is briefly sketched on the following pages. According to the size of its catchment, the river Saale drains very distinct landscape units. A large number of names for different sub regions is established, for the sake of simplicity a coarser, geology-based subdivision into three main units is made here: The paleozoic mountain ranges in the south and the north-west, the mesosoic mountainous forelands in the centre and the cenozoic lowlands in the north and the north-east of the watershed. Figure 2.8 depicts an extract of the geological map provided by the federal geological service.

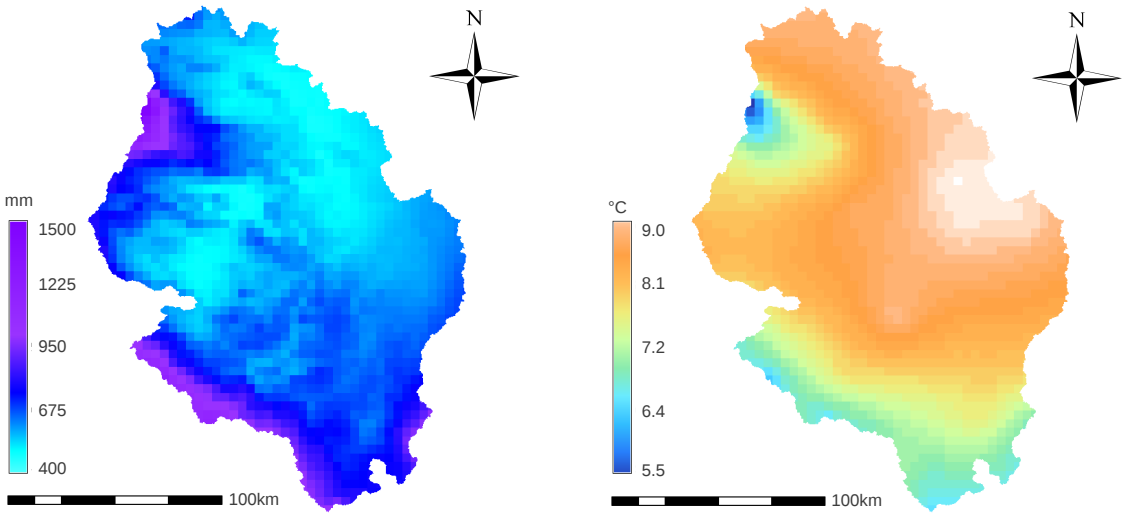


Figure 2.7: Maps of interpolated precipitation (l) and temperature (r) data, resolution: 4km, interpolation: External Drift Kriging (subsection 2.6.3). Source of weather station data: Deutscher Wetterdienst (DWD).

### The Cenozoic Lowlands

The lowlands, namely the Leipziger Tieflandsbucht and the Magdeburger Börde are considered to be the cenozioc transitional zone between the marine depositional environment of the North German Plain and the terrestrial domain in the south-west (Hennigsen and Katzung (2006)). The paleogene and neogene sediment package is widely superimposed by pleistocene glacial deposits and, on a regional scale, altered by human strip mining activities.

### The Mesozoic Forelands

From the Harz in the north to the Thüringer Wald in the south, limited by elongated faults in the east and the west, extend the mezosoic forelands, the broad Thüringer Becken and its framing plates. The overall shallow, bowl-like structure is filled with a sedimentary strata reaching from the upper Permian to the upper Triassic, overlaying the paleozoic basement and partly covered by cenozoic sediments, basically loess and in places of considerable thickness (Hennigsen and Katzung (2006)). The roughly concentric outcrops of sediments of different ages and composition are closely bound to tectonic processes, namely the descent of the basin centre and the evolution of a north-west/south-east striking system of faults. The actual topography is controlled by the resistance of the underlying geological formations. Moving up in the stratigraphy from the rims to the centre, the sand-, silt- and mudstones of the lower Triassic (Saale-Elster-Platte), but in particular the limestones of the middle Triassic (Saale-Ilm-Platte) favoured the evolution of a hilly cuesta dipping towards the basin centre. Deep fluvial cutting on the escarpment

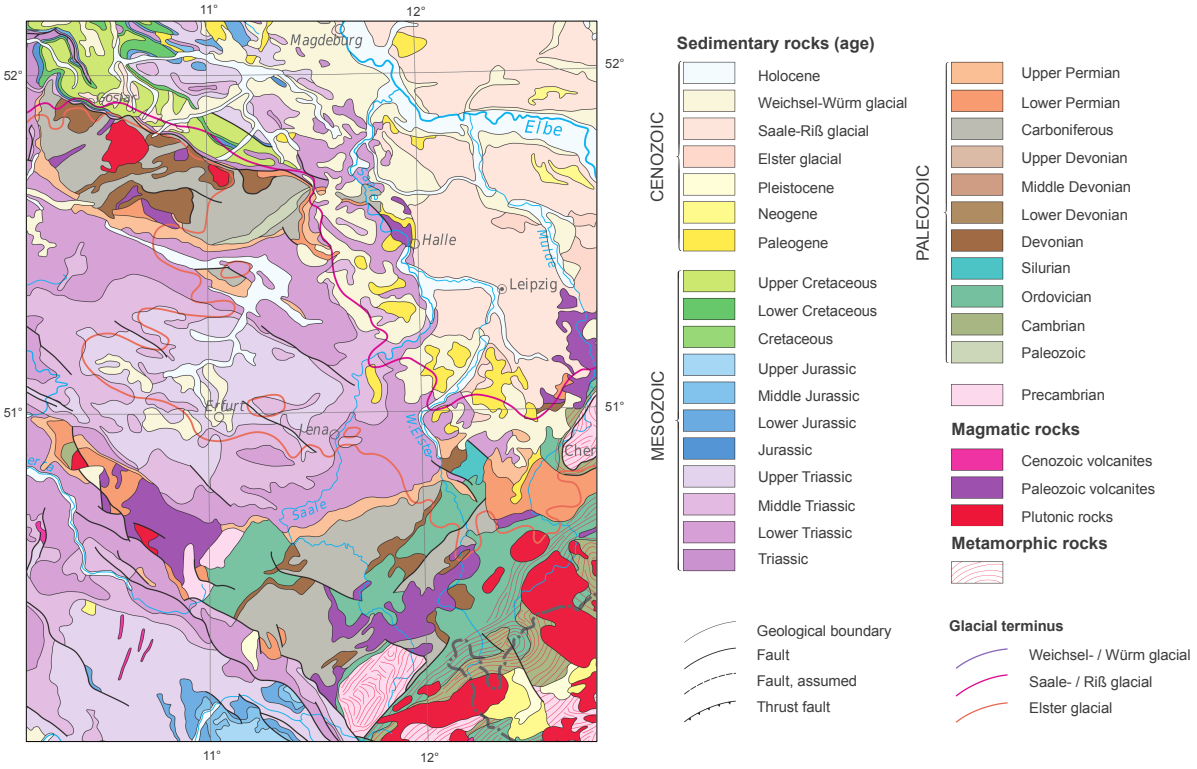


Figure 2.8: Geology of the Saale Catchment. Source: Geowissenschaftliche Karte der Bundesrepublik Deutschland 1:2000000 - Geologie (GK2000); Bundesanstalt für Geowissenschaften und Rohstoffe (BGR).

faces and a varying degree of karstification characterise the actual landscape (Liedtke and Marcinek (2002)). In the geographical and tectonical centre of the basin structure, the region around Erfurt, the youngest preserved autochthonal sediments are found. On a sea level of about 150-200 meters, approximately 200-300 meters lower then the framing plates, the heterogeneous late Triassic formations induced the development of a much smoother, undulating terrain with broad valleys and low hills (Bramer et al. (1991)).

### The mountain ranges

The north-west/south-east orientated morphological half-horst of the Harz mountains steeply arises out of its forelands in the north and the north-east and descents smoothly into the Thüringer Becken bordering in the south (Hennigsen and Katzung (2006)). The Harz is usually divided into tree units, the Upper-, Middle- and the Lower-Harz. In the geological literature (e.g. Rothe (2009), Walter (2007), Hennigsen and Katzung (2006)) a further internal subdivision into narrow north-east - south-west striking, with respect to their geology reasonably homogeneous, zones is made. This structure, with almost exclusively Paleozoic (Ordovicium to Permian) and mainly non-metamorphic rocks, is interpreted as a testimonial of the pre-orogeny, geological situation sketching the younger

tectonic directions (Rothe (2009)). Greywacke, mud- and sandstones with minor deposits of quarzite, schist and diabas of different ages are the most common rocks in the great petrographical variety of the Harz. Three mayor granite intrusions are found, the biggest one of them building the Brocken region in the Upper-Harz, with an elevation of 1141 meters the highest point of the watershed (Rothe (2009)). The topographical evolution of the Harz is more a result of tectonics, i.e. unequal elevation with highest rates in the north parts of the massive, and resulting erosion then of the underlying geology. Deep slopes and high precipitation rates in the Upper-Harz favoured the evolution of a system of deeply incised valleys at the northerly and the north-westerly rims, the half-horst itself is structured into different plateaus, each of them over topped by morphological resistant formations and with decreasing altitude towards the Thüringer Becken in the (Frühauf and Schwab (2008)).

The Thüringer Wald, morphological a narrow, elongated, north-westwards inclined skid, is the prominent limitation of the Thüringer Becken in the south of the Saale watershed. The mountainous range is limited by north-east - south-west oriented faults and clearly delimited from its forelands; the transition into the Thüringer Schiefergebirge in the south-east is of much smoother character and without any topographical distinct delimitation (Rothe (2009)). Due to the high relief ratio on either sides of the crest-line, both rims are deeply eroded by a close valley system (Bramer et al. (1991)). The internal structure is the result of the orogenesis of the Paleozoic high-mountains and its erosion. The crystalline core of gneisses and schists of varying age and metamorphism, the so called Rula-Kristallin is interrupted by granite intrusion and flanked by two major molasse basins, the Oberhöfer Mulde in the center and the Eisenacher Mulde in the nort-west of the mountain range. Both are filled with permian sediments (mainly sandstones, siltstones and conglomerates of different composition and sorting) and vulcanites of alkaline to rhyolitic chemistry (Walter (2007)).

Although without obvious borderline to the Thüringer Wald in the west, the Thüringer Schiefergebirge has to be examined as an independent geological formation. It is morphological a vast, smoothly northeastwards dipping horst with a more or less plain topography on the plateau and deeply cut valleys (Bramer et al. (1991)). Altitude decreases accordingly from about 800 m in the west to less then 500 m in the north-east. Built of mostly weakly metamorphic palaeozoic, but also proterozoic sediments (the name giving shists, greywackes and limestones) and sharply limited by faults in the southwest, the west and the east, the Thüringer Schiefergebirge is without natural limitation towards the crystalline mountains of the Fichtelgebirge in the very south of the catchment (Seidel (2003)).

### 2.1.4 Soils

The Soil Regions Map of the European Union and Adjacent Countries 1:5000000 (EUSR 5000) differentiates, based on regional climatology, four main soil regions within the watershed (figure 2.9). Each region is, according to dominant parent material, further subdivided into a number of sub regions, all characterised by a small-scale mosaic of different soils. Other regional classifications at the same mapping scale exist, nevertheless within the scope of this work the climatological approach seems to be appropriate.

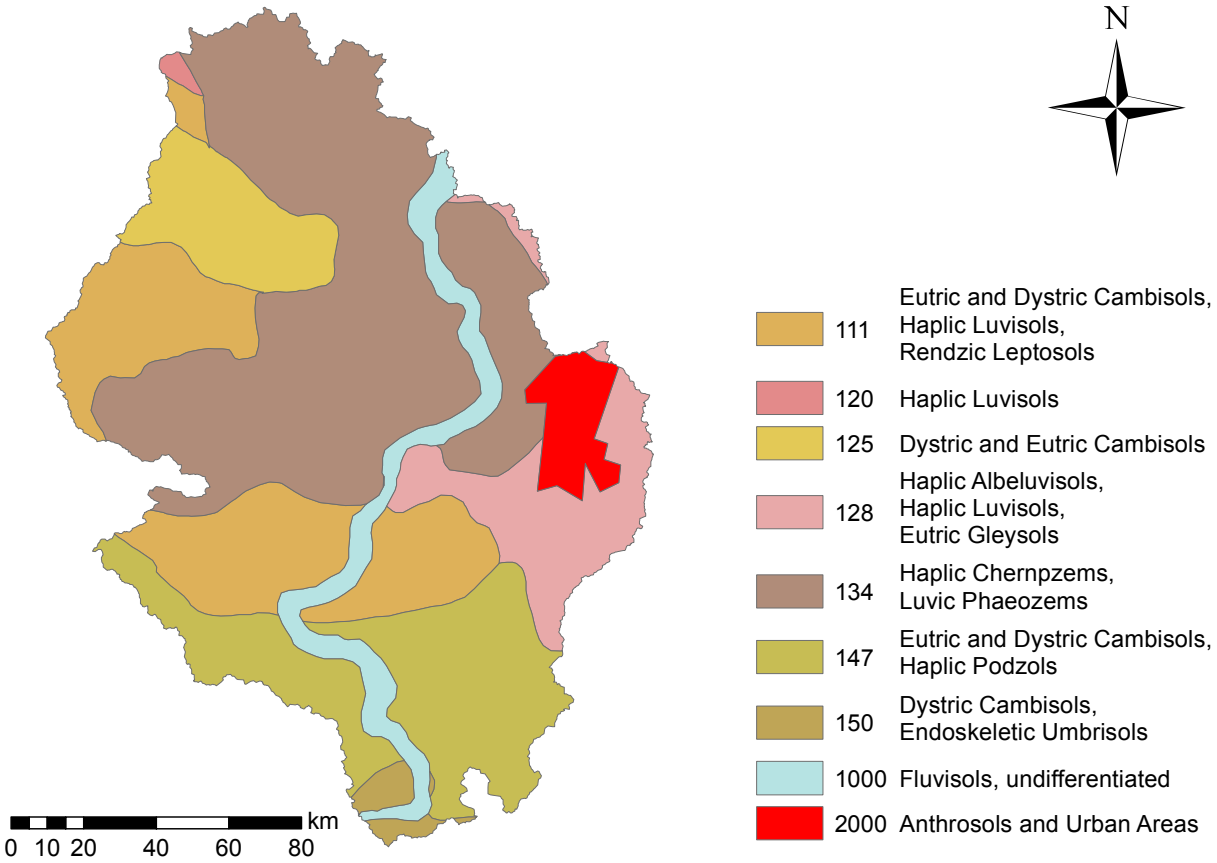


Figure 2.9: Soil region map of the Saale River basin. Source: Soil Regions Map of the European Union and Adjacent Countries 1:5000000 (EUSR 5000); Bundesanstalt für Geowissenschaften und Rohstoffe (BGR).

1. Soil region with predominant temperate sub-oceanic climate (legend label 111):

   On the Triassic sedimentary rocks framing the central Thüringer Basin, the european soil regions map lists Eutric and Dystric Cambisols, Haplic Luvisols and Rendzic Cambisols as dominating soils. The number of mentioned soils is the result of the heterogeneous geology and the complexity of overlaying periglacial regolith. On the sand-, silt- and mudstone of the lower Triassic usually Cambisols and Podzols are developed, depending on the parent material of varying fertility, in places pearched water influenced or of rendzic character at steeper slopes (Seidel (2003)).

On the limestone escarpment faces of the middle Triassic sediments catena-like soil formations dominate. A typical sequence reaches from deep Colluvia on the lower- to Rendzic Leptosols on the middle- and extremly shallow Syrosems at the upper-slopes. On the smoothly dipping plateaus mainly Rendzic Leptolsols and Chromic Cambisols are found, on loess often Eutric Podzoluvisols are developed and on the inner rim of the soil region the Haplic Luvisols and Luvic Chernozems from the adjacent region overlap Seidel (2003).

2. Soil region with predominant temperate sub-oceanic climate, influenced by mountains (legend label 125):

   The soil region is limited to the mountain range of the Harz. The large-scale soil map list Dystic and Eutric Cambisols, a somewhat insufficient generalisation for a in terms of geology, topography and climatology highly variable landscape. A smaller scale classification lists on the regolith of the Upper Harz, according to the acid parent rock material and the high amounts of precipitation, Podzols, in troughs and valleys Gleyic Podzols and Dystric Histolosols, on slopes and knolls shallow Rendzic Leptolos and Syrosems. On the loess and regolith deposits on the mainly non metamorphic sedimentary rocks of the Middle and Lower Harz Eutric and Dystic Cambisols and Dystric Podzoluvisols are dominating (Bachmann et al. (2008)).

3. Soil region with predominant temperate sub-oceanic to temperate sub-continental climate (legend labels 134 and 128):

   The soil region is roughly congruent with the lowlands within the watershed. On the central Thüringer Becken, the Magdeburger Börde and the Leipziger Tieflandsbucht, considerable amounts of loess are accumulated on the different sedimentary rocks of the upper Triassic and the Cenozoic. Highly fertile Haplic Chernozems are widespread. The upper slope soil profiles are often cut and degraded to Rendzic Leptosols, whereas the accumulation of eroded soil material at the low slope areas favoured the formation of Cumulic Anthrosols (Seidel (2003) and Pälchen (2008)). Towards the margins of the soil regions and on generally decreasing loess deposits, the dominating Chernozems are progressively replaced by Luvic Phaenozems of varying degree of degradation. In the very east of the catchment, in the eastern part of the Leipziger Tieflandsbucht the dominating soil types change towards Haplic and Eutric Luvisols, on impervious media also to Stagnic Gleysols. Within the soil region the floodplains and river terraces have to be considered seperately, generally high groundwater tables and periodically floodings determine the soil formation and consequently water influenced soils like Fluvisols, Gleysols and Mollic Fluvisols are common (Seidel (2003) and Pälchen (2008)).

4. Soil region with predominant temperate sub-oceanic to temperate sub-continental climate influenced by mountains (legend label 147):

   The region, according to the EUSR characterized by Eutric and Dystric Cambisols and Haplic Podzols, includes the landscape units Thüringer Wald and Thüringer Schiefergebirge. The mountain soils of the former show a slight altitude dependence, Haplic and Cambic Podzols on coarse regolith in the high precipitation crest areas and Spodic Arenosols and Eutric Cambisols on fine grained substrates at middle and low altitudes (Seidel (2003)). The soil mosaic of the Thüringer Schiefergebierge is usually developed in a covering layer of relocated weathering products of the underlying shists. In the fine grain substratum on the plateaus and moderately steep slopes Eutric Cambisols are common, in the higher areas Cambic Podzols, in the lower north and north-easterly parts Eutric Podzoluvisols on loess dominate the pattern (Seidel (2003)).

## 2.2 Climate Models

The A1B scenario output from four Regional Climate Models (RCM) nested into two Global Circulation Models (GCM) was chosen. The datasets are available through the ENSEMBLES-Project (van der Linden and Mitchell (2009)) and can be downloaded free of charge from the project homepage data archive (http://ensemblesrt3.dmi.dk/). The following section gives short delineations about climate models in general and the models used. As a complete description of the highly complex climate models is out of the scope of this work, the interested reader is referred to the cited literature and the references therein.

### 2.2.1 SRES Emission Scenarios

In order to asses the climatological impacts of human activities, emission scenarios projecting possible developments of human green-house gas emissions have been introduced by the 'Intergovernmental Panel on Climate Change' (IPCC). Since their first definition in 1990 as part of the IPCC First Assessment Report the scenarios have been updated twice, in the 1992 IPCC Second Assessment Report and in 2000 within the framework of the IPCC Third Assessment Report. The emission scenarios are based on scientific evidence, but are nevertheless no predictions or forecasts, rather then possible results of future population and economic development (Leggett et al. (1992)).

Four different scenarios were first defined in 1990, the SA90 A-D scenarios, a business-as-usual scenario (A), and three scenarios assuming a more ecological oriented development over the whole scenario period (B), during the second half of the century (C) and only in developed countries (D) (IPCC (1990)). In 1992 six alternative scenarios were published

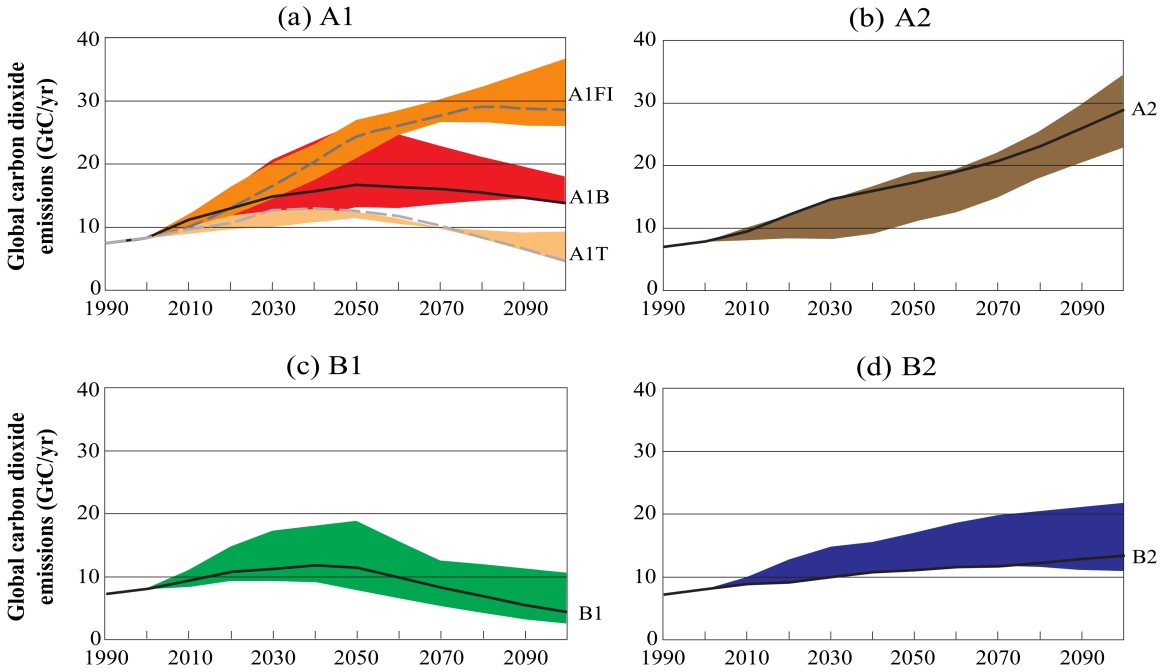


Figure 2.10: Total global annual $CO_2$ emissions from all sources (energy, industry and land-use change) from 1990 to 2100 (in gigatonnes of carbon [GtC/yr]) for the four families and six scenario groups. The coloured bands indicate the range of emission scenarios within the scenario groups (IPCC (2000): 8).

(IS92 a-f), to update and extend the existing ones. The scenarios IS92a and IS92b are pretty much comparable with the SA90 business-as-usual scenario. IS92c and IS92e mark the extremes of the emission range, the former one as the lower boundary, with emissions in 2100 being beneath the 1990 values and the latter as the upper end, projecting emissions to increase fivefold compared to 1990 (Leggett et al. (1992)). With the Third Assessment Report the scenario structure changed. Four different scenario families A1, A2, B1 and B2 were defined, each basing on a qualitative storyline on future development. Six scenario groups are derived, one group each in A2, B1, B2 and three in the A1 family, summarising the 40 different scenarios (IPCC (2000)). Figure 2.10 shows the corresponding global carbon dioxide emissions.

1. The A1 storyline is based on rapid economical growth, a global population maximum in the middle of the century and a decline afterwards. Cultural and social interaction between regions increase, differences in per capita income are reduced. Three groups describe the technological development and the energy sources it is based on: fossil fuels (A1FI), predominately non-fossil energy sources (A1T), and an equally balanced energy mix (A1B).

2. In the A2 storyline economical development is regionally oriented, but slow compared to other storylines. Differences in technological progress and per capita income remain large, world population increases continuously.

3. In the B1 storyline world population develops similar as within the A1 family but the future service and information economy is much less material intensive and more resource-efficient then nowadays. The solution of pestering challenges is globally oriented and with an emphasis on economic, social and environmental sustainability.

4. The B2 scenario is focused on environmental protection and social equity on the regional scale. World population is increasing continuously, but less than in the A2 scenario. Economic development and technological change are diverse but slower than in the A1 and B1 storyline.

### 2.2.2 Global Circulation Models

Global circulation models (GCM) mark the most complex hierarchical level in climate modelling, as they attempt to simulate all processes concerning the climate system. All state of the art GCM extend the mere atmospheric modelling by a number of sub-models simulating ocean, land surface and sea ice processes coupled internal or by an external coupling software (McGuffie and Henderson-Sellers (2008)). A number of synonyms like CGCM (Coupled Global Circulation Model) or AOGCM (Athmosphere Ocean Global Circulation Model) accounting for the multi-model structure are established. The two GCM providing boundary conditions for the Regional Climate Models used in this study, the models HadCM (Hadley Centre Coupled Model) and ECHAM5/MPI-OM (ECMWF Hamburg version 5 / Max Planck Institute - Ocean Model), both couple an atmospheric and an ocean part.

Beside a number of similarities within the basic formulations of atmospheric and ocean transport the two models do differ decisively with respect to the discretization of the atmospheric modelling domain. HadCM follows a finite grid approach, dividing the atmosphere from its lower boundary, the earth surface to its upper one, usually in the lower stratosphere (McGuffie and Henderson-Sellers (2008)) into a number of horizontally regularly shaped grid boxes with a latitude-longitude resolution of $2.5°/3.75°$. The atmospheric column on the other hand is divided irregularly into 19 layers, producing grid boxes with varying height. The vertical discretization is achieved by $\sigma$-coordinates (Pope et al. (2000)), dimensionless functions of lower and upper atmospheric boundary pressures ensuring continuity over the uneven earth surface (McGuffie and Henderson-Sellers (2008)). The model stores the diagnostic variables at different points on the grid, the Arakawa B grid used allows to define scalar values like temperature and precipitation at the grid cell centre and vector quantities like wind at the cell corners. The modelling

timestep is thirty minutes, a Fourier filtering is applied to account for decreasing absolute cell sizes towards the poles and the numerical problematic consequence of possible transfers over one ore more grid cells during one timestep (Stratton (1999)). The single variables at grid point scale are computed using a split-explicit finite difference method (Pope et al. (2000)).

The atmospheric part of ECHAM5/MPI-OM, a spectral model, follows a different discretization approach. Surface processes and vertical dynamics are still approximated on a rectangular grid but most of the atmospheric variables (i.e vorticity, divergence, temperature and surface pressure) are represented by spherical harmonics (Roeckner et al. (2006)). The spherical representation and the manipulation of atmospheric fields as waves simplifies the computation of gradients within the horizontal dimensions, but enforces constant transformation between the two discretization schemes. The resolution of a spherical atmospheric model is determined by the wave number of truncation (McGuffie and Henderson-Sellers (2008)). For the numerical experiments carried out in the ENSEMBLES-Project the ECHAM5 atmospheric model was run in T63 resolution giving a grid cell size of 1.875°/1.875°. The model uses 31 vertical layers in an hybrid vertical coordinate system where layers are defined as the pressures at the interfaces between them, the timestep in T63 resolution is set to 20 min and a weak time filter is implemented (Roeckner et al. (2006)).

### 2.2.3 Regional Climate Models

A way to at least partly overcome the limitations resulting from the coarse GCM resolutions, usually still in the range of degrees, are Regional Climate Models (RCM). Different approaches with characteristic properties exist, roughly classified into statistical and dynamical RCM. The former ones statistically relate observed meteorological data with large scale weather classifications to generate future climate from circulation patterns simulated by GCM (Wilby and Wigley (1997)). Dynamical RCM are autonomous climate models covering only the part of the earth surface of interest and in a considerably lower resolution (tens of km). They are coupled to GCM in a procedure called nesting (figure 2.11), where the RCM receives boundary conditions, i.e. large scale weather patterns like pressure fields, from the GCM to simulate regional climate in a scale more appropriate to resolve small-scale meteorological processes (von Storch et al. (1999)). The models used in this and described in the following passages all belong to the latter category.

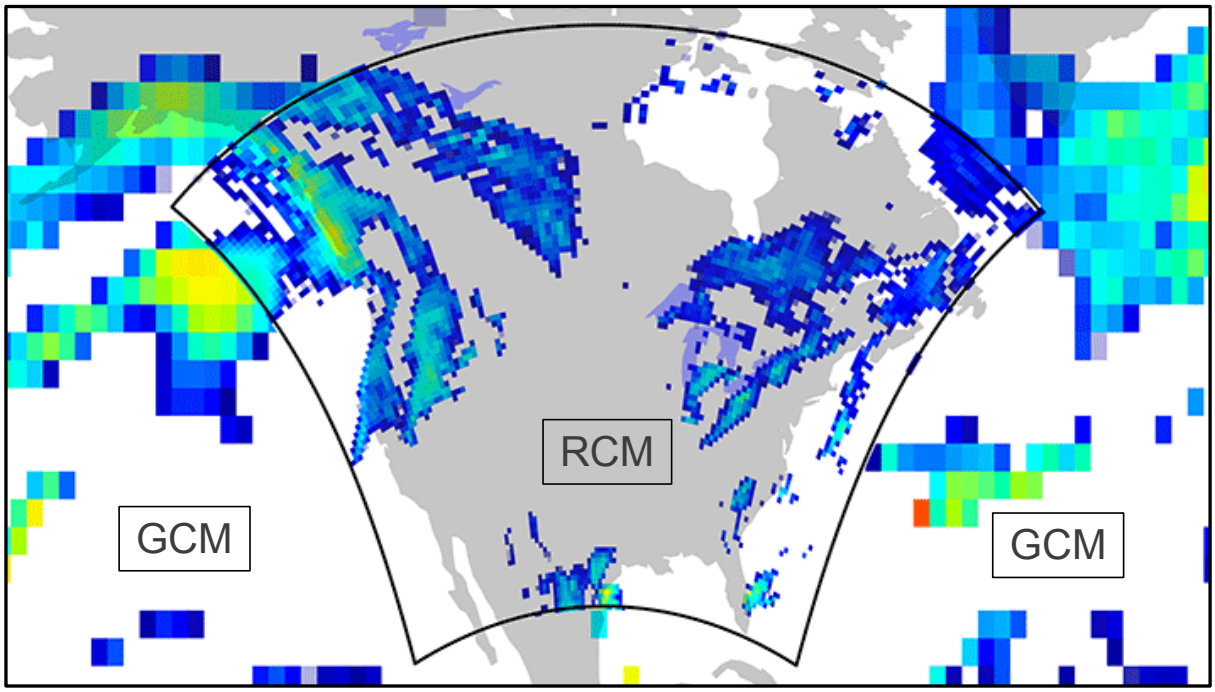


Figure 2.11: Nesting of a RCM into the driving GCM. Source: https://nar.ucar.edu/2011/lar/cisl/2000-cisl-science.

All RCM are available in horizontal resolutions of about 25 km, comparable grid cell sizes have been a directive of the ENSEMBLES-Project. All models handle the effects of meridian convergence and the resulting reduction of absolute cell areas towards the poles, ICTP-REGCM uses the Lambert Conformal Conic map projection, the other RCM a rotated grid, shifting the north pole to 39.25°/-162° latitude/longitude. As a result, the equator of the modelling coordinate system runs through the center of the modelling domain. (Doms (2011)). Major differences in model output concerning the time scheme exist. The ECHAM5/MPI-OM driven RCM provide output variables as timeseries using a standard calendar with months of unequal length and leap years, the HadCM models provide timeseries in a 360-day calendar, dividing the year into 12 equal months of 30 days. The following models have been used:

*ETHZ-CLM*

The Regional Climate Model CLM (Eidgenössische Technische Hochschule Zürich - Climate Version of Lokal Modell) is a community based extension of the non-hydrostatic operational forecasting system of the German Weather Service (DWD). A number of sub-modules have been implemented under the Consortium for Small-Scale Modelling (COSMO) in order to use the short range numerical weather prediction system as a RCM. External forcing in forecast mode, like the states of vegetation, atmosphere and ocean are included and a complex soil model is added to count for the water and energy

budget over multi-seasonal calculation periods (Boehm et al. (2006)).

*HadRM3Q0*
HadRM3Q0 (Hadley Centre Regional Model version 3Q0) is basically an advanced version of the atmospheric part of the Hadley Centre GCM, HadCM3. A number of improvements have been made (sulphur cycle, changes in the physical parametrisation), but the main formulations are adopted in order to ensure consistent projections on the regional and the global scale (Jones et al. (2004)).

*ICTP-REGCM3*
ICTP-REGCM3 (Abdus Salam International Centre for Theoretical Physics - Regional Climate Model version 3) was developed in Trieste, Italy, and implements, similar to the ETHZ-CLM model, a number of extension to an existing weather forecasting system (e.g. a land surface model, boundary layer scheme, parametrisation scheme for precipitation) (Pal et al. (2007)). The dynamical core of the model is provided by the non-hydrostatic Mesoscale Meteorology Model 5 (MM5), setup at the Pennsylvania State University (PSU) and the National Center for Atmospheric Research (NCAR) as a community model (Grell et al. (1994)).

*MPI-M-REMO*
The only hydrostatic RCM in the model ensemble is the regional climate model from the Max Planck Institute for Meteorology, REMO (Regional Modell). The model dynamics is based on the 'Europa-Modell', a former meso-scale weather forecasting system of the German Weather service (DWD). For the use in a climate prediction mode, the physical parametrization of the ECHAM4 GCM was implemented (Jacob et al. (2008)).

## 2.3 Bias Correction

Due to the bias inherent in climate models (Jacob et al. (2007), Christensen et al. (2008)) and described in much more detail and with particular focus on the study area in chapter 3, it is a common but controversial practice to correct climate model data in order to use it as forcing of impact models. A number of different approaches have been proposed and tested for their suitability in hydrological modelling (e.g. Haerter et al. (2011), Yang et al. (2010), Leander and Buishand (2007), Kunstmann et al. (2004), Hay et al. (2000)). The idea of correcting climate models for their deviation from observational data is however always based on at least two assumptions:

1. The data used for the bias correction, usually spatially interpolated measurement data, does adequately represent the actual climate.

2. The bias is consistent in time, correction functions derived for the past are suitable for future.

If these assumptions hold is questionable, however hydrological modelling relies on reasonably realistic forcing. For that reason a simple, monthly based bias correction, as suggested by Kunstmann et al. (2004) and employed by Senatore et al. (2011), is applied to correct climate model precipitation data. Correction factors are calculated for each grid cell and month individually as the quotient of longterm monthly precipitation sums (1961-1990) of modelled and observed data, the latter interpolation to the climate model grid using Inverse Distance Weighting (see subsection 2.6.3). All daily precipitation values are subsequently multiplied with the respective monthly correction factor. Formally written:

$$k_m(i,j) = \frac{\frac{1}{Y-y}\sum_{y}^{Y}\sum_{d}^{D} RCM_{y,m,d}(i,j)}{\frac{1}{Y-y}\sum_{y}^{Y}\sum_{d}^{D} OBS_{y,m,d}(i,j)} \tag{2.1}$$

with $k_m(i,j)$ denoting the correction factor $k$ for month $m$ and grid cell $i,j$, $RCM_{y,m,d}$ and $OBS_{y,m,d}$ the values for any specific date (year $y$, month $m$, day $d$) from modelled and observational data, $D$ the total number of days in given month and $Y$ the last year of the correction period.

The procedure results in a numeric adjustment of monthly precipitation sums of the RCM time series within the correction period but without explicitly correcting the entire distribution function. In contrast to other methods focusing on the empirical distribution (e.g. Yang et al. (2010), Leander and Buishand (2007), Shabalova et al. (2003)), the total number of rain days remains unchanged. This could be considered a shortcoming, the general idea here is anyhow not to achieve a perfect statistical fit but rather to generate a reasonably realistic database without changing RCM characteristics fundamentally.

## 2.4 The hydrological model mHM-UFZ

The hydrological model used for streamflow prediction, mHM-UFZ (mesoscale Hydrological Model - Umwelt Forschungs Zentrum) was developed during the recent years in the Department Computational Hydrosystems of the Helmeholtz-Zentrum für Umweltforschung in Leipzig, Germany. A brief description of the process based, spatially distributed, mesoscale, waterbalance model is given in the following subsections, much more detailed information can be found in Samaniego et al. (2010) and Kumar (2010).

### 2.4.1 Model Structure

Figure 2.12 depicts a general scheme of mHM and the different components included into the model. The core formulations are based on the hydrological model HBV (Bergström (1995), Hundecha (2004)). A number of new features have been included, namely canopy interception, a snow accumulation and melting scheme, effects of soil freezing and thawing, a two layer soil root zone and a cell to cell routing (Kumar (2010)). The model does furthermore account for up to three different spatial scales, each allowing different horizontal resolutions:

1. Level 0: The resolution of the morphological input data, such as terrain elevation, slope, aspect, soil physics, permeability of the main geological formation and land cover. For this study all physiographical input data is resampled to a resolution of 100 m.

2. Level 1: Modelling scale used to simulate the main hydrological processes, in the following a horizontal discretization of 4 km is used.

3. Level 2: Horizontal resolution of the meteorological forcing. Here set to 4 km (observed meteorological data used for calibration/validation) and 24 km (climate model data).

This differentiated spatial discretization allows the model to account for the variability in the different datasets on the scale they are available. There is no need and aggregate input data during preprocessing to the coarser modelling resolution rather then using it (quasi) as are (Samaniego et al. (2010)).

### 2.4.2 Model Parameters

For reasons as process and/or spatial complexity, a spatially explicit model must be an approximation of the main governing processes, accompanied by a number of simplifications, conceptualisations and errors due to the numerical solutions of the mathematical process formulation (Kirchner (2006)). Model parameters, i.e. not directly observable quantities, are used to compensate the inaccuracies introduced by model formulation and are usually estimated through calibration (Gupta et al. (2002)). mHM defines 28 model parameters, a complete list can be found in table 2.1.

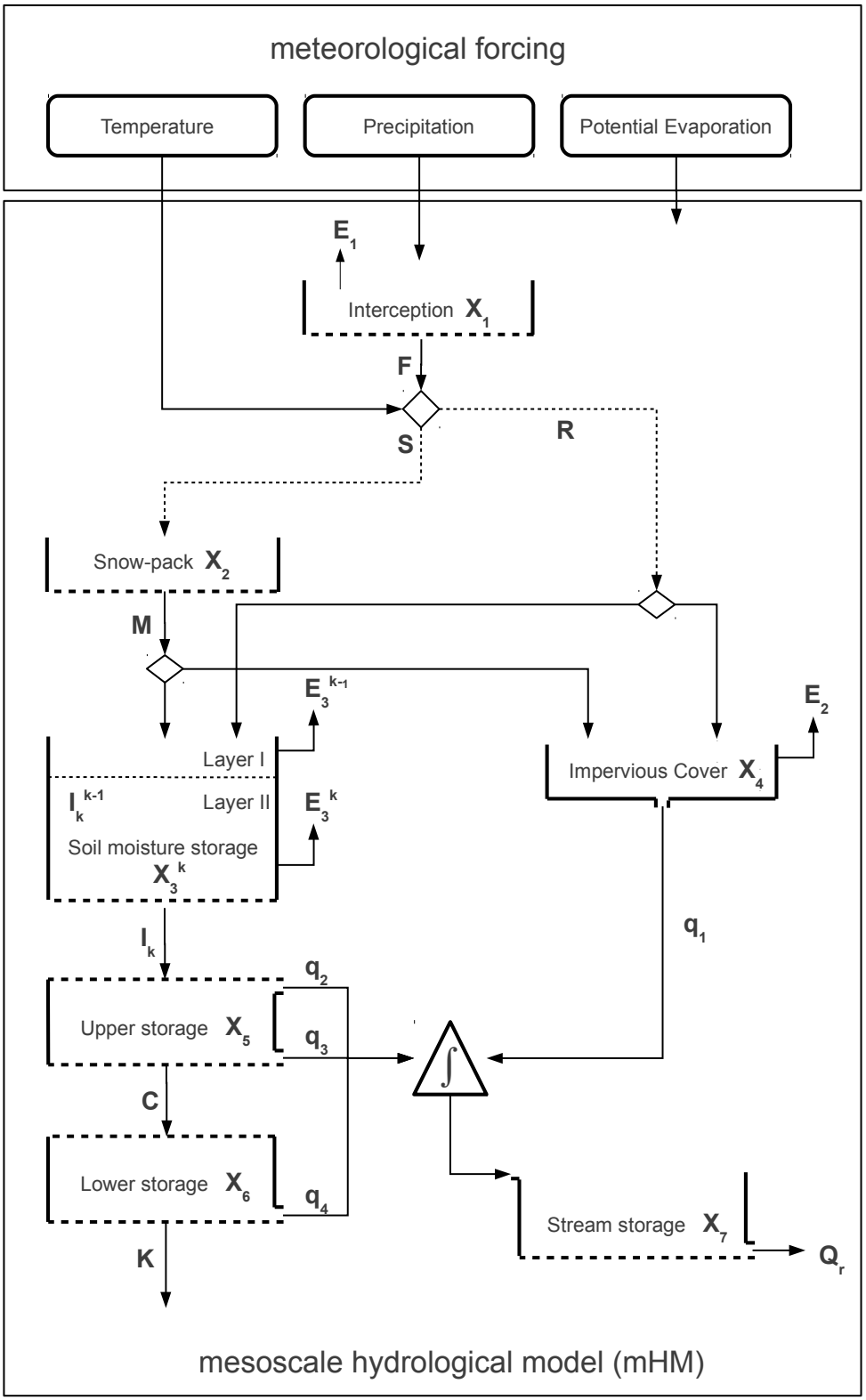


Figure 2.12: Schematic representation of different mHM components. $X$ = state variable, $E$ = actual evaporation, $q$ = component of runoff, $S$ = snow precipitation depth, $R$ = rain precipitation depth, $F$ = throughfall, $I$ = infiltration capacity, $C$ = percolation, $K$ = gain/loss flux in a leaking cell, $Q_r$ = runoff produced at cell outlet, $k$ = root zone layer index ($k = 1, 2$), $q$ = runoff component (Kumar 2010: 17f).

Table 2.1: mHM model Parameters (Kumar (2010), Samaniego et al. (2010))

| Parameter | Unit | Description |
|---|---|---|
| $\beta_1$ | mm | Effective maximum canopy storage. |
| $\beta_2$ | °C | Threshold temperature for phase transition sow/rain. |
| $\beta_3$ | - | Degree of day factor during rainless days. |
| $\beta_4$ | mm $d^{-1}$°C | Rate of increase of the degree day factor per unit of precipitation. |
| $\beta_5$ | mm $d^{-1}$°C | Maximum degree day factor reached during rainy days. |
| $\beta_6^k$ | mm | Maximum soil moisture content in the *kth* horizon. |
| $\beta_7$ | - | Parameter that determines the relative contribution of rain or snow melt to runoff. |
| $\beta_8$ | mm | Critical value of soil ice content above which the soil is practically impermeable. |
| $\beta_9$ | - | Shape factor of the gamma distribution that statistically estimates the virtual impermeable area due to frozen soil. |
| $\beta_{10}$ | K | Antecedent Temperature Index (ATI, a proxy for soil temperature) threshold below which unfrozen water content reaches its minimum. |
| $\beta_{11}$ | K | ATI threshold above which no frozen water exist. |
| $\beta_{12}$ | - | Minimum fraction of unfrozen water content. |
| $\beta_{13}$ | - | Weighting multiplier ranging from 0.1 to 1. |
| $\beta_{14}$ | mm | Maximum ponding retention in impervious areas. |
| $\beta_{15}$ | - | Permanent wilting point. |
| $\beta_{16}$ | - | Soil moisture limit above which the actual transpiration is equated with the potential evaporation (PET). |
| $\beta_{17}$ | - | Fraction of roots in the *kth* horizon. |
| $\beta_{18}$ | mm | Maximum holding capacity of the second reservoir (unsaturated zone). |
| $\beta_{19}$ | d | Fast recession constant. |
| $\beta_{20}$ | d | Slow recession constant. |
| $\beta_{21}$ | - | Exponent that quantifies the degree of nonlinearity of the cell response. |
| $\beta_{22}$ | d | Effective percolation rate. |
| $\beta_{23}$ | d | Baseflow recession rate. |
| $\beta_{24}$ | - | Fraction of the groundwater recharge that might be gained or lost either as deep percolation or as intercatchment groundwater flow in nonconservative catchments. |
| $\beta_{25}$ | h | Duration of the triangular unit hydrograph accounting for the discharge attenuation within the cell. |
| $\beta_{26}$ | h | Muskingum travel time parameter. |
| $\beta_{27}$ | - | Muskingum attenuation parameter. |
| $\beta_{28}$ | - | Aspect correction factor of the PET. |

### 2.4.3 Parameter Regionalization

Distributed hydrological models (e.g. TOP-MODEL (Beven et al. (1995)), the distributed HBV model (Lindström et al. (1997)), WASIM-ETH (Schulla and Jasper (2007))) account for the spatial variability of catchment properties by discretizing the modelling domain into small individual homogeneous units, the grid cells. This gain in model representativeness compared to lumped models, treating the basin as one single modelling unit, is accompanied by higher complexity of parametrisation (Kumar (2010)). With increasing modelling area and/or decreasing horizontal resolution the dimensionality of the parameter search space rapidly increases (Samaniego et al. (2010)). Considering the 28 mHM model parameters and the 29205 grid cells discretizing the Saale Catchment with a horizontal resolution of 4 km, 28*29205 = 788535 parameters needed to be estimated.

In order to reduce the number of model parameters, different parametrisation schemes have been applied, usually based on the grouping of grid-cells into a number of larger, considered to be homogeneous regions, the 'Hydrological Response Units' (HRU) (Leavesley et al. (1983), Flügel (1995)). Model parameters are then estimated for the HRU instead of the grid cells, reducing the complexity of the optimization problem in dependence of the simplification introduced by the classification procedure.

Although reasonably good model performances can be achieved applying the HRU concept (e.g. Das et al. (2008), Blöschl et al. (2008)) the classification is static, the delineation of the individual units arbitrary and a realistic simulation of small scale processes, like soil moisture patterns, is unlikely (Kumar (2010)). An approach to overcome this shortcomings is the regionalization of model parameters, i.e. the establishment of relationships between model parameters and catchment properties via regionalization or transfer functions and introduced quantities, the global parameters. In the general formulation:

$$\beta_{l,i}(t) = f_l(\mathbf{u}_i, \gamma) \tag{2.2}$$

$\beta_{l,i}(t)$ denotes the $l$th model parameter for grid cell $i$ at time step $t$. $\mathbf{u}_l$ refers to a vector of physiographical basin characteristics and $\gamma$ to a vector of global parameters (Samaniego et al. (2010)). Due to the predefined relationship between model parameters, global parameters and basin characteristics, the actual model parameters needed to solve the governing equations can be calculated for every grid cell individually, from the one set of global parameters. Instead of calibrating all model parameters for any grid cell, the optimization problem is reduced to the total number of global parameters, in mHM 68. Although parameter regionalization methods already have been applied in hydrological models (e.g. Hundecha (2004), Pokhrel et al. (2008)), the regionalization implemented in mHM and described in detail in Samaniego et al. (2010), follows a slightly different approach. The calculation of model parameters $\beta$ is usually accomplished on the modelling scale, thus after an aggregation of input data to a coarser resolution, implicating

a substantial loss of sub-grid variability (Samaniego et al. (2010)). With the so-called 'Multiscale Parameter Regionalization (MPR)' introduced in mHM, model parameters are always estimated on the lowest horizontal resolution (i.e. 100 m) and upscaled to modelling resolution later on. The effects of this parametrisation have been tested in extensive numerical experiments by Samaniego et al. (2010) and Kumar et al. (2010) and can be summarised as follows:

1. Global Parameters are quasi scale independent and transferable over different horizontal resolutions. The time consuming calibration procedure can be done on scale coarser than the modelling scale, without substantial loss of performance when using these parameters in finer scaled modelling.

2. Within mesoscale river basins, global parameters are quasi location independent. Modelling with parameters obtained by calibrating the model at the outlet gauge shows reasonable performance at internal stations.

### 2.4.4 Parameter Calibration

To identify feasible sets of global parameters the Dynamically Dimension Search (DDS) algorithm (Tolson and Shoemaker (2007)) was implemented in mHM, according to Kumar (2010) a robust and economical optimization method. The objective function to asses model performance and evaluate the quality of any parameter set generated during the iterative calibration process is based on daily discharge. The equally weighted average of the Nash-Sutcliff Efficiencies of daily discharge volumes and their logarithms are used (see section 2.6.1). The model is calibrated for the water years 2000-2004, using the discharge data of the basin outlet gauging station Calbe-Grizehne. This period is chosen as it covers an exceptional extreme event, the January 2003 high flood and distinctive below average conditions during the second half of the years 2000, 2003 and 2004.

## 2.5 Data Availability

The input data required to setup and run mHM can be grouped into three different categories: physiographical characteristics, land cover and meteorological forcing.

### 2.5.1 Physiographical Characteristics

Necessary morphological information is derived from a digital elevation model (DEM), the digital soil map 'Bodenübersichtskarte 1:1000000 (BÜK 1000)' and the hydrogeological map 'Hydrogeologische Übersichtskarte 1:200000 (HÜK 200)'. The DEM with resolution of 50 m is provided by the state agency for geoinformation 'Bundesamt für Kartographie

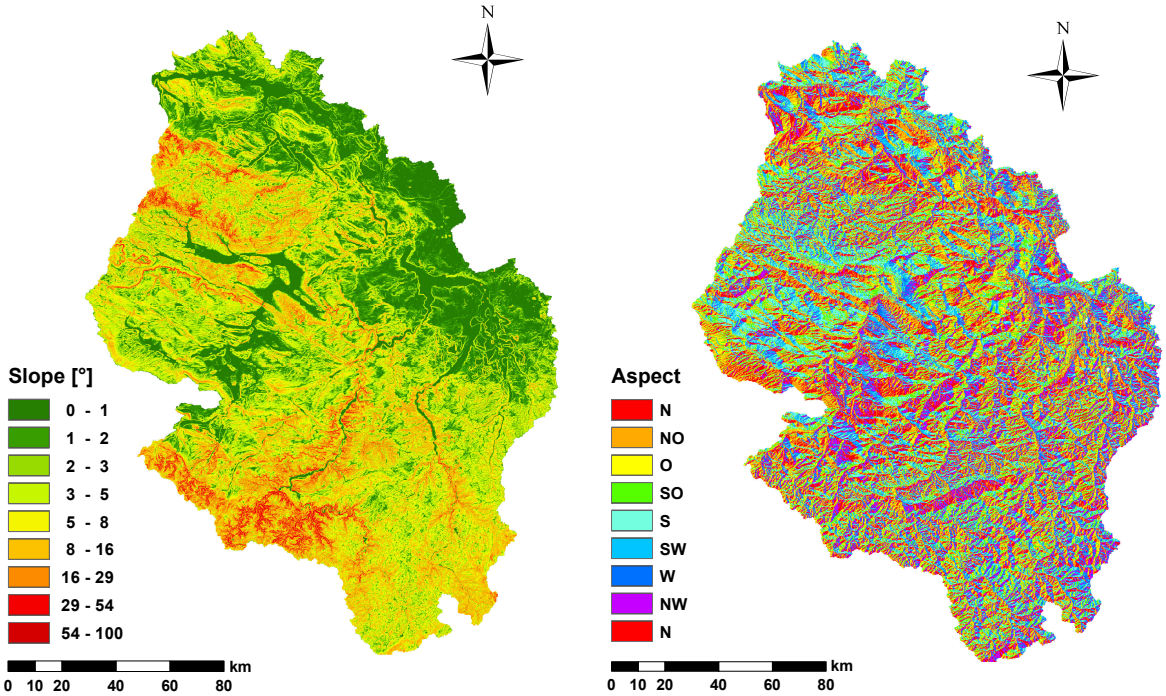


Figure 2.13: Maps of slope (l) and aspect (r). Calculated from digital elevation data, resolution: 100 m. Source of the DEM: Bundesamt für Kartographie und Geodäsie (BKG).

und Geodäsie (BKG)', the digital maps by the german geological service 'Budesanstalt für Geowissenschaften und Rohstoffe (BGR)'.

All datasets concerning the physiographical characteristics are resampled to a horizontal resolution of 100 m using the 'Resample' - tool and nearest neighbour assignment out of the 'ArcGIS - Data Management Toolbox'. The resulting DEM is further processes using the 'ArcGIS - Spatial Analyst Tools' in order to produce a sinkless DEM (Hydrology - Fill), calculate flow direction (Hydrology - Flow Direction), flow accumulation (Hydrology - Flow Accumulation), watershed boundaries (Hydrology - Watersheds), slope (Surface - Slope) and aspect (Surface - Aspect). Depth and textural composition of soils and soil horizons are estimated using the 'Bodenkundliche Kartieranleitung' (AG Boden (1994)), soil bulk density is calculated as a function of organic and mineral matter (Rawl (1983)). From the hydrogeological map information about the presence of karstic formations and the range of mean hydraulic conductivity of the upper groundwater reservoir is gathered, exact values of the latter are subject to calibration. Figure 2.13 exemplary shows selected mHM input catchment characteristics.

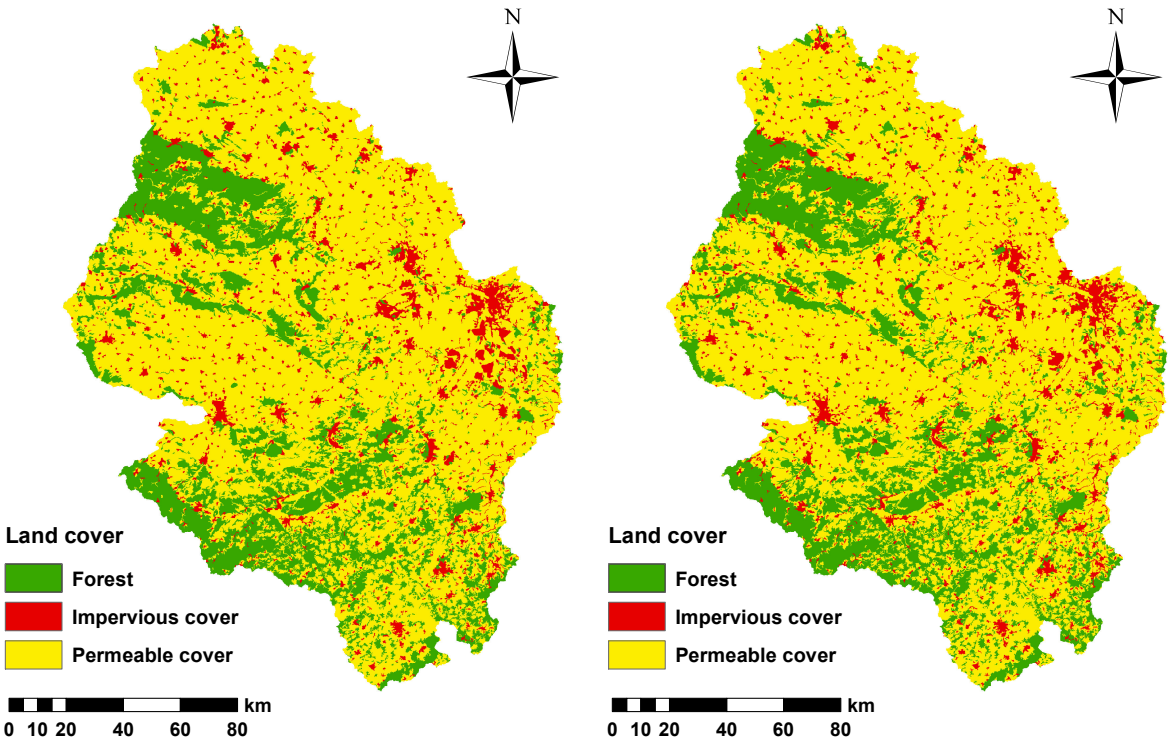


Figure 2.14: Land cover for the years 1990 (l) and 2006 (r). Maps derived from Landsat TM5 scenes, resolution: 100m.

### 2.5.2 Land Cover

To account for the change in land cover during the recent years, three different land cover datasets are derived from Landsat TM5 scenes for the years 1990, 2000 and 2006 (see figure 2.14). The satellite images with a horizontal resolution of 30 m are automatically classified (Bárdossy and Samaniego (2002)) and aggregated into three different land cover types as proposed by (Samaniego (2003)), namely Forest, impervious cover (e.g. settlement areas, traffic infrastructure) and permeable cover (e.g. agricultural areas, wetlands). The land cover information is subsequently resampled to a resolution of 100 m. In the hydrological modelling the 1990 land use patterns are used to simulated discharge for the years from 1951 to 2000, the second dataset for the years until 2006 and the most actual land cover information was considered to be valid until the end of the century.

### 2.5.3 Meteorological Data

The hydrological model mHM relies on spatial averages of three different meteorological forcings: daily mean temperature, daily precipitation sums and total daily potential evaporation. Gridded datasets of daily temperature and precipitation, interpolated from weather station data provided by the german meteorological service 'Deutscher Wetterdienst (DWD)', are available. Climate normals necessary in the bias correction procedure are freely gathered from the DWD-homepage.

Potential evaporation (PET), the water flux back into the atmosphere, is calculated using the Hargreaves and Samani method (Hargreaves and Samani (1985)), as direct measurements are not available. PET $E_p$ is calculated as function of temperature and extraterrestrial radiation:

$$E_p = 0.0023\, c\, R_a (T_{mean} + 17.8)(T_{max} - T_{min})^{0.5} \tag{2.3}$$

where $c = 0.408$, a constant to convert radiation in millimetre of evaporation equivalent, $T_{mean}$, $T_{max}$, $T_{min}$ denote daily mean, maximum and minimum temperatures and $R_a$ the extraterrestrial radiation as function of Julian day and geographical latitude (Duffie and Beckman (1980)):

$$R_a = 15.392\, d_r (\omega_s\ sin\,\phi\ sin\,\delta + cos\,\phi\ cos\,\delta\ sin\,\omega_s) \tag{2.4}$$

$d_r$ denotes the relative distance between earth and sun, $\omega_s$ the sunset hour angle, $\phi$ latitude in radians and $\delta$ solar inclination with:

$$d_r = 1 + 0.33\, cos\left(\frac{2\pi\, J}{365}\right) \tag{2.5}$$

$$\delta = 0.4093\, sin\left(\frac{2\pi\, J}{365} - 1.405\right) \tag{2.6}$$

$$\omega_s = arccos(-tan\phi\ tan\delta) \tag{2.7}$$

### 2.5.4 Discharge Data

The discharge data of five different gauging stations is available and used in calibration and validation of mHM. All datasets are provided as timeseries of daily mean discharge by the federal authority for flood control and water management of Saxony-Anhalt (Landesbetrieb für Hochwasserschutz und Wasserwirtschaft (LHW)) and the environmental and geological service of Thuringia (Thüringer Landesanstalt für Umwelt und Geologie (TLUG)). Due to data availability not all the main tributaries are covered explicitly. The basin of the river Unstrut is entirely covered by the station Laucha, the Bode catchment area at least to a waste extend by the gauge Hadmersleben. The river Weiße Elster is not covered directly, the next gauging station Halle-Trotha is located some 14 km after joining the receiving water. Streamflow data for the Saale itself is available at three stations, Rudolstadt, only a few kilometres downstream the large Saale dam-system, Halle-Trotha and the outlet gauge Calbe-Grizehene. Table 2.2 lists the main gauging station characteristics.

Table 2.2: Gauging station characteristics.

| Station name | Area ($km^2$) | Altitude ($m$) | River | Data source |
|---|---|---|---|---|
| Calbe-Grizehne | 23719 | 56 | Saale | LHW |
| Halle-Trotha | 17979 | 69 | Saale | LHW |
| Laucha | 6218 | 109 | Unstrut | LHW |
| Rudolstadt | 2678 | 190 | Saale | TLUG |
| Hadmersleben | 888 | 73 | Bode | LHW |

## 2.6 Statistics

A set of different statistical methods is used in order to preprocess the input to mHM and to analyse the generated output. In the following the main formulations and short descriptions are given.

### 2.6.1 Model Performance Criteria

To asses performance of the hydrological modelling, the four statistical criteria Nash-Sutcliff Efficiency (NSE) $E_Q$ (Nash and Sutcliffe (1970)), Nash-Sutcliff Efficiency of logarithmic discharge $E_{logQ}$, Pearson correlation coefficient $r$ and relative bias $bias$ are used. These are formally written as:

$$bias = \frac{\frac{1}{T}\sum_{t=1}^{T}(Q'(t) - Q(t))}{\overline{Q}} \tag{2.8}$$

$$r = \frac{1}{T-1}\sum_{t=1}^{T}\left(\frac{Q'(t) - \overline{Q'}}{S_{Q'}}\right)\left(\frac{(Q(t) - \overline{Q})}{S_Q}\right) \tag{2.9}$$

$$E_Q = 1 - \frac{\sum_{t=1}^{T}(Q_t - Q'_t)}{\sum_{t=1}^{T}(Q_t - \overline{Q}_t)} \tag{2.10}$$

$$E_{logQ} = 1 - \frac{\sum_{t=1}^{T}(log\ Q_t - log\ Q'_t)}{\sum_{t=1}^{T}(log\ Q_t - log\ \overline{Q}_t)} \tag{2.11}$$

where $t$ denotes an explicit time step, $T$ the total number of time steps, $Q(t)$ observed discharge at timestep $t$, $Q'(t)$ simulated discharge at timestep $t$, $S$ the standard deviation

and overbar the arithmetic mean.

### 2.6.2 Data Analysis

In order to analyse the characteristics of the meteorological data (i.e. precipitation) from the different Regional Climate Model (RCM), relative cumulative frequency distributions are estimated, their proximity to the distribution from observational data and, as a measure of extreme events, 95-percentiles are computed.

#### Cumulative Frequency Distribution

Cumulative distributions functions (CDF) are basically the integral of an histogram, i.e. the count of values falling into any of a arbitrarily high number of bins, subdividing the data usually into equally sized classes. The accumulation of these frequencies in the CDF-plot allows to asses on the vertical axis the relative probability that the corresponding value on the horizontal axis will not be exceeded (Wilks (2006)). The CDF-plots presented in the following are calculated from all daily precipitation sums in the dataset (including the zero precipitation days) with bin widths of 0.1 mm. The class size is determined by the resolution of precipitation measurement in the available observational dataset.

#### Percentiles

Percentiles or Quantiles, as well as their special cases Quartile and Median, are values limiting subsets of the data sample. The 95-percentiles calculated, are therefore the values greater than or equals to 95% of all values in the respective dataset. Percentiles are a common measure in extreme value statistics (Schönwiese (2006)) and as such used to asses the ability of RCM to reproduce heavy rainfall events.

#### Kolmogorow-Smirnow Test

The Kolmogorov-Smirnow test is a simple measure of similarity of two CDF and defined as the maximum value of the absolute difference between both. The Kolmogorov-Smirnow value $D$ is formally defined as:

$$D = max\ |C_{N1}(x) - C_{N2}(x)| \tag{2.12}$$

where $C_{N1}(x)$ and $C_{N2}(x)$ denote two different cumulative distributions functions (Wilks (2006)). Two datasets are considered to be drawn from the same distribution if the null-hypothesis is not rejected at a certain significance level $\alpha$, thus if:

$$D < \left[\frac{1}{2}\left(\frac{1}{n_1} + \frac{1}{n_2}\right) ln\left(\frac{\alpha}{2}\right)\right]^{\frac{1}{2}} \tag{2.13}$$

where $n_1$ and $n_2$ are the sample sizes of both datasets in comparison (Wilks (2006)).

### 2.6.3 Spatial Statistics

A number of interpolation schemes have been used in order to link climate model data to the hydrological model mHM. General principles and/or formulations are given in the following subsections and can be found in most textbooks on spatial statistics (e.g. Webster and Oliver (2007), Hengl (2007), Wackernagel (1995)).

#### Nearest Neighbour Search

In a Nearest Neighbour Search the unknown value of a variable $z$ at any position $x_0$ is set to the known value of $z'$ at a position $x_1$, where $x_1$ is the point out of $N$ observations in the dataset with a minimal distance to $x_0$.

$$z'(x_0) = z(x_1) \tag{2.14}$$

with

$$x_1 = min(d(x_0, x_i)\ \forall i \in N) \tag{2.15}$$

$d(x_0, x_i)$ denotes the distance between the points $x_0$ and $x_1$.

#### Inverse Distance Weighting

The spatial prediction technique Inverse Distance Weighting is described as a exact and convex spatial interpolation method (Hengl (2007)). The unknown value of a variable $z'$ at any location $x_0$ is given as:

$$z'(x_0) = \sum_{i=1}^{n} \lambda_i z(x_i) \tag{2.16}$$

where $\lambda_i$ denote the weighting factors for known values $z$ at locations $x_i$. The weighting factors $\lambda_i$ are estimated as a function of the inverse distance between any given location and the point in question:

$$\lambda_i(x_o) = \frac{\frac{1}{d(x_0,x_i)^\beta}}{\sum_{j=1}^{n} \frac{1}{d(x_0,x_j)^\beta}} \tag{2.17}$$

where $d(x_o, x_i)$ and $d(x_0, x_j)$ denote the distances between searched and known points, $\beta$ is an arbitrary power parameter adjusting weights. The relative weight of distance points will decrease with higher values of $\beta$ (Hengl (2007)). For all interpolation purposes within this work $\beta = 2$ and the absolute distance within points are included into the interpolation procedure was set to $d_{max} = 30000$ meters.

### External Drift Kriging

External Drift Kriging is an non stationary spatial interpolation technique. As with many other procedures spatial predictions are made as the weighted sum of neighbouring values (equation eq:IDW). In Ordinary Kriging the problem of weighting is solved by determining the differences between points mathematically; semivariances are plotted against distance in an experimental variogram from which an theoretical one is fitted. With the fitted variogram model the kriging weights can be solved. External Drift Kriging further sophisticates this approach as related auxiliary predictors are included into the computation of weights. The interpolation is therefore no longer only a function of the distance separating points rather then incorporating additional available spatial information. For more details on the procedure refer to the above mentioned literature, a concrete example using External Drift Kriging for the interpolation of meteorological data can be found in Samaniego (2003).

## 2.7 Data and Model Preprocessing

In order to run the hydrological model mHM with regional climate model (RCM) output, a number of preprocessing steps are necessary. After downloading the data from the ENSEMBLES-Project homepage, the files, each covering whole Europe and a period of 10 years were spatially cut and temporarily merged. Bias correction (subsection 2.3) was applied on this processing level, on the native grid defined by the respective RCM. Climate normals freely available from the homepage of the german meteorological service (DWD) were interpolated to the RCM grid resolution by the Inverse Distance Weighting (IDW) method (subsection 2.6.3). After correcting precipitation, all datasets were resampled to the mHM modelling grid using the nearest neighbour technique (subsection 2.6.3). A slight horizontal downscaling from 25 km to 24 km was not avoidable as mHM only accepts meteorological input data resolutions as a multiple of the modelling scale (i.e. 4 km). With the resampled data potential evaporation was calculated (subsection 2.5.3) and all files are converted from the NetCDF format in which they were provided (http://www.unidata.ucar.edu/software/netcdf) into the mHM native 4-byte floating point binary format. All these data preprocessing steps were done using the open source programming language Python (http://python.org), its standard library and the external modules numpy (http://numpy.scipy.org) for effective matrix manipulation and processing, scikits.timeseries (http://pytseries.sourceforge.net) for timeseries data handling, pyproj for map projection transformations (http://code.google.com/p/pyproj) and matplotlib (http://matplotlib.sourceforge.net) for plotting purposes. As the mHM structure uses explicit dates for input data handling in addition a FORTRAN 2003 subroutine was implemented to allow the processing of data provided in the 360-day calendar.

# 3 Climate Model Data

No matter how sophisticated and complex state-of-the-art climate models are, they still lack of a number of shortcomings leading to biased model results (e.g. Jacob et al. (2007), Christensen et al. (2008)). Biases can be found in all output variables, but are normally highest for precipitation. Reasons for the often poor representation of this hydrological important parameter are complex, but most likely a result of the coarse model resolutions and the difficulties to parametrise precipitation dynamics (Huang et al. (2010)). On the following pages a detailed evaluation of climate model performance and projected climatological changes are presented.

## 3.1 Model Evaluation

Two different studies evaluating the Regional Climate Model (RCM) runs realised in the ENSEMBLES-Project framework quantified model biases. In a comprehensive study Christensen et al. (2008) analysed biases over the whole modelling domain (i.e. Europe). The authors proved that three of the four models also used in the study on hand, tend to underestimated precipitation but to overestimated temperatures in the 1961-1990 control period, whereas the model ICTP-REGCM showed the opposite pattern. A more local study evaluating the performance of ENSEMBLES RCM data for the Rhine River basin was carried out by Hanel and Buishand (2011). All models also analysed on the following pages clearly overestimated river basin average precipitation in the 1961-1990 control period. Mean summer rainfall amounts were underestimated by the models ETHZ-CLM and HadRM3Q0 but overvalued by ICTP-REGCM and MPI-M-REMO and all RCM overestimated winter precipitation.

To evaluate climate model performance within the area of the Saale watershed, a number of figures and tables are presented in the following sections. All tabulated biases are calculated as relative deviations from gridded observational weather station data. The diverging coordinate systems were homogenised by resampling the RCM data to the hydrological model input grid with 24 km resolution using a Nearest Neighbour Search (see section 2.6.3). In order to equalise the different spatial discretization of 4 km an 24 km, the interpolated observational dataset was aggregated to the coarser RCM resolution by averaging the 36 cells within one RCM grid box. As the observational database was only available within the exact boarders of the Saale catchment, only these, after aggregation,

63 cells were selected from the RCM as well.

### 3.1.1 Precipitation

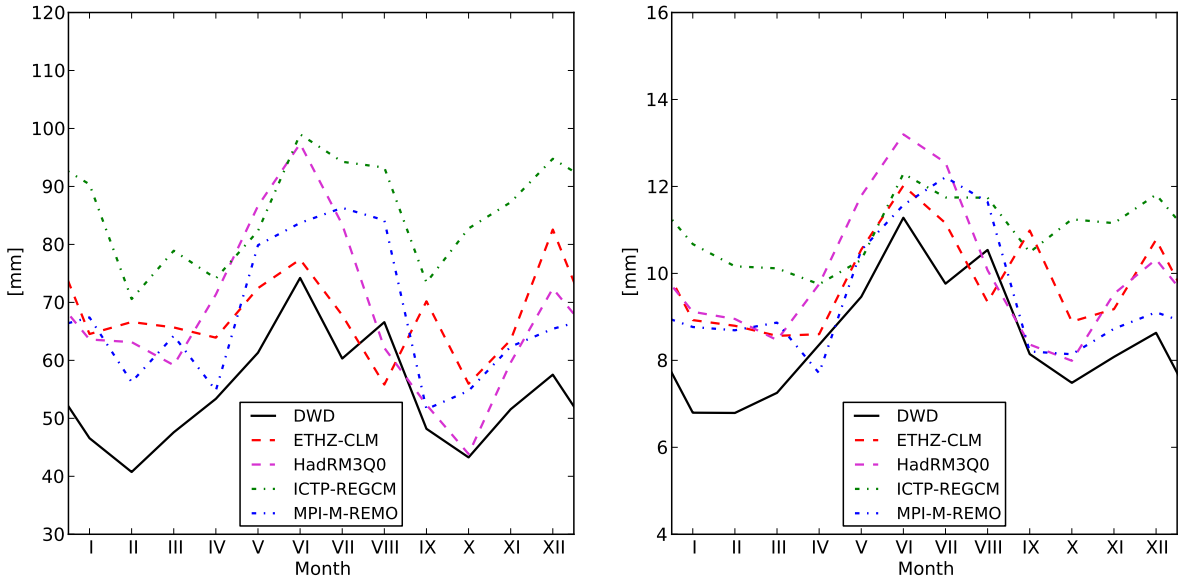


Figure 3.1: Monthly precipitation sums (l) and 95-percentiles of daily precipitation sums (r), 1961-1990.

The performance of RCM in representing precipitation is assessed using 30-year averages of monthly and seasonal rainfall amounts and the respective 95-percentiles. The latter ones are calculated month-wise from all daily precipitation sums available, i.e. including the zero precipitation events, in the thirty year period, and are subsequently averaged to obtain the seasonal or yearly values. The left hand side of figure 3.1 indicates that all models clearly overestimate precipitation throughout the entire year, but with higher biases during winter. Even on the monthly scale negative biases are restricted to one month, August, and two models, ETHZ-CLM and HadRM3Q0, both driven by the HadCM Global Circulation Model (GCM). In contrast to the results of Hanel and Buishand (2011), where exactly these two models showed negative biases for the entire summer season, the overall seasonal precipitation balance for the Saale Catchment is still positive. Not only the total monthly, seasonal and annual precipitation amounts exceed the measurements considerably (table 3.1), but also the annual cycle is only poorly represented. While the climate of the study area is characterised by a precipitation peak in summer and relatively low values in autumn and winter, only the models HadRM3Q0 and MPI-M-REMO, both nested into different GCM, could at least roughly fit this inter-annual variability. The remaining models either show only slight seasonal variance and comparable high values throughout the entire year (ICTP-REGCM) or even suggest

higher amounts during other seasons (ETHZ-CLM).

Table 3.1: Seasonal precipitation sums $\sum$ [mm] and biases [%], 1961-1990.

| | Winter | | Spring | | Summer | | Autumn | | Year | |
|---|---|---|---|---|---|---|---|---|---|---|
| | $\sum$ | bias | $\sum$ | bias | $\sum$ | bias | $\sum$ | bias | $\sum$ | bias |
| DWD | 146 | - | 161 | - | 201 | - | 144 | - | 651 | - |
| ETHZ-CLM | 216 | 49 | 204 | 26 | 202 | 1 | 189 | 32 | 811 | 24 |
| HadRM3Q0 | 200 | 38 | 217 | 34 | 241 | 20 | 158 | 10 | 816 | 25 |
| ICTP-REGCM | 257 | 78 | 238 | 47 | 283 | 41 | 243 | 70 | 1021 | 57 |
| MPI-M-REM0 | 192 | 32 | 199 | 23 | 252 | 25 | 167 | 17 | 810 | 24 |

The right hand side of figure 3.1 and table 3.2 indicate that all RCM fit the 95-percentiles of observational data better than monthly or seasonal sums. Although all models tend to overestimate winter values, especially summer heavy rainfall activity seems to be fairly well represented.

Table 3.2: Seasonally averaged 95-percentiles of daily precipitation sums [mm] and biases [%], uncorrected Climate Model data, 1961-1990.

| | Winter | | Spring | | Summer | | Autumn | | Year | |
|---|---|---|---|---|---|---|---|---|---|---|
| | p95 | bias | p95 | bias | p95 | bias | p95 | bias | p95 | bias |
| DWD | 6.5 | - | 7.3 | - | 9.2 | - | 6.8 | - | 7.4 | - |
| ETHZ-CLM | 8.5 | 31 | 8.2 | 12 | 9.3 | 1 | 8.5 | 25 | 8.6 | 16 |
| HadRM3Q0 | 8.4 | 30 | 8.8 | 21 | 10.5 | 14 | 7.5 | 10 | 8.8 | 19 |
| ICTP-REGCM | 9.9 | 52 | 9.0 | 23 | 10.6 | 15 | 9.8 | 44 | 9.8 | 32 |
| MPI-M-REM0 | 7.9 | 22 | 8.1 | 11 | 10.5 | 14 | 7.4 | 9 | 8.5 | 15 |

Figure 3.2 shows seasonal empirical cumulative distribution functions (CDF) of daily precipitation values, table 3.3 the corresponding Kolmogorov–Smirnov (K-S) values (subsection 2.6.2). The differences between the functions are quite striking, at the 5% significance level the statistical null hypothesis, i.e. the hypothesis that both samples are drawn from the same continuous distribution, has to be rejected for all models and seasons. Biases vary somehow accidentally, but models commonly underestimate the number of dry days, especially in summer. The HadCM models achieve best seasonal fits to observational data, ETHZ-CLM in summer (K-S: 0.07) and HadRM3Q0 in autumn (K-S: 0.06). Percentiles are mostly shifted towards higher precipitation amounts but deviations decrease towards the upper end of the CDF.

Table 3.3: Seasonal Kolmogorov–Smirnov test statistic values, uncorrected Climate Model data, 1961-1990.

| | Winter | Spring | Summer | Autumn |
|---|---|---|---|---|
| ETHZ-CLM | 0.16 | 0.15 | 0.07 | 0.09 |
| HadRM3Q0 | 0.1 | 0.15 | 0.09 | 0.06 |
| ICTP-REGCM | 0.2 | 0.19 | 0.23 | 0.22 |
| MPI-M-REM0 | 0.11 | 0.12 | 0.15 | 0.09 |

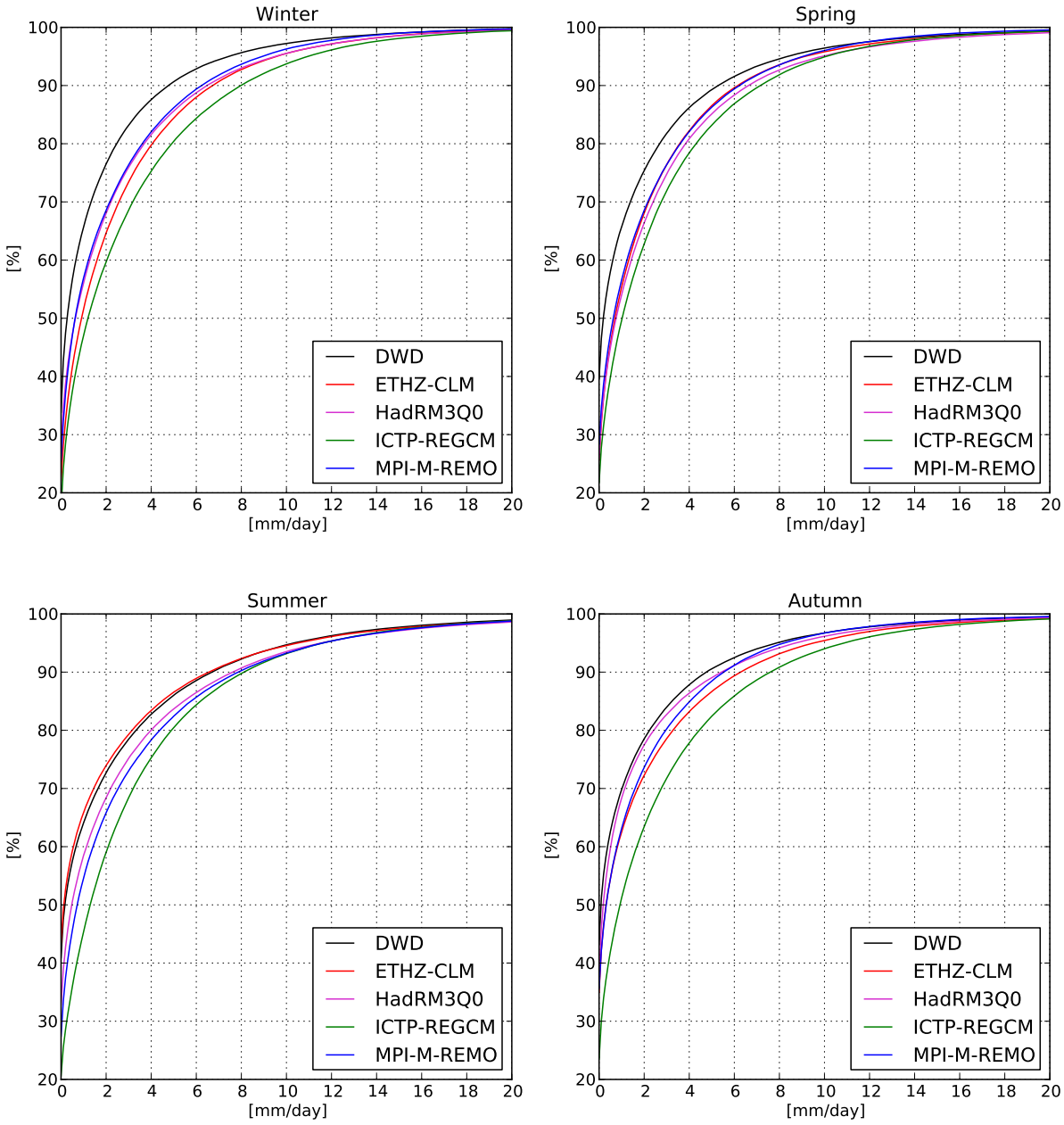


Figure 3.2: Cumulative seasonal frequency distributions of bias corrected daily precipitation sums, 1961-1990.

### 3.1.2 Temperature

With respect to temperature the models perform much better (left hand side of figure 3.3 and table 3.4). The remaining bias, ranging from -0.2° K to 0.9° K are controlled by driving GCM. The annual temperature curves for the HadCM driven models ETHZ-CLM and HadRM3Q0 are largely identical. Both models overvalue temperatures in summer and underestimate temperatures during the rest of the year, summing up to average biases about zero. The ECHAM5/MPI-OM driven RCM indeed delimit the span of model biases at the lower and the upper end. The temperature curved diverge until July before gradually converging until December, but show anyhow a remarkable analogy in their yearly cycles. Both models are too warm in winter, as MPI-M-REMO also is during spring and autumn. ICTP-REGCM produces underestimates temperatures during the rest of the year.

Table 3.4: Seasonal mean temperatures ∅ [°C] and biases [°K], 1961-1990.

| | Winter | | Spring | | Summer | | Autumn | | Year | |
|---|---|---|---|---|---|---|---|---|---|---|
| | ∅ | bias | ∅ | bias | ∅ | bias | ∅ | bias | ∅ | bias |
| DWD | -0.8 | - | 6.8 | - | 15.6 | - | 8.0 | - | 7.5 | - |
| ETHZ-CLM | -0.9 | -0.1 | 6.0 | -0.8 | 17.3 | 1.7 | 7.7 | -0.3 | 7.5 | 0 |
| HadRM3Q0 | -0.7 | 0.1 | 6.4 | -0.4 | 17.5 | 1.9 | 8.0 | 0 | 7.8 | 0.3 |
| ICTP-REGCM | 0.6 | 1.4 | 6.3 | -0.5 | 14.1 | -1.5 | 7.8 | -0.2 | 7.3 | -0.2 |
| MPI-M-REM0 | 0.7 | 1.5 | 8.0 | 1.2 | 15.9 | 0.3 | 9.1 | 1.1 | 8.4 | 0.9 |

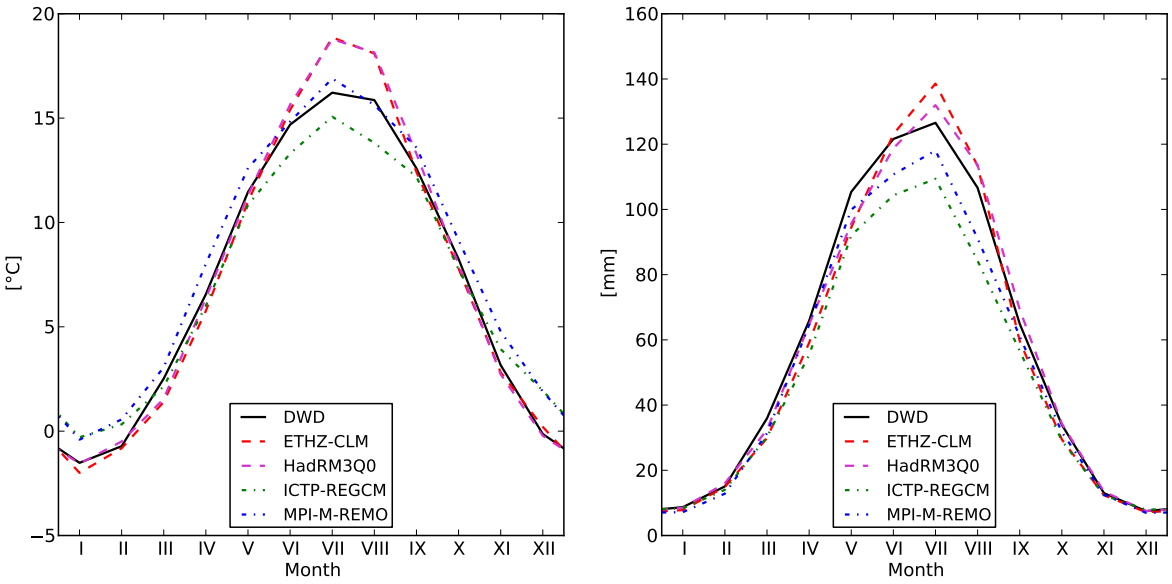


Figure 3.3: Monthly mean temperatures (l) and monthly potential evaporation sums (r), 1961-1990.

### 3.1.3 Potential Evaporation

Potential evaporation (PET), here a function of geographical position and daily maximum and minimum temperatures (see subsection 2.5.3), is mainly controlled by summer temperatures (right hand side of figure 3.3). While the monthly evaporation sums are roughly identical during winter, spring and autumn, basically unaffected of temperature differences, even small variations during summer lead to considerably altered PET rates. Yearly model biases range from -3% to 0% in the HadCM and from -8% to -14% in the ECHAM5/MPI-OM driven RCM. Deviations between the yearly averages calculated from observational and modelled climate data are rather small. The comparison to precipitation totals reveals in turn major differences, as PET exceeds the total yearly rainfall amount for observational but not for RCM data. The relative biases given in table 3.5 can be misleading, as absolute values for winter, spring and autumn are rather low.

Table 3.5: Seasonal potential evaporation sums $\sum$ [mm] and biases [%], 1961-1990.

| | Winter | | Spring | | Summer | | Autumn | | Year | |
|---|---|---|---|---|---|---|---|---|---|---|
| | $\sum$ | bias | $\sum$ | bias | $\sum$ | bias | $\sum$ | bias | $\sum$ | bias |
| DWD | 31 | - | 207 | - | 355 | - | 112 | - | 705 | - |
| ETHZ-CLM | 30 | -3 | 183 | -12 | 371 | 5 | 102 | -9 | 685 | -3 |
| HadRM3Q0 | 32 | 2 | 193 | -7 | 364 | 3 | 117 | 5 | 706 | 0 |
| ICTP-REGCM | 30 | -3 | 178 | -14 | 299 | -16 | 97 | -13 | 604 | -14 |
| MPI-M-REM0 | 27 | -13 | 197 | -5 | 321 | -9 | 104 | -7 | 649 | -8 |

## 3.2 Validation of Bias Correction

The bias correction of climate model data (section 2.3) does change daily precipitation sums and their variability in time and space considerably. For the period the correction factors where calculated, 1961-1990, the monthly sums and their annual cycles, are adjusted (figure 3.4 and table 3.6). The remaining deviations from observational data are rather low and a relict of the data homogenisation. In order to asses the effects of bias correction in a time-slice not entirely covered by the correction period, figure 3.5 opposes monthly mean precipitation sums from uncorrected and corrected datasets for the years 1980-2009, table 3.7 lists the corresponding seasonal values.

Table 3.6: Seasonal precipitation sums $\sum$ [mm] and biases [%], 1961-1990, bias corrected climate model data.

| | Winter | | Spring | | Summer | | Autumn | | Year | |
|---|---|---|---|---|---|---|---|---|---|---|
| | $\sum$ | bias | $\sum$ | bias | $\sum$ | bias | $\sum$ | bias | $\sum$ | bias |
| DWD | 146 | - | 161 | - | 201 | - | 144 | - | 651 | - |
| ETHZ-CLM | 155 | 7 | 170 | 5 | 210 | 4 | 154 | 8 | 689 | 6 |
| HadRM3Q0 | 155 | 7 | 173 | 7 | 213 | 6 | 151 | 6 | 692 | 6 |
| ICTP-REGCM | 159 | 10 | 168 | 4 | 211 | 5 | 154 | 8 | 693 | 6 |
| MPI-M-REM0 | 150 | 3 | 166 | 2 | 206 | 2 | 149 | 4 | 670 | 3 |

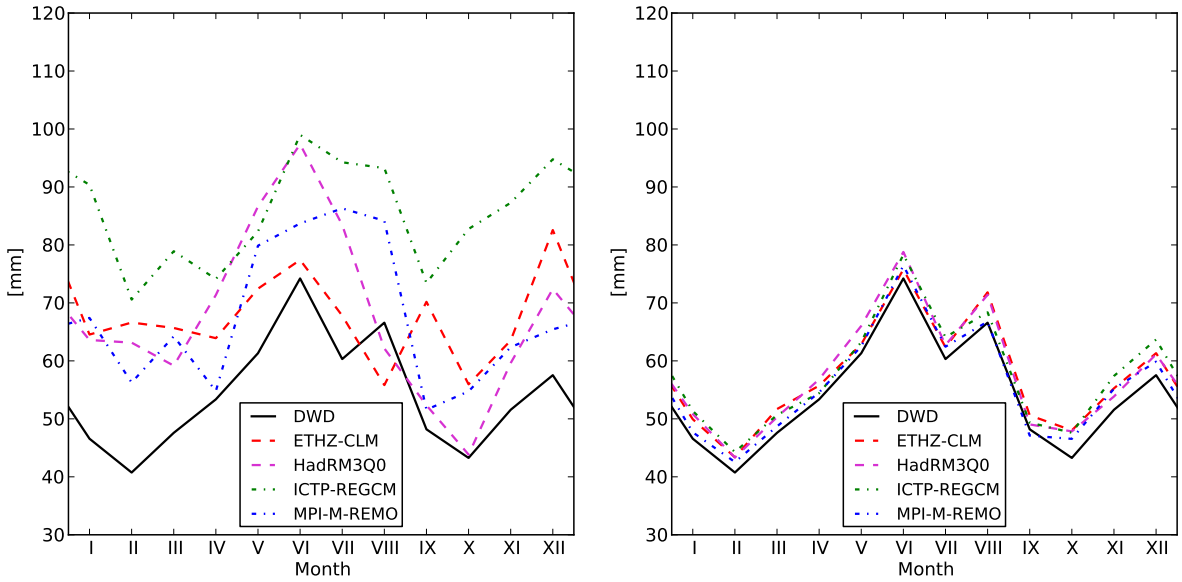


Figure 3.4: Monthly precipitation sums of uncorrected (l) and bias corrected (r) Climate Model data, 1961-1990.

Table 3.7: Seasonal precipitation sums $\sum$ [mm] and biases [%], 1980-2009.

| | Winter | | Spring | | Summer | | Autumn | | Year | |
|---|---|---|---|---|---|---|---|---|---|---|
| | $\sum$ | bias | $\sum$ | bias | $\sum$ | bias | $\sum$ | bias | $\sum$ | bias |
| DWD | 156 | - | 162 | - | 203 | - | 160 | - | 681 | - |
| *not corrected* | | | | | | | | | | |
| ETHZ-CLM | 213 | 37 | 210 | 30 | 218 | 7 | 215 | 34 | 856 | 26 |
| HadRM3Q0 | 192 | 23 | 224 | 38 | 263 | 30 | 160 | 0 | 838 | 23 |
| ICTP-REGCM | 252 | 62 | 225 | 39 | 283 | 39 | 243 | 52 | 1003 | 47 |
| MPI-M-REM0 | 190 | 22 | 187 | 15 | 249 | 23 | 174 | 9 | 800 | 17 |
| *bias corrected* | | | | | | | | | | |
| ETHZ-CLM | 154 | -1 | 177 | 9 | 230 | 13 | 174 | 9 | 736 | 8 |
| HadRM3Q0 | 149 | -4 | 179 | 10 | 231 | 14 | 155 | -3 | 714 | 5 |
| ICTP-REGCM | 156 | 0 | 161 | -1 | 208 | 2 | 154 | -4 | 679 | 0 |
| MPI-M-REM0 | 151 | -3 | 156 | -4 | 200 | -1 | 154 | -4 | 661 | -3 |

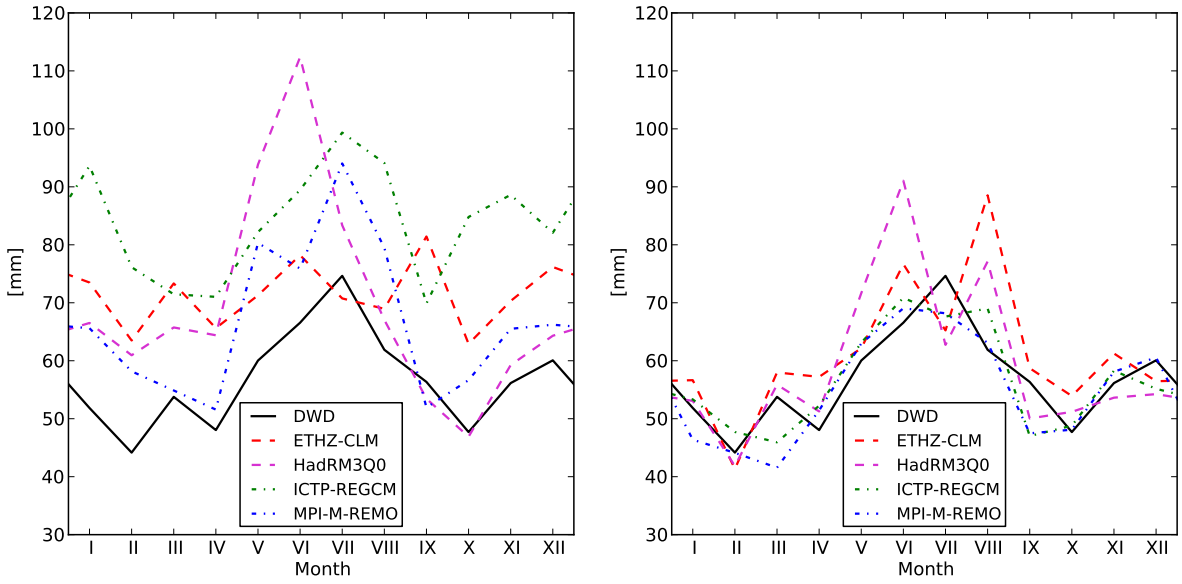


Figure 3.5: Monthly precipitation sums of uncorrected (l) and bias corrected (r) Climate Model data, 1980-2009.

In the 1980-2009 period RCM data characteristics is largely comparable to the 1961-1990 period. Precipitation is generally overestimated and the yearly variability is not or only roughly represented (figure 3.5). The bias corrected datasets are much closer to observation (table 3.7), but longterm stability of the correction depends on driving GCM. The ECHAM5/MPI-OM models deviate only slightly, whereas the bias corrected HadCM models overestimate precipitation, especially in summer. The RCM climate dynamics is obviously able to counteract the intended correction. Although the seasonal biases are

not excessively large, they point to the fact, that the assumption of temporarily stable biases in climate model output is not necessarily fulfilled.

Table 3.8: Seasonally averaged 95-percentiles of daily precipitation sums [mm] and biases [%], 1961-1990.

| | Winter | | Spring | | Summer | | Autumn | | Year | |
|---|---|---|---|---|---|---|---|---|---|---|
| | p95 | bias | p95 | bias | p95 | bias | p95 | bias | p95 | bias |
| DWD | 6.5 | - | 7.3 | - | 9.2 | - | 6.8 | - | 7.4 | - |
| *not corrected* | | | | | | | | | | |
| ETHZ-CLM | 8.5 | 31 | 8.2 | 12 | 9.3 | 1 | 8.5 | 25 | 8.6 | 16 |
| HadRM3Q0 | 8.4 | 30 | 8.8 | 21 | 10.5 | 14 | 7.5 | 10 | 8.8 | 19 |
| ICTP-REGCM | 9.9 | 52 | 9.0 | 23 | 10.6 | 15 | 9.8 | 44 | 9.8 | 32 |
| MPI-M-REM0 | 7.9 | 22 | 8.1 | 11 | 10.5 | 14 | 7.4 | 9 | 8.5 | 15 |
| *bias corrected* | | | | | | | | | | |
| ETHZ-CLM | 6.2 | -5 | 6.9 | -6 | 9.7 | 5 | 6.9 | 2 | 7.4 | 0 |
| HadRM3Q0 | 6.6 | 2 | 7.0 | -4 | 9.3 | 1 | 7.3 | 7 | 7.5 | 1 |
| ICTP-REGCM | 6.2 | -5 | 6.5 | -11 | 7.8 | -15 | 6.2 | -9 | 6.7 | -10 |
| MPI-M-REM0 | 6.3 | -3 | 6.7 | -8 | 8.4 | -9 | 6.5 | -5 | 7.0 | -5 |

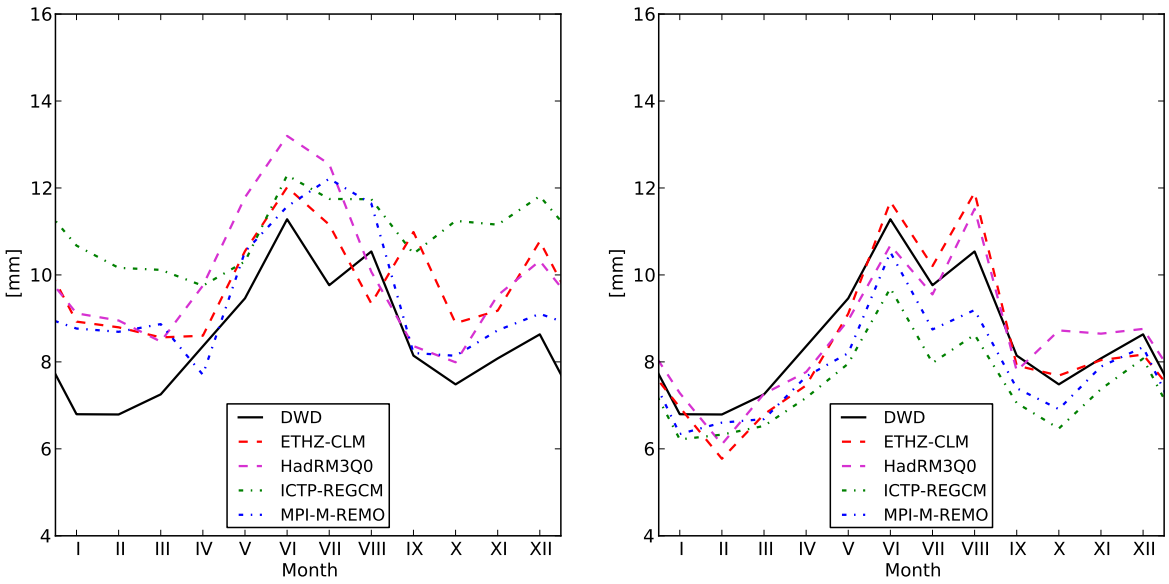


Figure 3.6: Averaged 95-percentiles of uncorrected (l) and bias corrected (r) daily precipitation sums, 1961-1990.

Figure 3.6 and table 3.8 indicate that the correction of monthly precipitation sums does not intrinsically optimise all moments of the distribution equally. 95-percentile biases are clearly reduced in the HadCM driven models with a tendency to underestimate observation

in the first and to overestimate it in the second half of the year. The ECHAM5/MPI-OM RCM biases are larger and in any case negative. In the 1980-2009 period the differences between both RCM groups are larger. Biases of ETHZ-CLM and HadRM3Q0 are reduced to good yearly fits, positive deviations are only found in summer but winter percentiles are represented poorly (figure 3.7, table 3.9). The deviations from observational data are again always negative for the ECHAM5/MPI-OM models. MPI-M-REMO output deviates after bias correction even slightly more than before.

Table 3.9: Seasonally averaged 95-percentiles of daily precipitation sums [mm] and biases [%], 1980-2009.

| | Winter | | Spring | | Summer | | Autumn | | Year | |
|---|---|---|---|---|---|---|---|---|---|---|
| | p95 | bias | p95 | bias | p95 | bias | p95 | bias | p95 | bias |
| DWD | 7.0 | - | 7.5 | - | 9.1 | - | 7.6 | - | 7.8 | - |
| *not corrected* | | | | | | | | | | |
| ETHZ-CLM | 8.5 | 21 | 8.5 | 13 | 10.0 | 10 | 9.6 | 26 | 9.1 | 16 |
| HadRM3Q0 | 8.1 | 16 | 9.1 | 21 | 11.0 | 21 | 7.6 | 0 | 8.9 | 14 |
| ICTP-REGCM | 9.7 | 39 | 8.7 | 16 | 10.5 | 14 | 10.1 | 33 | 9.8 | 26 |
| MPI-M-REM0 | 7.9 | 13 | 7.8 | 4 | 10.4 | 14 | 7.8 | 3 | 8.5 | 9 |
| *bias corrected* | | | | | | | | | | |
| ETHZ-CLM | 6.1 | -13 | 7.2 | -4 | 10.5 | 15 | 7.7 | -1 | 7.9 | 1 |
| HadRM3Q0 | 6.3 | -10 | 7.2 | -4 | 9.7 | 7 | 7.4 | -3 | 7.7 | -1 |
| ICTP-REGCM | 6.0 | -14 | 6.3 | -16 | 7.7 | -14 | 6.4 | -16 | 6.6 | -15 |
| MPI-M-REM0 | 6.3 | -10 | 6.5 | -13 | 8.2 | -10 | 6.9 | -9 | 7.0 | -10 |

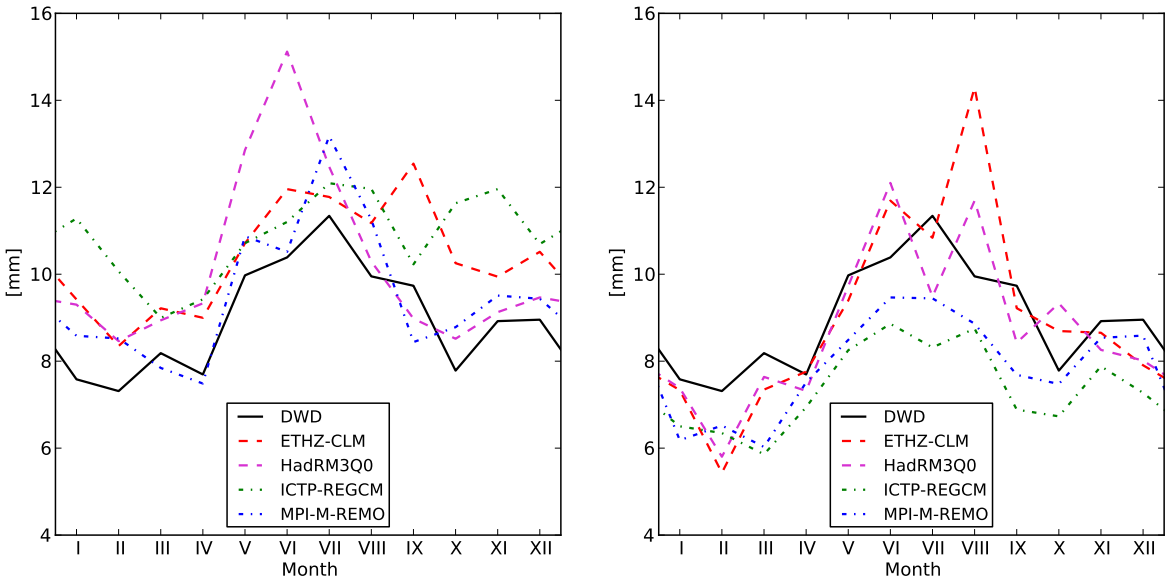


Figure 3.7: Averaged 95-percentiles of uncorrected (l) and bias corrected (r) daily precipitation sums, 1980-2009.

Figure 3.8 shows the empirical cumulative distribution functions (CDF) of seasonally aggregated, bias corrected, daily precipitation sums. The fitting has improved for all seasons and models compared to uncorrected data, but the selective impact of the method becomes apparent. The procedure, a single multiplication, does not alter the general dichotomy of dry and rain days in the datasets. values at the upper extreme are therefore disproportionally reduced to fit the total sums to observation. The mostly sharp intersections of all CDF, located between the 80- and the 90-percentile and 4 to 5 mm/d, indicate the described effect. The transition marks the shift from overestimation of low precipitation events to the correction induced underestimation of large rainfall amounts. Tabulated Kolmogorov–Smirnov values (table 3.10) do not directly reflect the improved fittings and reveal only slight differences between corrected and uncorrected RCM data. The differences in number of dry days, obviously close to the maximum differences between the CDF from observational and uncorrected climate model data, determine the K-S values. No clear pattern of how modelled CDF fit observed seasonal distributions is found, the HadCM based models show largest K-S values for spring, the ECHAM5/ MPI-OM nested RCM for summer. Lowest values are distributed almost equally over all seasons.

Table 3.10: Seasonal Kolmogorov–Smirnov test statistic values, bias corrected Climate Model data, 1961-1990.

| | Winter | Spring | Summer | Autumn |
|---|---|---|---|---|
| ETHZ-CLM | 0.12 | 0.14 | 0.07 | 0.08 |
| HadRM3Q0 | 0.06 | 0.13 | 0.09 | 0.05 |
| ICTP-REGCM | 0.15 | 0.17 | 0.21 | 0.18 |
| MPI-M-REM0 | 0.09 | 0.11 | 0.13 | 0.08 |

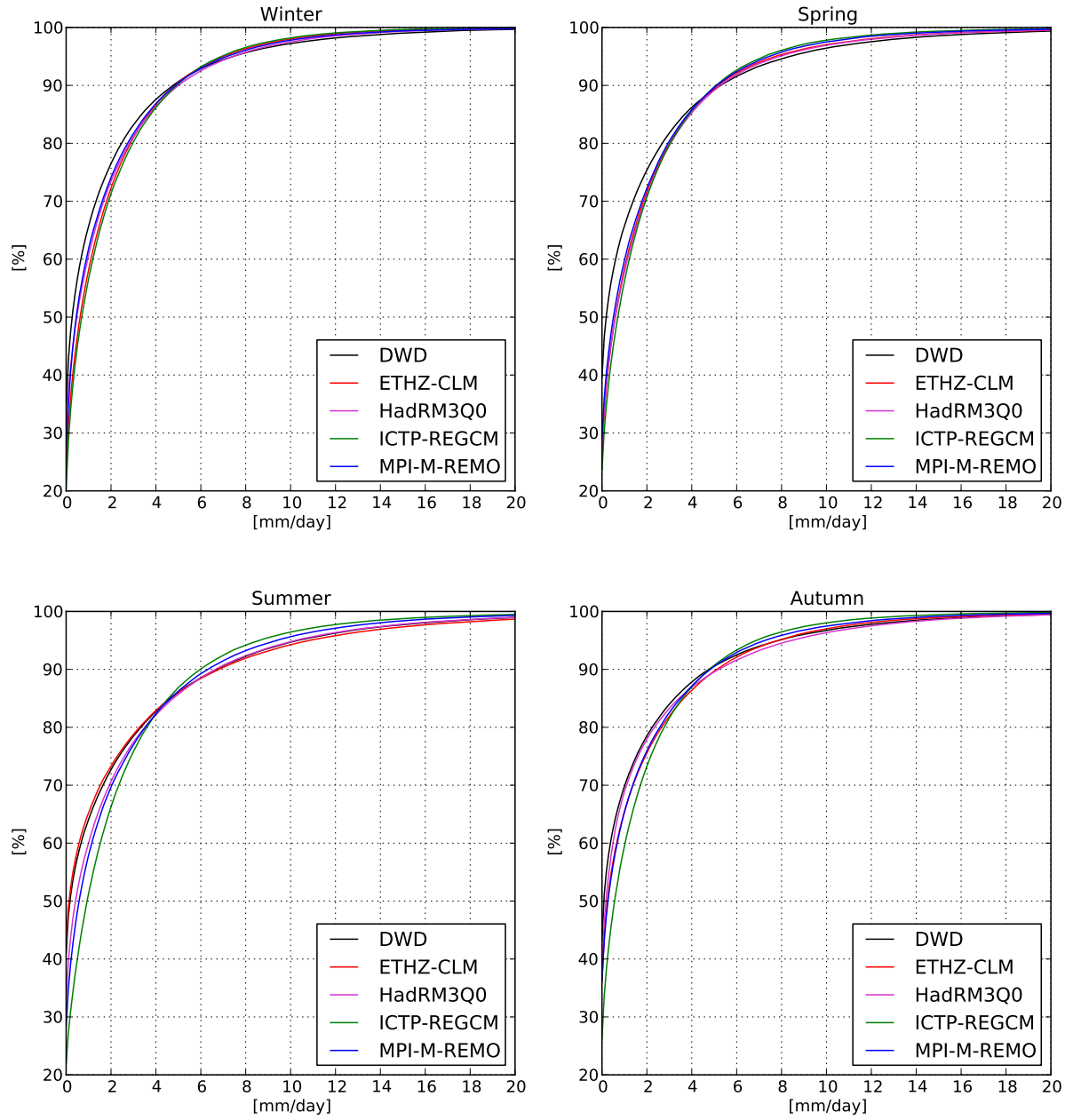


Figure 3.8: Cumulative seasonal frequency distributions of bias corrected daily precipitation sums, 1961-1990.

Three conclusions can be drawn from the results presented on the previous pages:

1. The bias correction applied is able to approximate a given model variable (i.e. longterm averages of monthly precipitation sums) to observational data.

2. A correction based on any one statistical parameter, does not necessarily adjust other comparably well.

3. The effects of bias correction are in circumstances temporarily limited as model dynamics may counteract the intended adjustments.

## 3.3 Projected Climate Change

All remarks about climate model data made hitherto where focused on model performance with respect to past climate. The evaluation against measurements does deliver import information about the ability of the models to adequately reproduce the climatic system. The intrinsic motivation in climate modelling is anyhow the projection of future climate trends and changes to be expected. As alterations in the variables precipitation and temperature most likely enforce an hydrological response, possible climate changes (i.e. changes in precipitation and temperature) for the two scenario periods 2011-2040 and 2061-2090 are examined and presented in the following subsections. Relative or absolute changes are all calculated from differences between the longterm average values of the corresponding time-slice and the reference period 1961-1990.

### 3.3.1 Temperature

All models project raising temperatures as shown in figure 3.9 and the table 3.11. A grouping of the RCM by driving GCM can be stated. The models MPI-M-REM0 and ICTP-REGCM project a raise of yearly mean temperatures of 0.9° K and 0.8° K for the 2011-2040 and 2.5° K and 2.6° K for the 2061-2090 time-slice, respectively. The nearly identical changes of monthly mean temperatures are striking. In the 2011-2040 scenario time-slice MPI-M-REM0 projects maximum temperature differences for autumn (1.2° K), ICTP-REGCM for spring (0.9° K). Both models project minimum temperature differences for winter (0.6° K and 0.5° K). In the 2061-2090 period minimal warming is projected for spring (1.9° K and 2.1° K), highest for winter (2.9° K each). The HadCM driven models, ETHZ-CLM and HadRM3Q0, represent a less stable temperature regime. Changes are in general higher (2011-2040: 1.5° K and 1.8° K, 2061-2090: 3.3° K and 3.9° K) and although main warming trends are comparable, monthly values deviate discernible. For the first half of the century both RCM project highest temperature increases for winter (2° K and 2.2° K), especially predicted January temperature changes are twice as high as the yearly mean, and lowest for spring (ETHZ-CLM, 1.2° K) or autumn (HadRM3Q0, 1.4° K). The warming peak is shifted into autumn in the second scenario period (3.8° K and 4.2° K), lowest temperature change is projected for spring (2.4° K and 3.4° K).

Table 3.11: Seasonal mean temperatures ⌀ [°C] and changes Δ [°K] since 1961-1990. DJF: Winter, MAM: Spring, JJA: Summer, SON: Autumn.

| | Winter | | Spring | | Summer | | Autumn | | Year | |
|---|---|---|---|---|---|---|---|---|---|---|
| *2011-2040* | ⌀ | Δ | ⌀ | Δ | ⌀ | Δ | ⌀ | Δ | ⌀ | Δ |
| ETHZ-CLM | 1.2 | 2 | 7.3 | 1.2 | 18.8 | 1.4 | 9.2 | 1.5 | 9.1 | 1.5 |
| HadRM3Q0 | 1.5 | 2.2 | 8.3 | 1.9 | 19.3 | 1.8 | 9.5 | 1.4 | 9.6 | 1.8 |
| ICTP-REGCM | 1.2 | 0.5 | 7.4 | 1 | 15.1 | 0.9 | 8.8 | 0.9 | 8.1 | 0.8 |
| MPI-M-REM0 | 1.3 | 0.6 | 8.9 | 0.9 | 16.9 | 1 | 10.3 | 1.2 | 9.4 | 0.9 |
| *2061-2090* | | | | | | | | | | |
| ETHZ-CLM | 2.8 | 3.6 | 8.5 | 2.4 | 20.8 | 3.4 | 11.5 | 3.8 | 10.9 | 3.3 |
| HadRM3Q0 | 3.2 | 3.9 | 9.8 | 3.4 | 21.6 | 4.1 | 12.3 | 4.2 | 11.7 | 3.9 |
| ICTP-REGCM | 3.6 | 2.9 | 8.5 | 2.1 | 16.9 | 2.7 | 10.6 | 2.7 | 9.9 | 2.6 |
| MPI-M-REM0 | 3.6 | 2.9 | 9.9 | 1.9 | 18.5 | 2.6 | 11.9 | 2.8 | 11 | 2.5 |

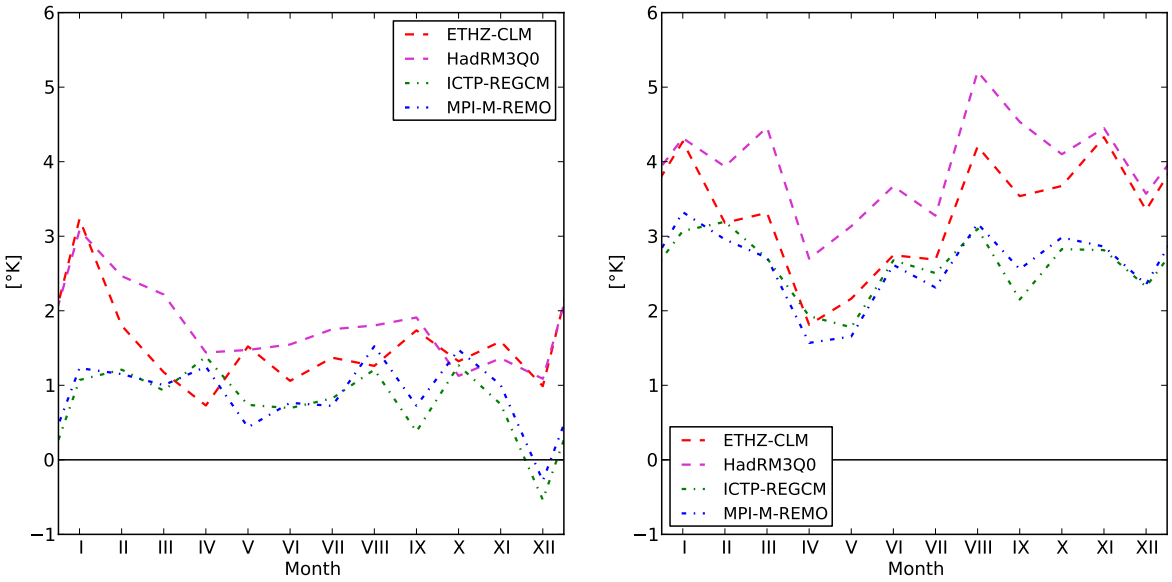


Figure 3.9: Changes of monthly mean temperatures [°K] between 1961-1990 and 2011-2040 (l), 1961-1990 and 2061-2090 (r).

## 3.3.2 Precipitation

The figures 3.10, 3.11 and 3.12, 3.13 depict the relative changes to the 1961-1990 control period of the selected statistical parameters, longterm monthly and 95-percentiles of daily precipitation sums, for the time-slices 2011-2040 and 2061-2090. The single figures each oppose uncorrected and bias corrected climate model data for any one period, the corresponding values are given in the tables 3.12 and 3.13.

Table 3.12: Changes in seasonal precipitation sums [%] since 1961-1990. DJF: Winter, MAM: Spring, JJA: Summer, SON: Autumn.

| | 2011-2040 | | | | | 2061-2090 | | | | |
|---|---|---|---|---|---|---|---|---|---|---|
| *not corrected* | DJF | MAM | JJA | SON | Year | DJF | MAM | JJA | SON | Year |
| ETHZ-CLM | 10 | -3 | 5 | 2 | 4 | 19 | 1 | -8 | -4 | 3 |
| HadRM3Q0 | 6 | 0 | 2 | 10 | 4 | 13 | 8 | -11 | 3 | 3 |
| ICTP-REGCM | 8 | -4 | -6 | 12 | 2 | 12 | 13 | 1 | 9 | 9 |
| MPI-M-REMO | 10 | -12 | -8 | 15 | 0 | 12 | 3 | -8 | 13 | 4 |
| *bias corrected* | DJF | MAM | JJA | SON | Year | DJF | MAM | JJA | SON | Year |
| ETHZ-CLM | 11 | -3 | 6 | 4 | 4 | 19 | 2 | -6 | -2 | 2 |
| HadRM3Q0 | 6 | 0 | 1 | 11 | 4 | 13 | 8 | -12 | 3 | 2 |
| ICTP-REGCM | 8 | -4 | -6 | 13 | 2 | 12 | 14 | 1 | 10 | 9 |
| MPI-M-REMO | 11 | -11 | -8 | 15 | 1 | 13 | 5 | -8 | 14 | 4 |

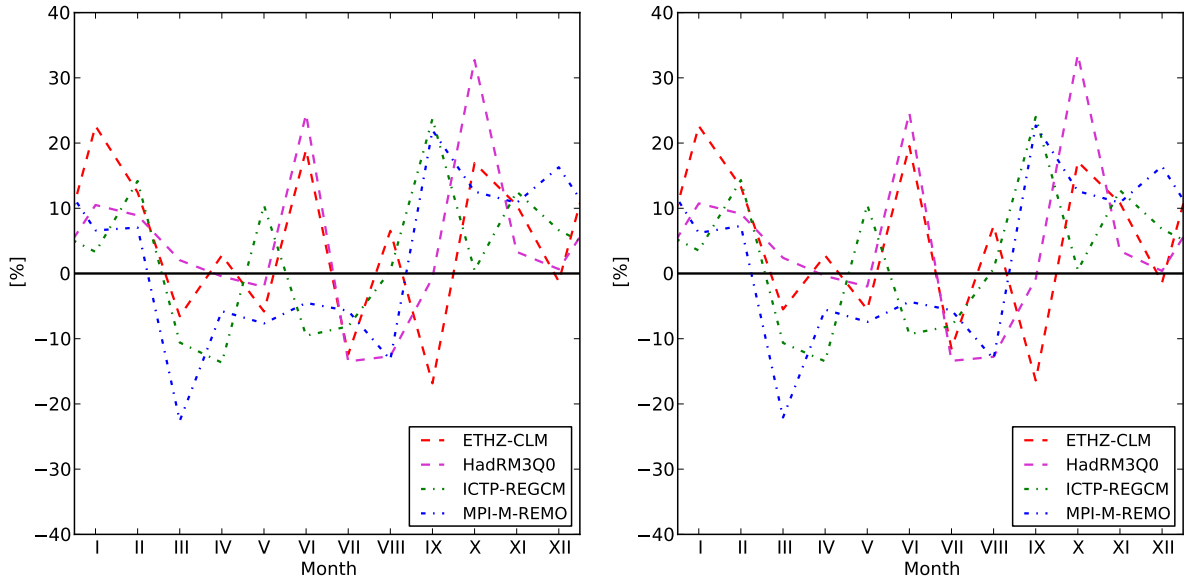


Figure 3.10: Changes of monthly precipitation sums [%] between 1961-1990 and 2011-2040, uncorrected (l) and bias corrected (r) Climate Model data.

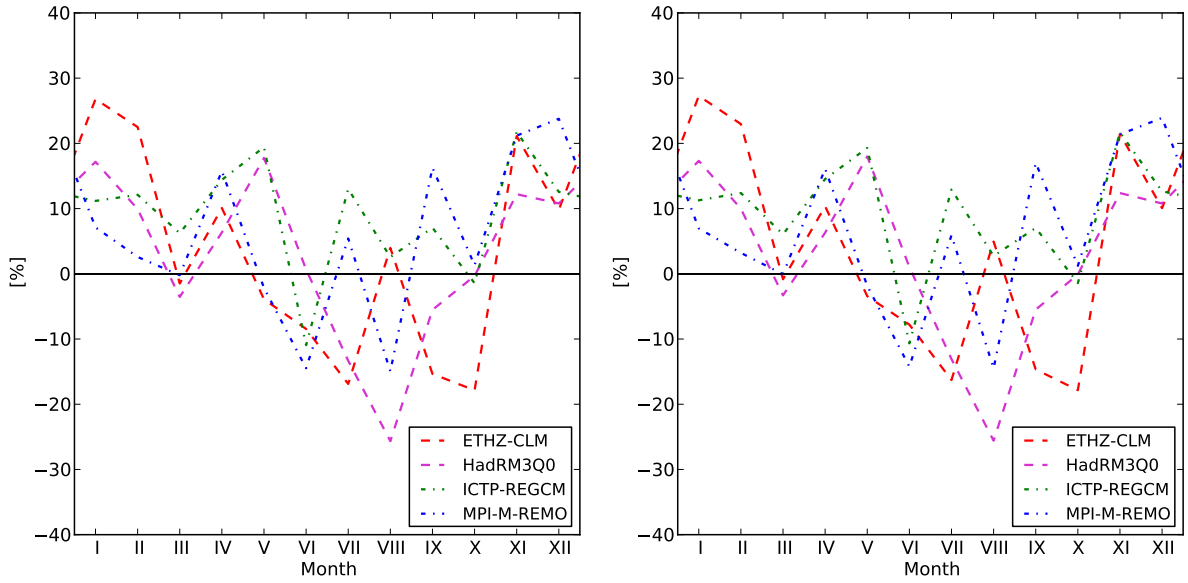


Figure 3.11: Changes of monthly precipitation sums [%] between 1961-1990 and 2061-2090, uncorrected (l) and bias corrected (r) Climate Model data.

Although monthly trends in mean precipitation may deviate distinctively, they are more stable on a seasonal basis. For the 2011-2040 period all models project increasing precipitation amounts for winter and autumn. Changes in yearly rainfall are moderate and in the range from 0% to 4%. The ECHAM5/MPI-OM based RCM indicate a shifted inter-seasonal variability, less precipitation in spring and summer, more during autumn and winter. The HadCM nested RCM project also slight upward or stable trends for the latter seasons. Positive trends for winter precipitation are, in all projections, even stronger in the second scenario period. The models commonly indicate positive climate change signals for spring and the overall annual rainfall amounts. Yearly trends show a GCM controlled pattern. The HadCM models indicate a weaker upward trend, the ECHAM5/MPI-OM RCM a more pronounced raise for the second scenario period.

Table 3.13: Changes in seasonally averaged 95-percentiles of daily precipitation sum [%] since 1961-1990. DJF: Winter, MAM: Spring, JJA: Summer, SON: Autumn.

| | 2011-2040 | | | | | 2061-2090 | | | | |
|---|---|---|---|---|---|---|---|---|---|---|
| *not corrected* | DJF | MAM | JJA | SON | Year | DJF | MAM | JJA | SON | Year |
| ETHZ-CLM | 10 | 3 | 5 | 5 | 6 | 14 | 8 | -3 | 2 | 5 |
| HadRM3Q0 | 6 | 0 | 3 | 10 | 5 | 11 | 14 | -7 | 5 | 5 |
| ICTP-REGCM | 3 | -1 | -1 | 15 | 4 | 8 | 14 | 9 | 13 | 11 |
| MPI-M-REMO | 7 | -7 | -4 | 18 | 3 | 11 | 6 | -1 | 20 | 8 |
| *bias corrected* | DJF | MAM | JJA | SON | Year | DJF | MAM | JJA | SON | Year |
| ETHZ-CLM | 10 | 4 | 6 | 7 | 7 | 15 | 8 | -1 | 2 | 5 |
| HadRM3Q0 | 7 | 0 | 1 | 12 | 5 | 12 | 14 | -9 | 4 | 4 |
| ICTP-REGCM | 4 | 0 | -1 | 15 | 4 | 9 | 14 | 8 | 13 | 11 |
| MPI-M-REMO | 7 | -6 | -4 | 17 | 3 | 12 | 6 | -1 | 19 | 8 |

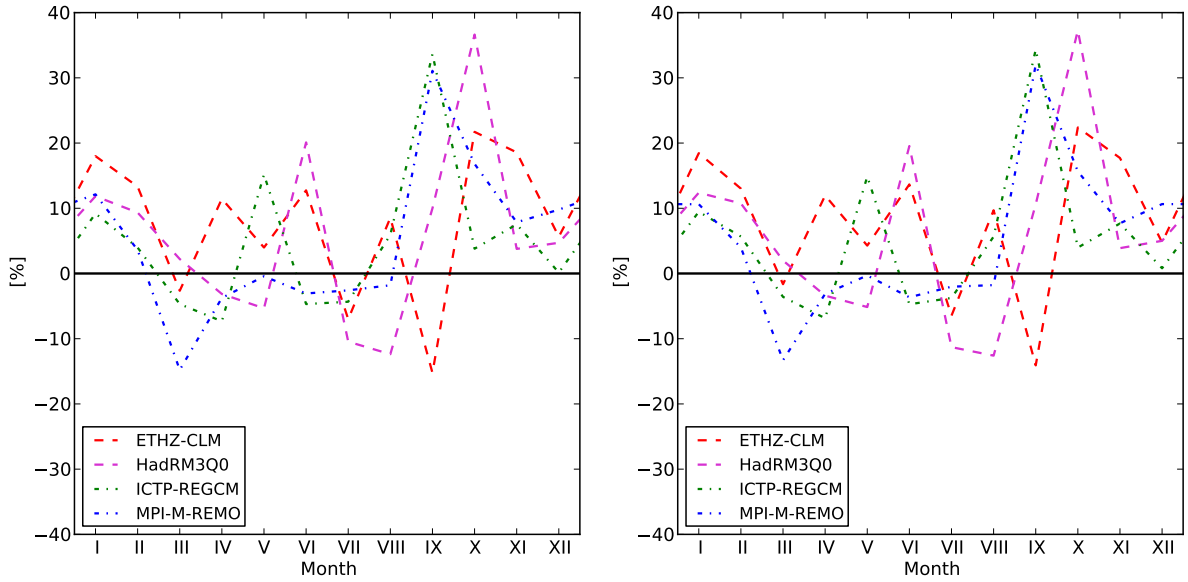


Figure 3.12: Changes of averaged 95-percentiles between 1961-1990 and 2011-2040, uncorrected (r) and bias corrected (r) Climate Model data.

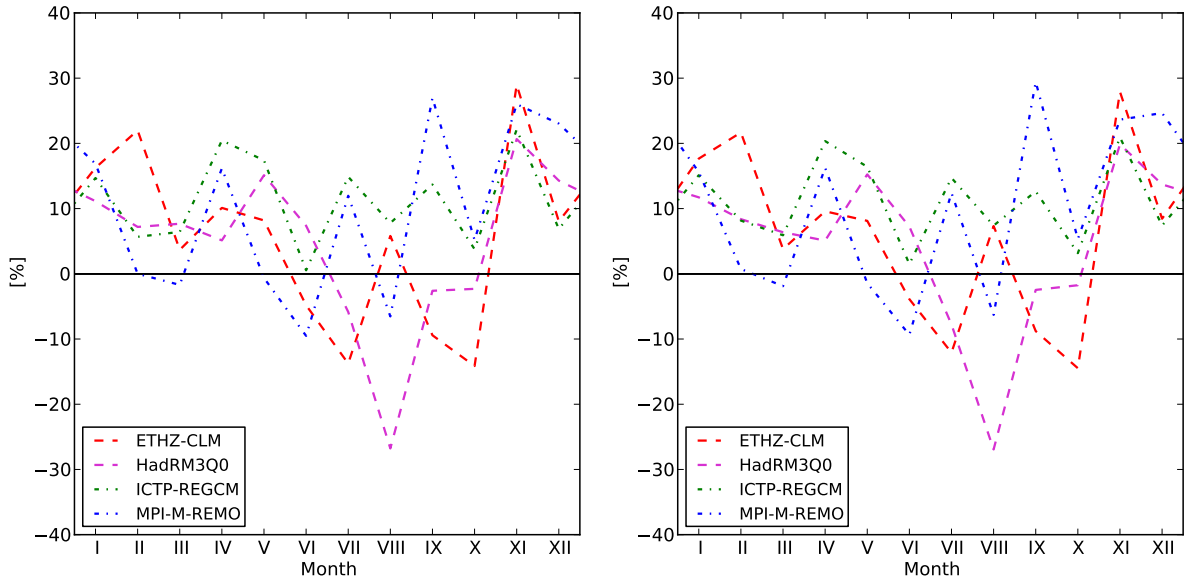


Figure 3.13: Changes of averaged 95-percentiles between 1961-1990 and 2061-2090, uncorrected (l) and bias corrected (r) Climate Model data.

The whole ensemble indicates increasing 95-percentiles for winter, autumn and the entire for both scenario periods, as well as additionally an upward trend for spring in the second time-slice. The actual values vary largely but sign and magnitude are closely related to the trends in monthly and seasonal precipitation sums. The changes in 95-percentiles usually exceed trends in the latter in most seasons, but fall behind in winter.

Tabulates values 3.12 and 3.13 show that the applied method preserves the general data characteristics and model dynamics pretty well. None of the projected trends is disturbed. Differences in relative changes from bias corrected and uncorrected data never exceed two percentage points but are usually lower.

# 4 Hydrological Modelling

A number of hydrological simulation have been carried out using the hydrological model mHM, observational meteorological data and Regional Climate Model (RCM) output as forcing. These simulations are in the following also referred to as control and model runs. To assess general performance of uncorrected and bias corrected RCM driven modelling and possible trends in future hydrology, the generated discharge is analysed at five gauging stations for different three time-slices: the 1961-1990 reference and two scenario periods, 2011-2040 and 2061-2090.

## 4.1 Model Validation

Plots of monthly mean discharge generated with uncorrected and bias corrected RCM data are presented in the figures 4.1 to 4.5. Seasonal and yearly averages plus their respective biases are given in the tables 4.2 to 4.6. Table 4.1 list typical model performance criteria as defined in subsection 2.6.1 for control (1961-1990) and calibration (2000-2004) runs. Given biases are defined as relative deviations from observed discharge and aggregated from monthly values. rounding errors may occur when averaging tabulated seasonal values.

Table 4.1: Model performance criteria for calibration (2000-2004) and validation (1961-1990), bias in [%]. mHM driven by observational meteorlogical data.

| | Calibration | | | Validation | | |
|---|---|---|---|---|---|---|
| Gauge | NSE | r | bias | NSE | r | bias |
| Calbe-Grizehne | 0.81 | 0.91 | 2 | 0.75 | 0.9 | -17 |
| Halle-Trotha | 0.83 | 0.92 | 5 | 0.75 | 0.9 | -17 |
| Laucha | 0.75 | 0.9 | -3 | 0.74 | 0.9 | -19 |
| Rudolstadt | 0.8 | 0.91 | -10 | 0.65 | 0.83 | -18 |
| Hadmersleben | 0.47 | 0.88 | 25 | 0.68 | 0.85 | -4 |

### 4.1.1 Gauge Calbe-Grizehne, Saale

Beside of the good model performance for calibration (NSE: 0.81, r: 0.91) and control run (NSE: 0.75, r: 0.9, see table 4.1), modelling with observational forcing is still negatively biased. Yearly mean discharge deviates by -17% from observed data, seasonal biases range from -20% (autumn) to -15% (winter) (table 4.2). Modelling with uncorrected Regional Climate Model (RCM) data clearly reflects the extensive positive precipitation bias described in chapter 3. Discharge is in any case overestimated, yearly biases range from 52% (MPI-M-REMO) to 180% (ICTP-REGCM). Variability of biases is high for all models, the most stable modelling output (i.e. minimal differences in seasonal biases) is produced with MPI-M-REMO forcing. Each model performs least in a different season (ETHZ-CLM: spring, HadRM3Q0: summer, ICTP-REGCM: autumn, MPI-M-REMO: winter), both HadCM driven simulations (ETHZ-CLM, HadRM3Q0) fit observation best in autumn, ICTP-REGCM forced modelling in spring, MPI-M-REMO in summer.

Bias corrected meteorological data produces more reasonable hydrological timeseries. Generated discharge is in three cases closer to streamflow observation than modelling with observed meteorological data. Yearly deviations range from -1% for the HadRM3Q0 to 25% for the ICTP-REGCM forcing. The HadRM3Q0 driven run not only produces lowest yearly, but with exception of autumn also seasonal biases. On a monthly basis, the good accordance of the HadCM based simulations becomes apparent. Even though the absolute generated discharge values do deviate from each other, their yearly cycle is remarkable similar (figure 4.1). The ECHAM5/MPI-OM RCM driven runs are less close related. The spring high flow period starts later and summer low flood conditions last longer in the MPI-M-REMO generated results. Bias correction affects the MPI-M-REMO driven run much as expected, monthly mean values and yearly cycle are comparable to observation, discharge is however systematically underestimated during the second half of the hydrological year. Timeseries generated with ICTP-REGCM forcing preserve much of its former characteristics. Absolute values are reduced to a plausible range, but the early and distinct winter/spring high flood period is not adjusted.

Table 4.2: Seasonal mean discharge ∅ $[m^3/s]$ and biases [%], gauge Calbe-Grizehne, 1961-1990.

| | Winter | | Spring | | Summer | | Autumn | | Year | |
|---|---|---|---|---|---|---|---|---|---|---|
| | ∅ | bias | ∅ | bias | ∅ | bias | ∅ | bias | ∅ | bias |
| Observation | 136 | - | 173 | - | 98 | - | 86 | - | 126 | - |
| Validation | 116 | -15 | 145 | -16 | 78 | -20 | 69 | -20 | 105 | -17 |
| *not corrected* | | | | | | | | | | |
| ETHZ-CLM | 226 | 65 | 321 | 86 | 157 | 61 | 137 | 59 | 218 | 72 |
| HadRM3Q0 | 193 | 42 | 290 | 67 | 178 | 83 | 110 | 27 | 198 | 57 |
| ICTP-REGCM | 439 | 221 | 426 | 146 | 244 | 150 | 280 | 224 | 354 | 180 |
| MPI-M-REMO | 217 | 59 | 267 | 54 | 139 | 43 | 127 | 47 | 192 | 52 |
| *bias correcetd* | | | | | | | | | | |
| ETHZ-CLM | 140 | 3 | 193 | 11 | 110 | 13 | 91 | 5 | 138 | 9 |
| HadRM3Q0 | 133 | -2 | 175 | 1 | 97 | -1 | 80 | -7 | 125 | -1 |
| ICTP-REGCM | 194 | 42 | 201 | 16 | 112 | 14 | 107 | 24 | 158 | 25 |
| MPI-M-REMO | 134 | -2 | 179 | 3 | 83 | -15 | 78 | -10 | 122 | -4 |

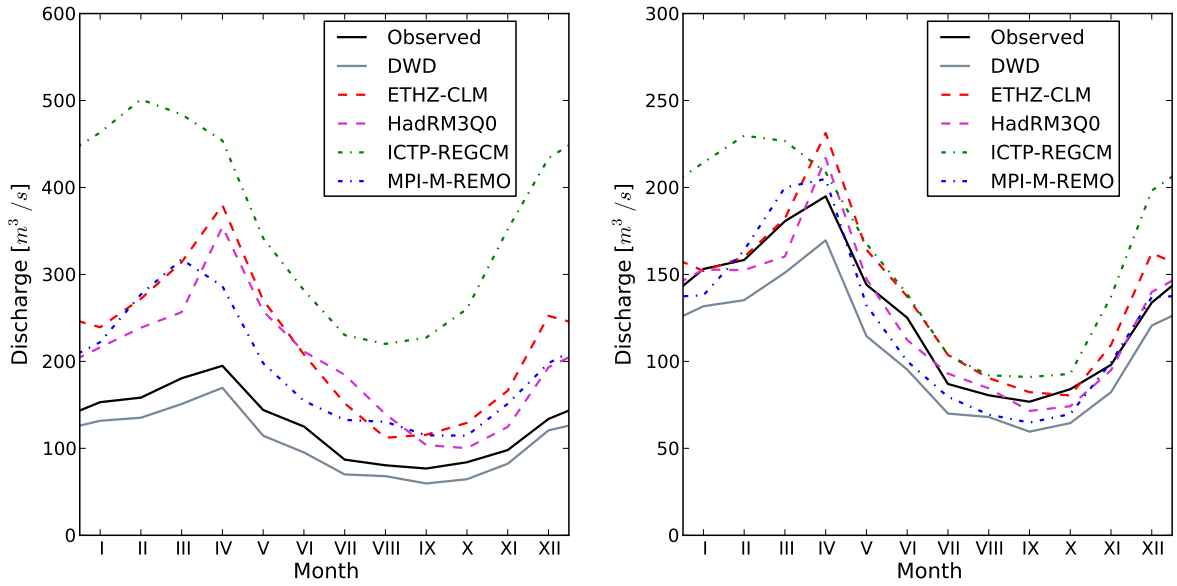


Figure 4.1: Monthly mean discharge values, gauge Calbe-Grizehne, 1961-1990. Modelled with uncorrected (l) and bias corrected (r) climate model data.

### 4.1.2 Gauge Halle-Trotha, Saale

At gauge Halle-Trotha control run performance is quite similar to gauging station Calbe-Grizehne (see figure 4.1), although NSE and r values are slightly higher for calibration (0.89 and 0.92). Uncorrected RCM data driven simulations are similarly biased as the results at the former station (table 4.3). The MPI-M-REMO forced simulation is closest to observation, seasonal biases are considerable but stable (range from 40% to 52%). Largest seasonal biases produced by any RCM data forcing are equally distributed over the year (ETHZ-CLM: spring, HadRM3Q0: summer, ICTP-REGCM: autumn, MPI-M-REMO: winter), the runs forced by the HadCM models deviate least from observation in autumn, ICTP-REGCM modelling results in spring and timeseries generated with MPI-M-REMO in summer.

Bias correction could overcome most of the shortcomings, with exception of ICTP-REGCM forcing all model runs are closer to observation than the control run (table 4.3). Yearly biases range between -4% and 21% (for HadRM3Q0 and ICTP-REGCM forcing, respectively). Modelling with corrected MPI-M-REMO data does exactly reproduce the observed spring discharge average, but the results from the HadRM3Q0 simulation are in general most reasonable. Plotted monthly values in figure 4.2 indicate that the characteristics of the simulated yearly discharge cycles are related to driving GCM.

Table 4.3: Seasonal mean discharge ∅ $[m^3/s]$ and biases [%], gauge Halle-Trotha, 1961-1990.

| | Winter | | Spring | | Summer | | Autumn | | Year | |
|---|---|---|---|---|---|---|---|---|---|---|
| | ∅ | bias | ∅ | bias | ∅ | bias | ∅ | bias | ∅ | bias |
| Observation | 111 | - | 141 | - | 78 | - | 70 | - | 102 | - |
| Validation | 94 | -15 | 117 | -17 | 63 | -19 | 56 | -20 | 85 | -17 |
| *not corrected* | | | | | | | | | | |
| ETHZ-CLM | 180 | 63 | 264 | 88 | 125 | 60 | 110 | 57 | 176 | 71 |
| HadRM3Q0 | 152 | 37 | 232 | 64 | 140 | 80 | 87 | 24 | 158 | 54 |
| ICTP-REGCM | 346 | 212 | 336 | 138 | 188 | 142 | 221 | 215 | 278 | 171 |
| MPI-M-REMO | 168 | 52 | 211 | 50 | 109 | 40 | 100 | 43 | 150 | 46 |
| *bias correcetd* | | | | | | | | | | |
| ETHZ-CLM | 109 | -2 | 152 | 8 | 87 | 12 | 72 | 2 | 108 | 6 |
| HadRM3Q0 | 104 | -6 | 137 | -3 | 77 | -1 | 63 | -10 | 98 | -4 |
| ICTP-REGCM | 150 | 36 | 158 | 12 | 88 | 12 | 84 | 20 | 124 | 21 |
| MPI-M-REMO | 104 | -6 | 141 | 0 | 66 | -16 | 62 | -11 | 96 | -7 |

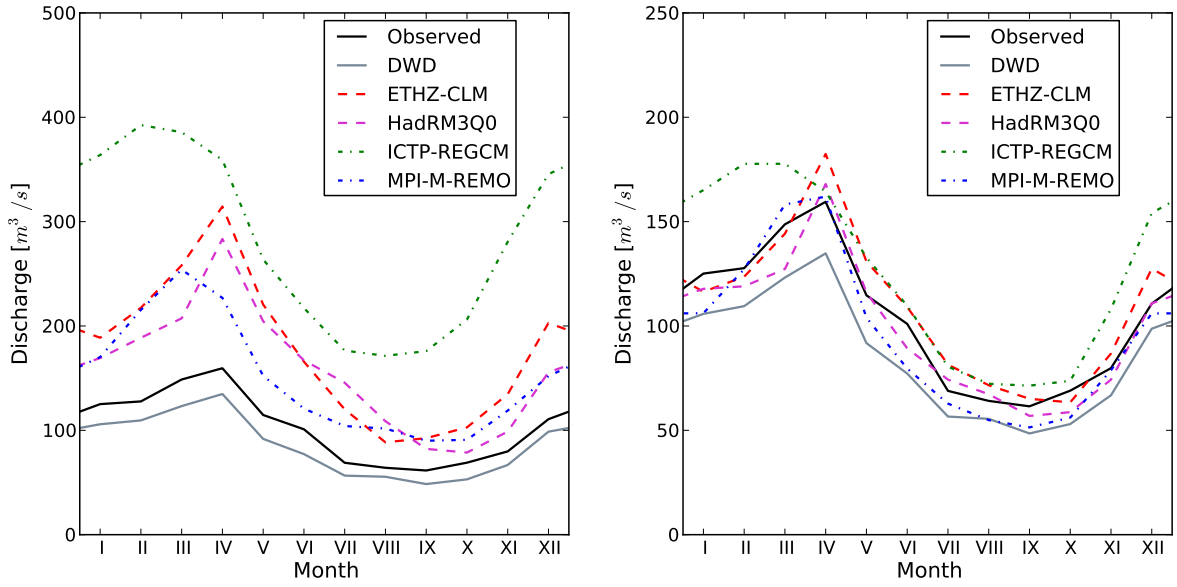


Figure 4.2: Monthly mean discharge values, gauge Halle-Trotha, 1961-1990. Modeled with uncorrected (l) and bias corrected (r) climate model data.

### 4.1.3 Gauge Laucha, Unstrut

mHM control run performance is lower than at the previous stations, NSE and r values are pretty stable for calibration (0.75, 0.9) and control run (0.74, 0.9). Biases in the discharge timeseries generated with uncorrected RCM data range from 30% (HadRM3Q0) to 160% (ICTP-REGCM), whereas three of the four runs produce biases between 30% and 36%. Biases in the MPI-M-REMO driven simulations are most stable, HadRM3Q0 data forcing produces minimal seasonal deviation (autumn: 4%). Three model runs perform best in autumn (exception ICTP-REGCM: spring), and least in summer (exception ICTP-REGCM: autumn) (table 4.4).

Bias correction brakes these similarities, highest and lowest deviations from observational data are distributed more equally. With yearly biases between -1% (ETHZ-CLM) and 18% (ICTP-REGCM) model runs forced with corrected RCM data are in any case closer to observation than the control run. Deviations are usually higher in the first half of the hydrological year, the HadCM RCM generated timeseries match the April discharge peak, the MPI-M-REMO forced simulation produces comparable values for March (figure 4.3). Compared to the previous stations, monthly biases are more balanced and discharge generated with corrected RCM data is usually lower than observation (exception ICTP-REGCM) but higher than control run discharge. Especially MPI-M-REMO modelling results are clearly negatively biased during the months June to October and preserve the misrepresentation of the April discharge peak.

Table 4.4: Seasonal mean discharge ∅ $[m^3/s]$ and biases [%], gauge Laucha, 1961-1990.

| | Winter | | Spring | | Summer | | Autumn | | Year | |
|---|---|---|---|---|---|---|---|---|---|---|
| | ∅ | bias | ∅ | bias | ∅ | bias | ∅ | bias | ∅ | bias |
| Observation | 36 | - | 45 | - | 24 | - | 21 | - | 32 | - |
| Validation | 30 | -16 | 37 | -17 | 18 | -25 | 15 | -27 | 26 | -19 |
| *not corrected* | | | | | | | | | | |
| ETHZ-CLM | 48 | 32 | 62 | 38 | 34 | 39 | 26 | 24 | 44 | 36 |
| HadRM3Q0 | 43 | 18 | 61 | 36 | 38 | 55 | 22 | 4 | 42 | 30 |
| ICTP-REGCM | 109 | 202 | 101 | 123 | 56 | 130 | 64 | 204 | 85 | 160 |
| MPI-M-REMO | 49 | 34 | 59 | 31 | 33 | 35 | 27 | 29 | 43 | 32 |
| *bias correcetd* | | | | | | | | | | |
| ETHZ-CLM | 35 | -4 | 45 | -1 | 26 | 6 | 20 | -8 | 32 | -1 |
| HadRM3Q0 | 33 | -9 | 41 | -9 | 22 | -8 | 17 | -18 | 30 | -9 |
| ICTP-REGCM | 48 | 32 | 49 | 9 | 27 | 11 | 24 | 14 | 38 | 18 |
| MPI-M-REMO | 34 | -7 | 42 | -8 | 19 | -21 | 17 | -20 | 29 | -12 |

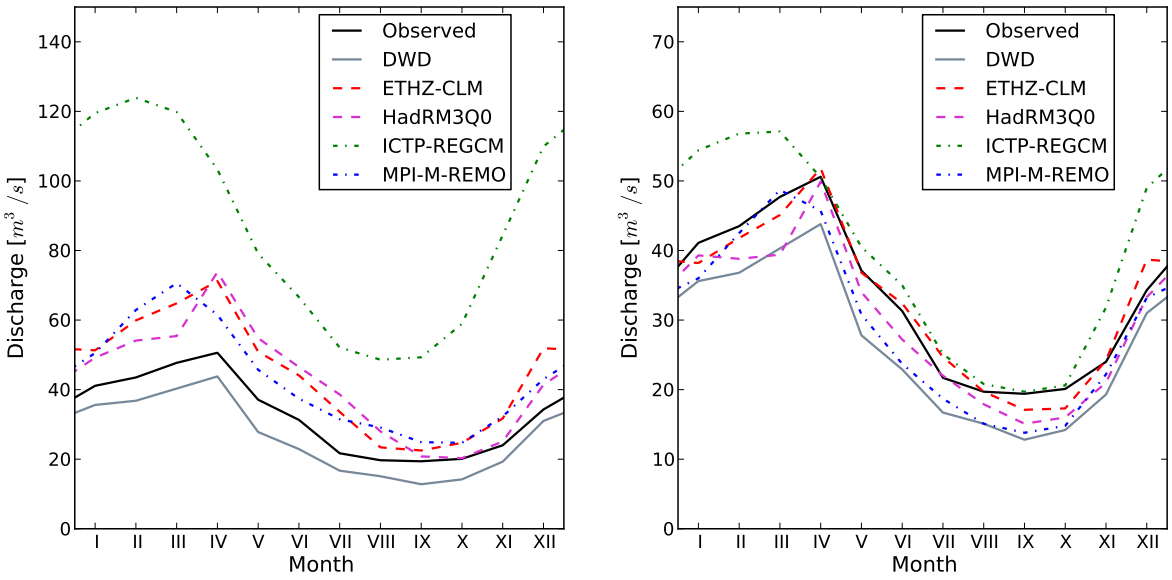


Figure 4.3: Monthly mean discharge values, gauge Laucha, 1961-1990. Modelled with uncorrected (l) and bias corrected (r) climate model data.

### 4.1.4 Gauge Rudolstadt, Saale

mHM performance is rather low at gauge Rudolstadt (table 4.1), NSE and r values are reduced from 0.8 and 0.91 for calibration to 0.65 and 0.83 for the control run simulation. Biases are lower than at gauge Laucha, although seasonal deviations show a greater dynamics (-10% to -27%). The results from the uncorrected RCM data runs are special compared to other stations. Both HadCM RCM driven simulations produce highly variable seasonal biases, spring discharge is overestimated about 100% but summer and autumn values are considerably lower. Biases from the ICTP-REGCM model run are again largest, but lower than at the remaining stations. The good model fit achieved with MPI-M-REMO data (yearly bias: -3%, seasonal biases between -7% and 18%) is the only case where modelling with uncorrected climate model data outperforms the control run simulation. Three of the model runs deviate most from observation in spring (exception ICTP-REGCM: autumn). Forcing mHM with on of the HadCM models gives least performance in autumn, with ICTP-REGCM in summer and with MPI-M-REMO in winter (table 4.5).

Bias correction is less effective than at the former stations. All model runs are still positively biased, yearly deviations range from 9% to 31%, two runs perform better than the control run simulation. The considerable spring discharge surplus produced with ETHZ-CLM and HadRM3Q0 data is only slightly reduced and basically a result of overestimated April discharge (figure 4.4) . While the ICTP-REGCM model run is affected like at other stations, effects on the MPI-M-REMO simulation are rather unwanted. The slight yearly bias of -3% increases to 9% and even though autumn deviations could be reduced to 0%, spring discharge is now considerably biases (34%).

Table 4.5: Seasonal mean discharge ∅ $[m^3/s]$ and biases [%], gauge Rudolstadt, 1961-1990.

| | Winter | | Spring | | Summer | | Autumn | | Year | |
|---|---|---|---|---|---|---|---|---|---|---|
| | ∅ | bias | ∅ | bias | ∅ | bias | ∅ | bias | ∅ | bias |
| Observation | 30 | - | 36 | - | 20 | - | 20 | - | 27 | - |
| Validation | 25 | -17 | 32 | -10 | 15 | -24 | 15 | -27 | 22 | -18 |
| *not corrected* | | | | | | | | | | |
| ETHZ-CLM | 41 | 36 | 72 | 103 | 29 | 42 | 28 | 42 | 44 | 60 |
| HadRM3Q0 | 42 | 41 | 69 | 93 | 36 | 80 | 25 | 26 | 45 | 63 |
| ICTP-REGCM | 75 | 152 | 72 | 104 | 40 | 95 | 52 | 158 | 61 | 122 |
| MPI-M-REMO | 28 | -7 | 42 | 18 | 18 | -12 | 18 | -12 | 27 | -3 |
| *bias correcetd* | | | | | | | | | | |
| ETHZ-CLM | 33 | 9 | 51 | 43 | 24 | 19 | 23 | 14 | 34 | 23 |
| HadRM3Q0 | 32 | 8 | 44 | 25 | 21 | 5 | 20 | -1 | 30 | 12 |
| ICTP-REGCM | 45 | 52 | 46 | 29 | 22 | 11 | 26 | 27 | 36 | 31 |
| MPI-M-REMO | 31 | 3 | 48 | 34 | 18 | -9 | 20 | 0 | 30 | 9 |

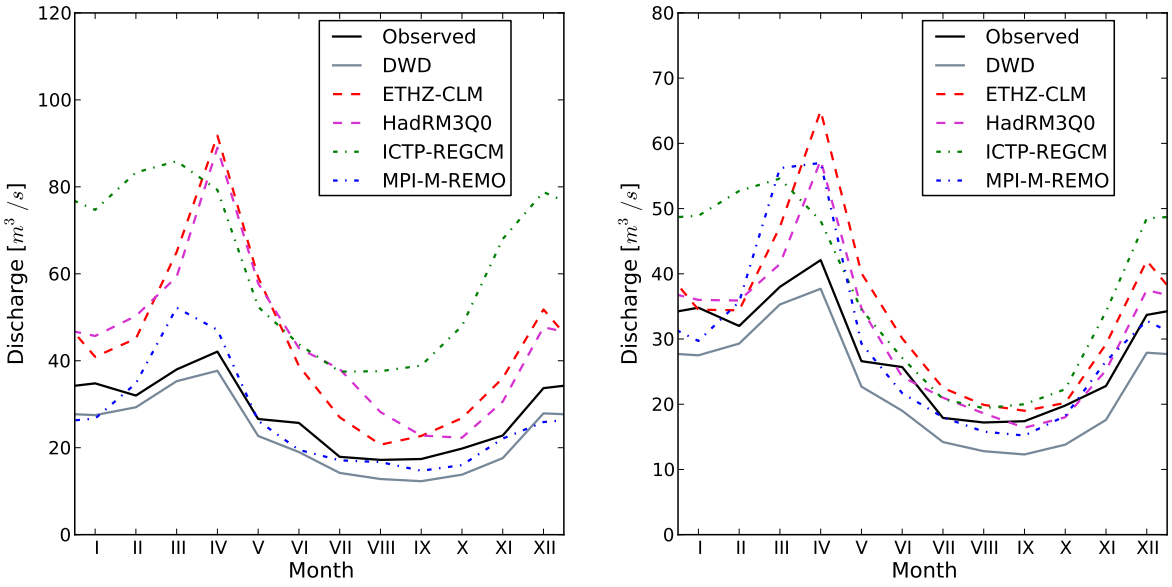


Figure 4.4: Monthly mean discharge values, gauge Rudolstadt, 1961-1990. Modelled with uncorrected (l) and bias corrected (r) climate model data.

### 4.1.5 Gauge Hadmersleben, Bode

At the smallest gauging station model performance for calibration is rather low (NSE: 0.47, r: 0.88) but slightly higher for the control run (NSE: 0.68, r: 0.85) (table 4.1). Relative deviations between simulated and observed streamflow volume, ranging from -10% (winter) to 0% (summer), are anyhow lower than at the other gauging stations. The direct use of RCM data in mHM results in yearly biases between 48% (MPI-M-REMO) and 220% (ICTP-REGCM), whereas seasonal values always from all model runs exceed 39%. The simulations forced with any of the HadCM RCM are closest to observation in winter and deviate most in autumn, the ECHAM5/MPI-OM runs perform best in spring and worst in autumn (ICTP-REGCM) and summer (MPI-M-REMO) (table 4.6).

Bias correction could, with exception of the results generated with ICTP-REGCM data, not significantly improve results. Yearly biases are still in the range of 36% (MPI-M-REMO) to 78% (ICTP-REGCM), all simulations are higher biased than the control run and none could approximate observed streamflow. Plotted monthly values indicate that bias correction leads to a convergence of modelling results and a slightly better fit to observed data, but also that modelling is not improved the same way it is at the stations Calbe-Grizehne, Halle-Trotha or Laucha (figure 4.5).

Table 4.6: Seasonal mean discharge ∅ $[m^3/s]$ and biases [%], gauge Hadmersleben, 1961-1990.

| | Winter | | Spring | | Summer | | Autumn | | Year | |
|---|---|---|---|---|---|---|---|---|---|---|
| | ∅ | bias | ∅ | bias | ∅ | bias | ∅ | bias | ∅ | bias |
| Observation | 18 | - | 21 | - | 10 | - | 9 | - | 15 | - |
| Validation | 16 | -10 | 21 | -1 | 10 | 0 | 9 | -2 | 14 | -4 |
| *not corrected* | | | | | | | | | | |
| ETHZ-CLM | 26 | 47 | 34 | 62 | 20 | 98 | 17 | 87 | 25 | 68 |
| HadRM3Q0 | 28 | 59 | 39 | 88 | 24 | 147 | 16 | 70 | 28 | 86 |
| ICTP-REGCM | 58 | 231 | 54 | 159 | 35 | 257 | 39 | 324 | 47 | 220 |
| MPI-M-REMO | 26 | 47 | 29 | 39 | 16 | 62 | 15 | 61 | 22 | 48 |
| *bias correcetd* | | | | | | | | | | |
| ETHZ-CLM | 24 | 38 | 31 | 51 | 17 | 71 | 14 | 58 | 22 | 52 |
| HadRM3Q0 | 23 | 33 | 30 | 42 | 15 | 49 | 13 | 45 | 21 | 41 |
| ICTP-REGCM | 34 | 94 | 32 | 53 | 18 | 79 | 18 | 98 | 26 | 78 |
| MPI-M-REMO | 23 | 33 | 29 | 41 | 13 | 29 | 12 | 37 | 20 | 36 |

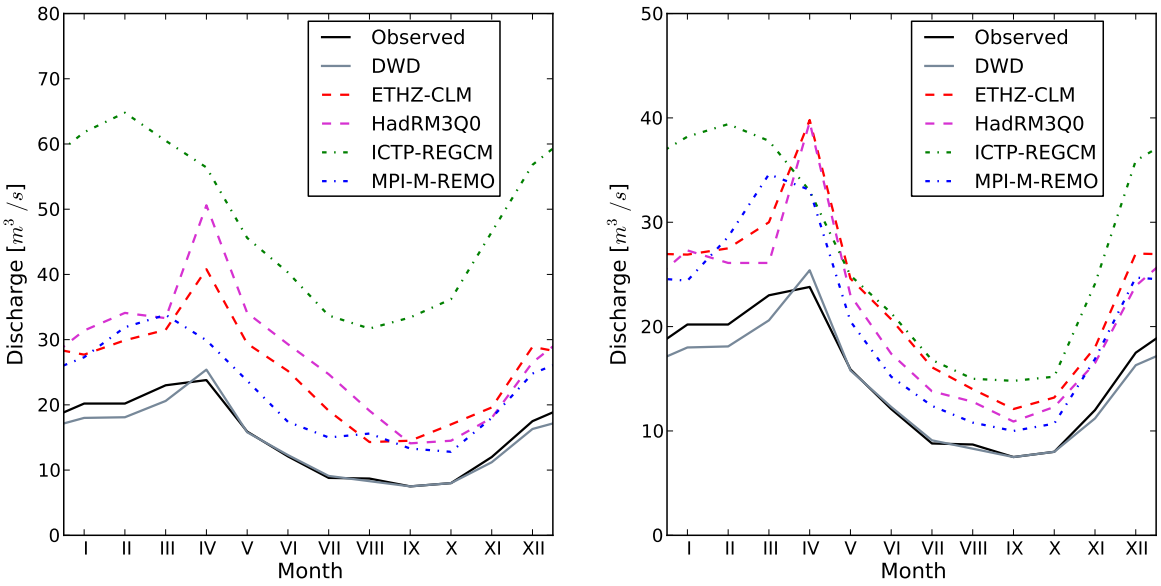


Figure 4.5: Monthly mean discharge values, gauge Hadmersleben, 1961-1990. Modelled with uncorrected (l) and bias corrected (r) climate model data.

### 4.1.6 General modelling performance

A number of common trends can be extracted from the results presented in the last five subsections. Most important, the improvements of generated hydrological data caused by bias correcting the meteorological forcing and differences in modelling performance obviously related to catchment size. Forcing mHM with uncorrected RCM data usually multiplies precipitation biases. Bias corrected input data generates in contrary in most cases reasonably realistic results.

Streamflow generated with bias corrected ETHZ-CLM, HadRM3Q0 and MPI-M-REMO data is close to observation at the gauging stations Calbe-Grizehne, Halle-Trotha and Laucha. There is no or only little positive effect in simulations for the gauges Rudolstadt and Hadmersleben, both covering considerably smaller sub-catchments. Uncorrected MPI-M-REMO forcing produced at all station results closest to observation even though biases are still high, simulations driven with ICTP-REGCM data are always biased most. Beside the propagated spatial dependency of bias correction, the climate model further determines the efficiency of the method. ETHZ-CLM and HadRM3Q0 driven hydrological simulations are more sensitive to bias correction of input data than ICTP-REGCM and MPI-M-REMO generated results.

## 4.2 Hydrological Impacts of Climate Change

To asses the impact of projected climate change on the hydrology of the Saale River and its main tributaries as well as the numerical effects of bias correction on future trends in hydrology, simulation results for each station and the two scenario periods, 2011-2040 and 2061-2090, are presented in the following subsections. Changes in the hydrological regime, whether on the monthly basis as depicted in the figures 4.6 to 4.15 or tabulated in the tables 4.7 to 4.11 are defined as relative deviations from the 1961-1990 reference period simulations of the respective model. Seasonal and yearly averages are calculated from monthly changing rates, rounding errors may occur when aggregating tabulated values.

### 4.2.1 Gauge Calbe-Grizehne, Saale

For the 2011-2040 timeslice a considerable increase of winter, accompanied by a slightly lower decrease of spring discharge is projected. Three of the uncorrected Regional Climate Model (RCM) driven hydrological simulations prognosticate highest increases for January and most substantial decreases for April (see figure 4.6). Climate change impacts are generally higher driving mHM with one of the HadCM RCM. Changes are less distinctive and univocal in the second half of the hydrological year. Summer discharge is projected to decrease in the ICTP-REGCM (-6%) and MPI-M-REMO (-11%), to be stable in the HadRM3Q0 and to increase in the ETHZ-CLM (9%) simulations. The latter model

forcing produces furthermore a stable, all other RCM inputs a raised autumn discharge regime. Modelling results are more consistent with respect to yearly average discharge, as all simulations indicate a slight increase (table 4.7). For the 2061-2090 scenario period mHM simulations indicate a further increase of winter discharge, mainly the result of considerably higher December values (figure 4.7) when forced with ICTP-REGCM (22%) and MPI-M-REMO (31%) data. The streamflow timeseries generated with ETHZ-CLM input shows no other increase, HadRM3Q0 a decrease of winter discharge compared to the 2011-2040 time-slice. Both models simulate stable negative trends for the remaining seasons. The development of yearly mean discharge until the end of the century is ambiguous. The HadCM based simulations indicate a decrease (ETHZ-CLM: -2%, HadRM3Q0: -7%), the ECHAM5/MPI-OM models an increase (ICTP-REGCM: 11%, MPI-M-REMO: 8%).

The effect of bias correction on modelling results is rather small in the first scenario period. Seasonal differences in the timeseries generated with uncorrected and bias corrected RCM data are inconsistent, but round up to zero for HadRM3Q0 and ICTP-REGCM, and to three percentage points for ETHZ-CLM and MPI-M-REMO forcing. The projected increase of winter discharge is cushioned in the HadRM3Q0 and elevated in the remaining RCM driven modelling runs. The decrease of spring discharge is generally not altered substantially. Simulated changes in summer and autumn discharge are elevated compared to uncorrected input in the ETHZ-CLM and MPI-M-REMO simulations, are almost identical in the ICTP-REGCM and inconsistently modified in the HadRM3Q0 driven modelling runs. The hydrological change signal is more sensitive to bias correction in the second scenario period. The differences are, with exception of the ETHZ-CLM forced simulations, higher than in the 2011-2040 time-slice. The numerical impact of bias correction on hydrological modelling is most problematic for the MPI-M-REMO forced modelling chain. Projected changes in seasonal mean discharge conditions are altered considerably and the arithmetic sign of the summer discharge trend has changed (table 4.7).

Table 4.7: Changes in seasonal mean discharge [%] since 1961-1990 at gauging station Calbe-Grizehne, simulated with uncorrected and bias corrected climate model data. DJF: Winter, MAM: Spring, JJA: Summer, SON: Autumn.

| | 2011-2040 | | | | | 2061-2090 | | | | |
|---|---|---|---|---|---|---|---|---|---|---|
| *not corrected* | DJF | MAM | JJA | SON | Year | DJF | MAM | JJA | SON | Year |
| ETHZ-CLM | 27 | -15 | 9 | 0 | 4 | 27 | -14 | -13 | -16 | -2 |
| HadRM3Q0 | 26 | -17 | 0 | 7 | 2 | 18 | -19 | -11 | -16 | -7 |
| ICTP-REGCM | 12 | -9 | -6 | 8 | 2 | 22 | 4 | 7 | 6 | 11 |
| MPI-M-REMO | 19 | -13 | -11 | 9 | 1 | 31 | -6 | -1 | 5 | 8 |
| *bias corrected* | DJF | MAM | JJA | SON | Year | DJF | MAM | JJA | SON | Year |
| ETHZ-CLM | 29 | -13 | 14 | 5 | 7 | 25 | -14 | -12 | -12 | -2 |
| HadRM3Q0 | 24 | -17 | -3 | 8 | 2 | 12 | -21 | -16 | -19 | -10 |
| ICTP-REGCM | 13 | -8 | -6 | 7 | 2 | 22 | 7 | 10 | 6 | 13 |
| MPI-M-REMO | 26 | -13 | -8 | 15 | 4 | 42 | -8 | 2 | 11 | 12 |

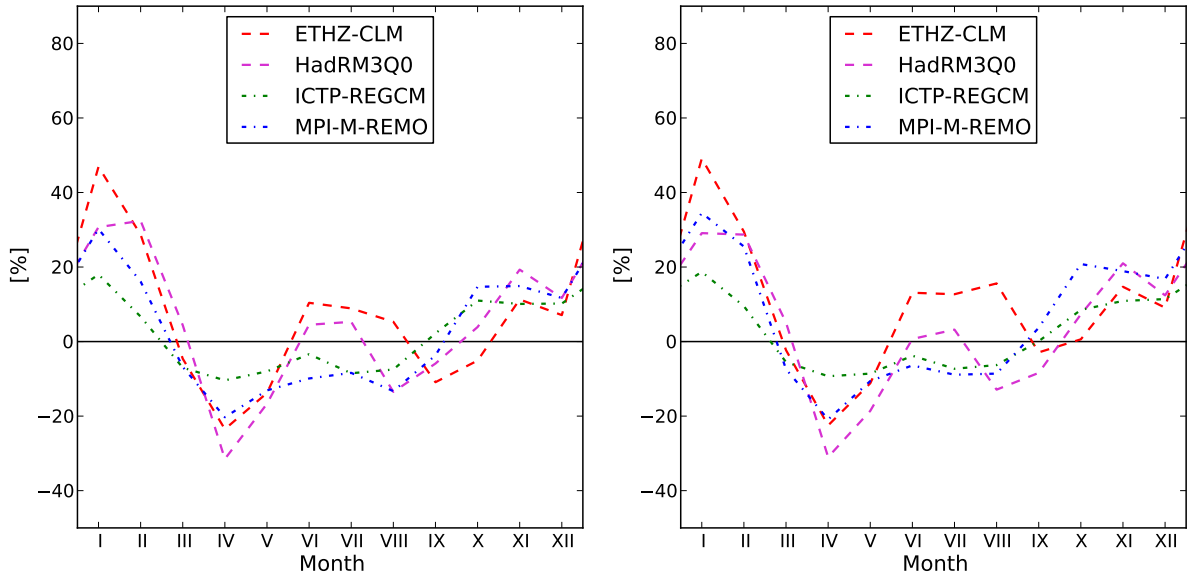


Figure 4.6: Changes in monthly mean discharge at gauge Calbe-Grizehne between 1961-1990 and 2011-2040, modelled with uncorrected (l) and bias corrected (r) climate model data.

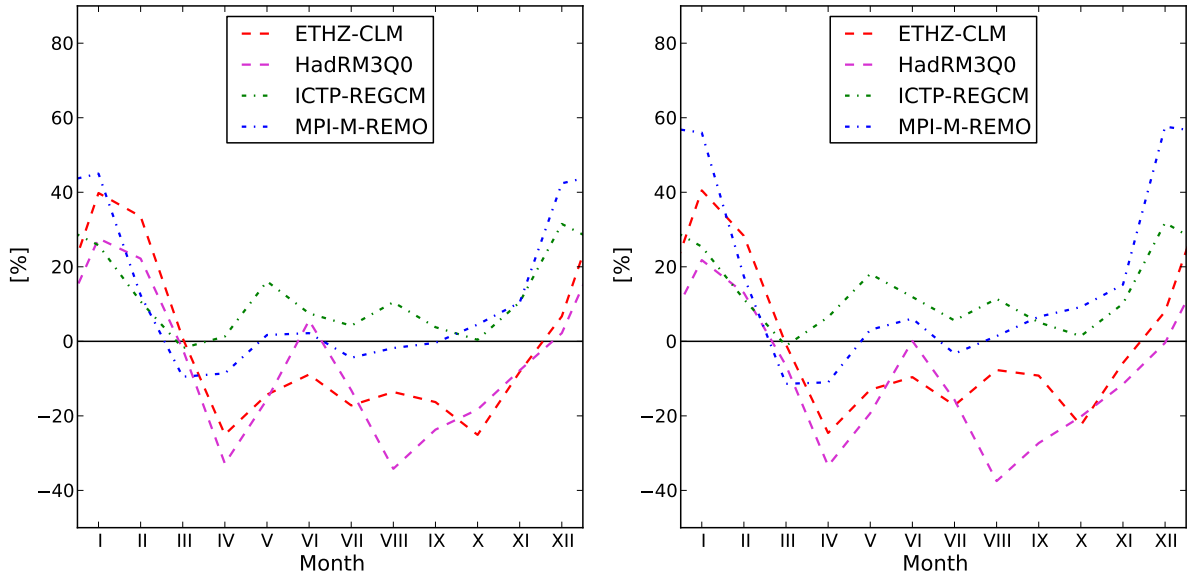


Figure 4.7: Changes in monthly mean discharge at gauge Calbe-Grizehne between 1961-1990 and 2061-2090, modelled with uncorrected (l) and bias corrected (r) climate model data.

### 4.2.2 Gauge Halle-Trotha, Saale

In the 2011-2040 scenario period all RCM driven simulation project a considerable increase of winter discharge, highest relative changes result from modelling with ETHZ-CLM (28%), lowest from ICTP-REGCM data (13%). Spring discharge is reduced with rates between -18% (HadRM3Q0) and -8% (ICTP-REGCM), all model runs simulate highest discharge reduction for April (figure 4.8). ICTP-REGCM and MPI-M-REMO forcing of the hydrological model indicates lower summer (-5% and -10%) and higher autumn discharge (9% and 10%). The ETHZ-CLM driven simulation points to increased summer (8%) and unchanged autumn, HadRM3Q0 to stable summer but higher autumn discharge. Yearly mean streamflow is projected to be roughly stable, the shift in seasonal conditions does balance out to yearly relative changes between 1% (MPI-M-REMO) and 3% (ETHZ-CLM, ICTP-REGCM). In the 2061-2090 scenario period climate change impacts on the annual discharge average are more significant but ambiguous. Mean discharge is reduced in both HadCM and heightened in the ECHAM5/MPI-OM RCM driven modelling runs. The winter discharge surplus is projected to be lower than in the previous time-slice modelling river hydrology with RCM from the former model group. The simulations driven with ICTP-REGCM and MPI-M-REMO indicate in contrary a further increase, whereas especially the raise of December discharge is more distinct (figure 4.7). Spring, summer and autumn discharge is decreasing according to the ETHZ-CLM and HadRM3Q0 driven mHM runs, increasing for ICTP-REGCM and inconsistent for MPI-M-REMO forcing

(table 4.8).

Bias correction does affect modelling results not at all or positively in arithmetic sign in the first scenario period. The climate change signals from HadRM3Q0 and ICTP-REGCM forced simulations are barely altered, the relative changes from ETHZ-CLM and MPI-M-REMO driven modelling are slightly raised. The synthetic hydrological timeseries are more sensitive to bias correction of the input data in the 2061-2090 period. The changes projected from the MPI-M-REMO modelling chain deviate most significantly, from ICTP-REGCM least. The stable climate change signals in both HadRM3Q0 driven simulations during the first scenario period are not preserved that exactly in the second, whereas they are in the ETHZ-CLM forced simulations.

Table 4.8: Changes in seasonal mean discharge [%] 1961-1990 at gauging station Halle-Trotha, simulated with uncorrected and bias corrected climate model data. DJF: Winter, MAM: Spring, JJA: Summer, SON: Autumn.

| | 2011-2040 | | | | | 2061-2090 | | | | |
|---|---|---|---|---|---|---|---|---|---|---|
| *not corrected* | DJF | MAM | JJA | SON | Year | DJF | MAM | JJA | SON | Year |
| ETHZ-CLM | 28 | -17 | 8 | 0 | 3 | 28 | -17 | -15 | -19 | -4 |
| HadRM3Q0 | 26 | -18 | 0 | 7 | 2 | 21 | -20 | -10 | -13 | -6 |
| ICTP-REGCM | 13 | -8 | -5 | 9 | 3 | 23 | 3 | 6 | 4 | 10 |
| MPI-M-REMO | 21 | -14 | -10 | 10 | 1 | 33 | -9 | -3 | 5 | 7 |
| *bias corrected* | DJF | MAM | JJA | SON | Year | DJF | MAM | JJA | SON | Year |
| ETHZ-CLM | 29 | -15 | 13 | 5 | 6 | 23 | -18 | -15 | -17 | -6 |
| HadRM3Q0 | 24 | -18 | -3 | 9 | 2 | 13 | -22 | -16 | -16 | -9 |
| ICTP-REGCM | 15 | -7 | -4 | 8 | 3 | 23 | 6 | 9 | 4 | 12 |
| MPI-M-REMO | 28 | -14 | -8 | 15 | 4 | 43 | -9 | -1 | 10 | 11 |

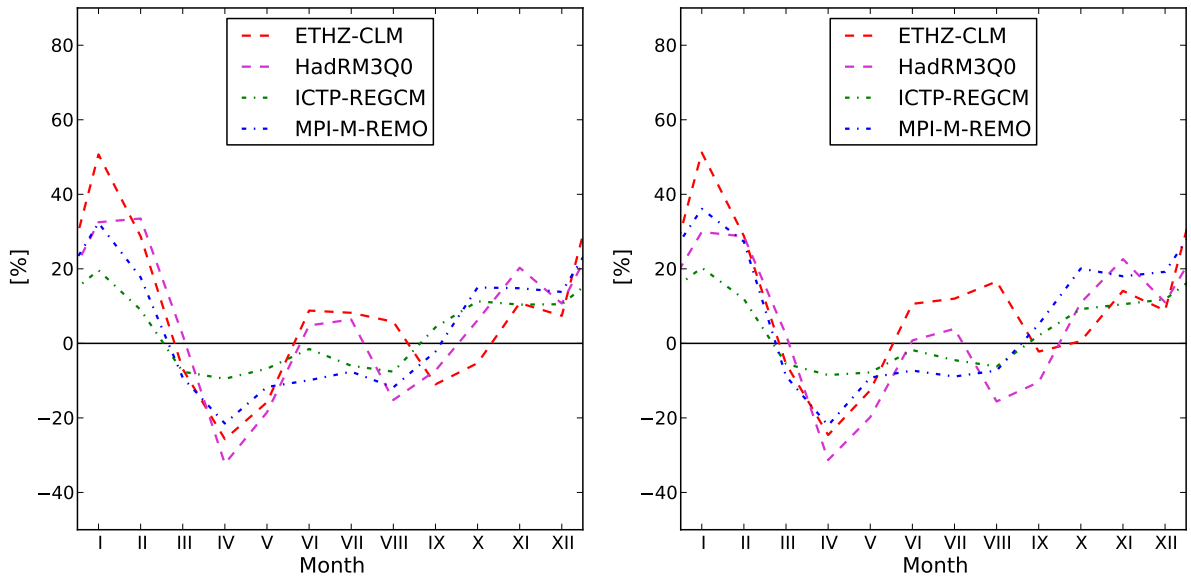

Figure 4.8: Changes in monthly mean discharge at gauge Halle-Trotha between 1961-1990 and 2011-2040, modelled with uncorrected (l) and bias corrected (r) climate model data.

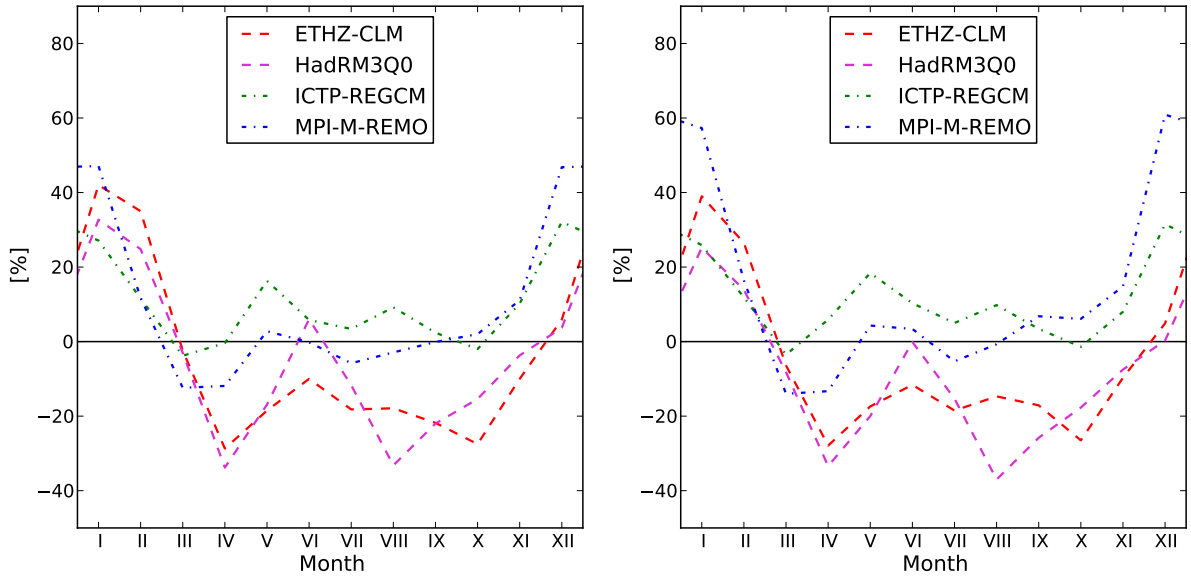


Figure 4.9: Changes in monthly mean discharge at gauge Halle-Trotha between 1961-1990 and 2061-2090, modelled with uncorrected (l) and bias corrected (r) climate model data.

### 4.2.3 Gauge Laucha, Unstrut

For the 2011-2040 scenario period all model runs project a considerable shift in the discharge regime of the river Unstrut. With exception of ETHZ-CLM forcing and summer, seasonal projections generated with all RCM point in the same direction, higher mean discharge during Winter and Autumn with a peak in January or February, lower discharge during spring and summer (figure 4.10). Three runs indicate higher yearly mean discharge (1% to 6%), only MPI-M-REMO a slightly reduced one (-3%) (table 4.9). 2061-2090 scenario period simulations differ more explicitly. Forcing mHM with one of the HadCM RCM indicates a decrease of yearly mean discharge (-2% and -10%), while both ECHAM5/MPI-OM RCM driven modelling runs simulate the opposite (12% and 5%). All models project an increase of winter discharge. The surplus is, compared to the 2011-2040 scenario period, lower modelling with ETHZ-CLM and HadRM3Q0 and higher using ICTP-REGCM and MPI-M-REMO data. The former two model runs project a considerable decrease of seasonal mean discharge for spring, summer and autumn as well as for all individual months (figure 4.11). ICTP-REGCM forcing indicates an increase during

all seasons and months, the MPI-M-REMO driven simulation an increase of autumn and a decrease of spring and summer discharge.

Simulated climate change impacts are in generally positively altered by biases correction, i.e. upward trends in streamflow are consolidated, downward trends cushioned. In the 2011-2040 scenario period changes in hydrology are influenced most substantially in the ETHZ-CLM driven simulations. The change in yearly mean discharge is increased (from 6% to 10%), as are all seasonal values. Impact projections from the remaining models are affected less, changes in yearly mean discharge are altered little or not at all in the HadRM3Q0, ICTP-REGCM and MPI-M-REMO driven runs. The disparity in discharge dynamics simulated with uncorrected and bias corrected climate model data gets greater in the 2061-2090 period. Yearly mean discharge changes produced with any model are affected, highest differences are found between the MPI-M-REMO simulations, and the arithmetic sign has changed in the bias corrected ETHZ-CLM simulation (table 4.9).

Table 4.9: Changes in seasonal mean discharge [%] 1961-1990 at gauging station Laucha, simulated with uncorrected and bias corrected climate model data. DJF: Winter, MAM: Spring, JJA: Summer, SON: Autumn.

| | 2011-2040 | | | | | 2061-2090 | | | | |
|---|---|---|---|---|---|---|---|---|---|---|
| *not corrected* | DJF | MAM | JJA | SON | Year | DJF | MAM | JJA | SON | Year |
| ETHZ-CLM | 25 | -11 | 7 | 5 | 6 | 21 | -8 | -17 | -13 | -2 |
| HadRM3Q0 | 24 | -15 | -4 | 5 | 1 | 12 | -18 | -18 | -23 | -10 |
| ICTP-REGCM | 12 | -5 | -5 | 11 | 4 | 21 | 7 | 6 | 10 | 12 |
| MPI-M-REMO | 13 | -14 | -15 | 4 | -3 | 27 | -5 | -8 | 4 | 5 |
| *bias corrected* | DJF | MAM | JJA | SON | Year | DJF | MAM | JJA | SON | Year |
| ETHZ-CLM | 27 | -9 | 12 | 13 | 10 | 22 | -7 | -13 | -4 | 1 |
| HadRM3Q0 | 21 | -14 | -6 | 7 | 2 | 5 | -20 | -21 | -25 | -13 |
| ICTP-REGCM | 15 | -4 | -5 | 10 | 5 | 23 | 11 | 8 | 10 | 14 |
| MPI-M-REMO | 17 | -14 | -15 | 8 | -1 | 34 | -5 | -6 | 9 | 10 |

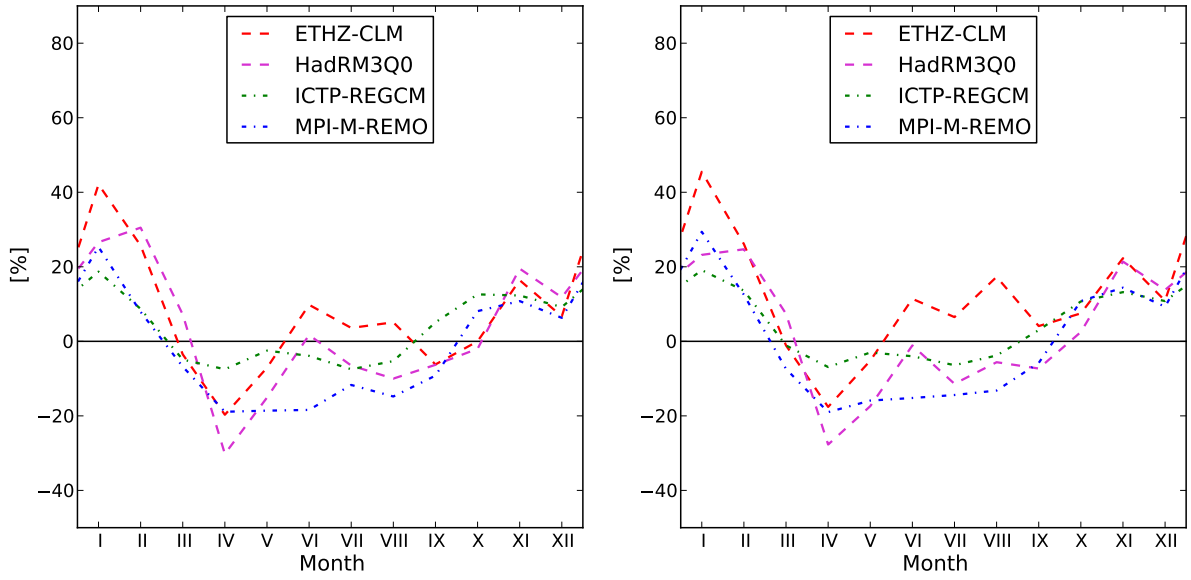


Figure 4.10: Changes in monthly mean discharge at gauge Laucha between 1961-1990 and 2011-2040, modelled with uncorrected (l) and bias corrected (r) climate model data.

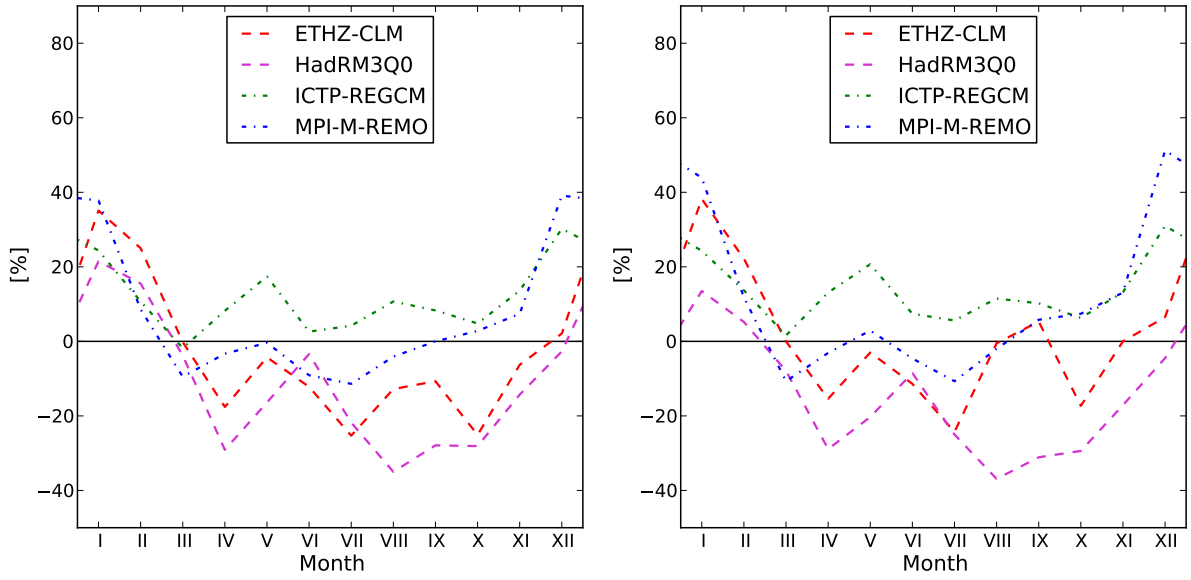


Figure 4.11: Changes in monthly mean discharge at gauge Laucha between 1961-1990 and 2061-2090, modelled with uncorrected (l) and bias corrected (r) climate model data.

### 4.2.4 Gauge Rudolstadt, Saale

The most substantial alterations of river discharge are projected for the gauging station Rudolstadt, although changes in yearly average discharge do not directly reflect seasonal ones. Winter changing rates range from 17% (ICTP-REGCM) to 41% (ETHZ-CLM) in the 2011-2041 period, with also exceptional high values for HadRM3Q0 (31%) and MPI-M-REMO (40%). The ETHZ-CLM and ICTP-REGCM driven simulations project highest discharge increases for January, the HadRM3Q0 and MPI-M-REMO forced runs for February (figure 4.12). Spring discharge is also stronger affected than at other stations, projected reductions ranges from -11% (ICTP-REGCM) to -24% (HadRM3Q0). Summer discharge change is simulated to be positive in arithmetic sign in ETHZ-CLM and HadRM3Q0 driven modelling and negative in the ICTP-REGCM and MPI-M-REMO forced runs. Simulated autumn discharge is more stable as three out of four simulations (exception ETHZ-CLM) indicate higher seasonal mean discharge (table 4.10). In the 2061-2090 scenario period the drastic shift of peak discharge into winter is even more pronounced. All model runs indicate higher increases compared to the previous period. Differences in the inter-seasonal variability of changing rates exist. ECHAM5/MPI-OM RCM driven simulations indicate similar increases for the months December and January, modelling with any of the HadCM RCM indicates a clear peak for the first month of the year (figure 4.13). Spring discharge decreases according to all simulations, as summer and autumn streamflow volumes in ETHZ-CLM and HadRM3Q0 forced runs. The ICTP-REGCM driven simulation indicates no major changes for the second half of the hydrological year, MPI-M-REMO input to mHM a slight decrease for summer and an increase for autumn. Projected changes of yearly mean discharge are controlled by driving GCM, the HadCM based modelling chains show an upward, the ECHAM5/MPI-OM RCM forced simulations a downward trend.

Bias correction affects results in the first scenario period non-uniformly. Winter discharge changes are reduced modelling with bias corrected ETHZ-CLM and HadRM3Q0 input, but are elevated using the corrected ICTP-REGCM and MPI-M-REMO datasets. Other seasonal changes are only slightly altered, highest differences occur for HadRM3Q0 forcing in summer. In the 2061-2090 period simulated winter discharge changes are reduced in three out of four cases, only corrected MPI-M-REMO forcing indicates a stronger seasonal climate change signal. Spring, summer and autumn discharge changes are, as in the 2011-2040 period, only slightly altered, whereas the HadCM based model runs are generally more sensitive (table 4.10).

Table 4.10: Changes in seasonal mean discharge [%] 1961-1990 at gauging station Rudolstadt, simulated with uncorrected and bias corrected climate model data. DJF: Winter, MAM: Spring, JJA: Summer, SON: Autumn.

| | 2011-2040 | | | | | 2061-2090 | | | | |
|---|---|---|---|---|---|---|---|---|---|---|
| *not corrected* | DJF | MAM | JJA | SON | Year | DJF | MAM | JJA | SON | Year |
| ETHZ-CLM | 41 | -22 | 5 | 0 | 3 | 50 | -27 | -12 | -21 | -3 |
| HadRM3Q0 | 31 | -24 | 1 | 5 | 0 | 34 | -27 | -8 | -12 | -4 |
| ICTP-REGCM | 17 | -11 | -8 | 9 | 3 | 28 | -7 | 1 | 0 | 7 |
| MPI-M-REMO | 40 | -17 | -5 | 19 | 6 | 56 | -19 | -1 | 7 | 9 |
| *bias corrected* | DJF | MAM | JJA | SON | Year | DJF | MAM | JJA | SON | Year |
| ETHZ-CLM | 38 | -21 | 7 | 3 | 4 | 39 | -27 | -13 | -22 | -5 |
| HadRM3Q0 | 27 | -24 | -4 | 7 | 0 | 25 | -28 | -14 | -15 | -8 |
| ICTP-REGCM | 18 | -10 | -7 | 7 | 3 | 26 | -4 | 4 | -1 | 8 |
| MPI-M-REMO | 43 | -17 | -3 | 22 | 8 | 64 | -21 | -1 | 10 | 11 |

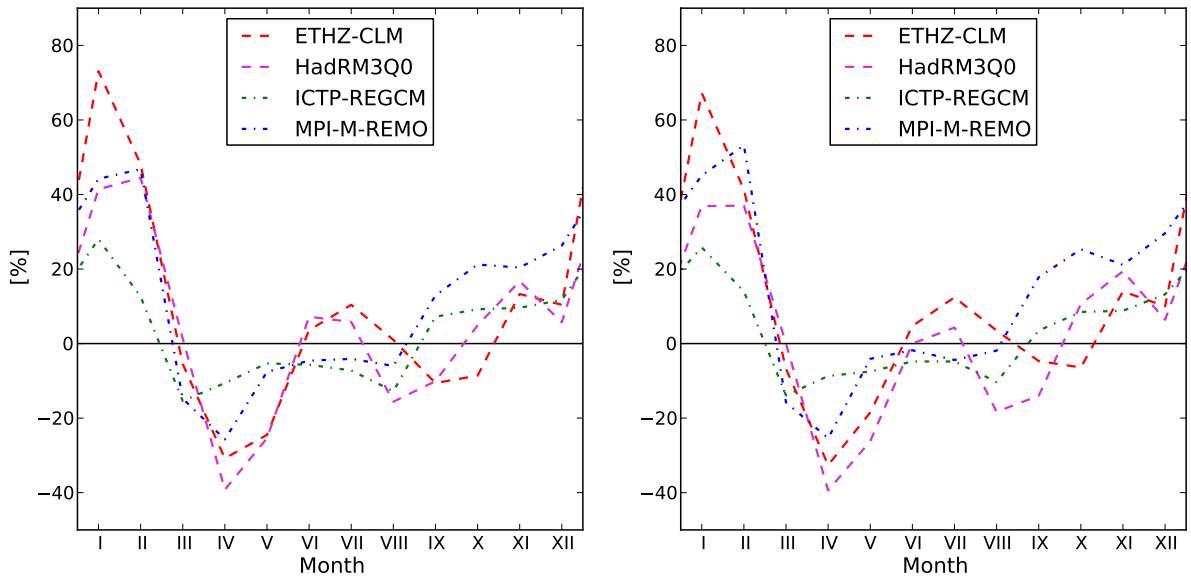


Figure 4.12: Changes in monthly mean discharge at gauge Rudolstadt between 1961-1990 and 2011-2040, modelled with uncorrected (l) and bias corrected (r) climate model data.

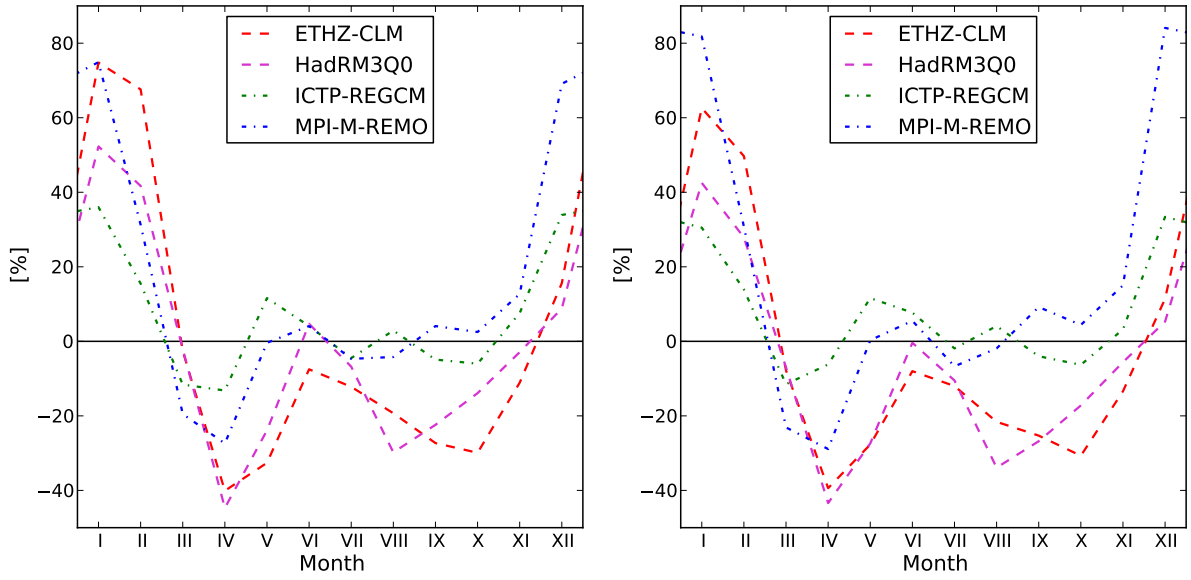


Figure 4.13: Changes in monthly mean discharge at gauge Rudolstadt between 1961-1990 and 2061-2090, modelled with uncorrected (l) and bias corrected (r) climate model data.

### 4.2.5 Gauge Hadmersleben, Bode

The increase of winter discharge in the 2011-2040 scenario period is, especially for the modelling based on ECHAM5/MPI-OM RCM less distinct than at the former gauging stations. Both timeseries indicate further highest seasonal decreases for summer rather than spring (14% each). The simulations forced with the HadCM RCM deviate less from the modelling results obtained for other stations. Winter discharge is simulated to increase by 24% (ETHZ-CLM) and 23% (HadRM3Q0), spring discharge to decrease by -8% and -14%, respectively. The projections for the second half of the hydrological year are inconsistent, ETHZ-CLM forcing indicates an increase of summer discharge (6%) with a peak in June (figure 4.14) and a decrease of autumn discharge (-2%), HadRM3Q0 opposing seasonal impacts (-2% and 2%). The development of yearly mean discharge is not univocal, ICTP-REGCM and MPI-M-REMO driven simulations indicate a slight reduction (-1% and -2%), the ETHZ-CLM and HadRM3Q0 modelling runs an heightening (5% and 2%). In the 2061-2090 period the results are more uniformly. ICTP-REGCM, MPI-M-REMO and ETHZ-CLM driven simulations project an increase of yearly mean discharge. The significant reduction in the HadRM3Q0 modelling results is reflected in negative trends for spring, summer and autumn. ETHZ-CLM driven modelling simulates raising winter, reduced summer/autumn and spring discharge on the 1961-1990 control period level. Both HadCM based modelling chains indicate highest negative changes for summer months, ETHZ-CLM in July, HadRM3Q0 in August (figure 4.15). The ICTP-

REGCM forced simulation prognosticates higher discharge throughout all seasons, but most pronounced for winter. MPI-M-REMO driven modelling shows a dichotomy between lower spring/summer and higher autumn/winter streamflow (table 4.11).

Bias correction affects changes in seasonal average discharge simulated with HadRM3Q0 and ICTP-REGCM data in the 2011-2040 period barely. Projected changes in river hydrology are altered more decisively for the ETHZ-CLM and MPI-M-REMO driven simulations, whereas in the latter the general direction of simulated changes is reversed. The second scenario period results are more distinct from modelling forced with uncorrected RCM data. The general pattern of moderate differences in the HadRM3Q0 and ICTP-REGCM generated streamflow timeseries and considerably higher in the ETHZ-CLM and MPI-M-REMO based simulations is however preserved. The climate change signal is again especially distorted in the MPI-M-REMO forced simulations, the main trend are however preserved (table 4.11).

Table 4.11: Changes in seasonal mean discharge [%] 1961-1990 at gauging station Hadmersleben, simulated with uncorrected and bias corrected climate model data. DJF: Winter, MAM: Spring, JJA: Summer, SON: Autumn.

| | 2011-2040 | | | | | 2061-2090 | | | | |
|---|---|---|---|---|---|---|---|---|---|---|
| *not corrected* | DJF | MAM | JJA | SON | Year | DJF | MAM | JJA | SON | Year |
| ETHZ-CLM | 24 | -8 | 6 | -3 | 5 | 29 | 0 | -10 | -3 | 6 |
| HadRM3Q0 | 23 | -14 | -1 | 1 | 2 | 9 | -17 | -20 | -29 | -12 |
| ICTP-REGCM | 7 | -11 | -14 | 6 | -2 | 17 | 7 | 8 | 9 | 11 |
| MPI-M-REMO | 11 | -12 | -14 | 7 | -2 | 27 | 2 | 5 | 8 | 11 |
| *bias corrected* | DJF | MAM | JJA | SON | Year | DJF | MAM | JJA | SON | Year |
| ETHZ-CLM | 28 | -8 | 8 | 3 | 8 | 37 | -1 | -4 | 6 | 11 |
| HadRM3Q0 | 24 | -15 | -2 | 2 | 2 | 8 | -20 | -21 | -31 | -14 |
| ICTP-REGCM | 9 | -11 | -14 | 5 | -2 | 19 | 7 | 9 | 12 | 12 |
| MPI-M-REMO | 18 | -14 | -9 | 15 | 2 | 39 | -5 | 9 | 14 | 14 |

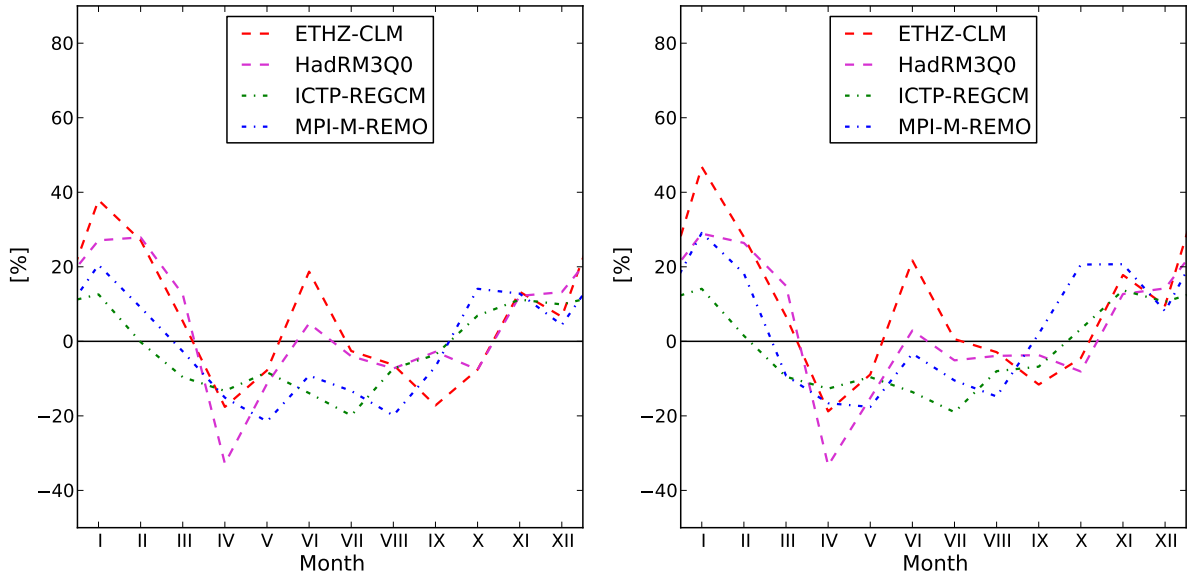


Figure 4.14: Changes in monthly mean discharge at gauge Hadmersleben between 1961-1990 and 2011-2040, modelled with uncorrected (l) and bias corrected (r) climate model data.

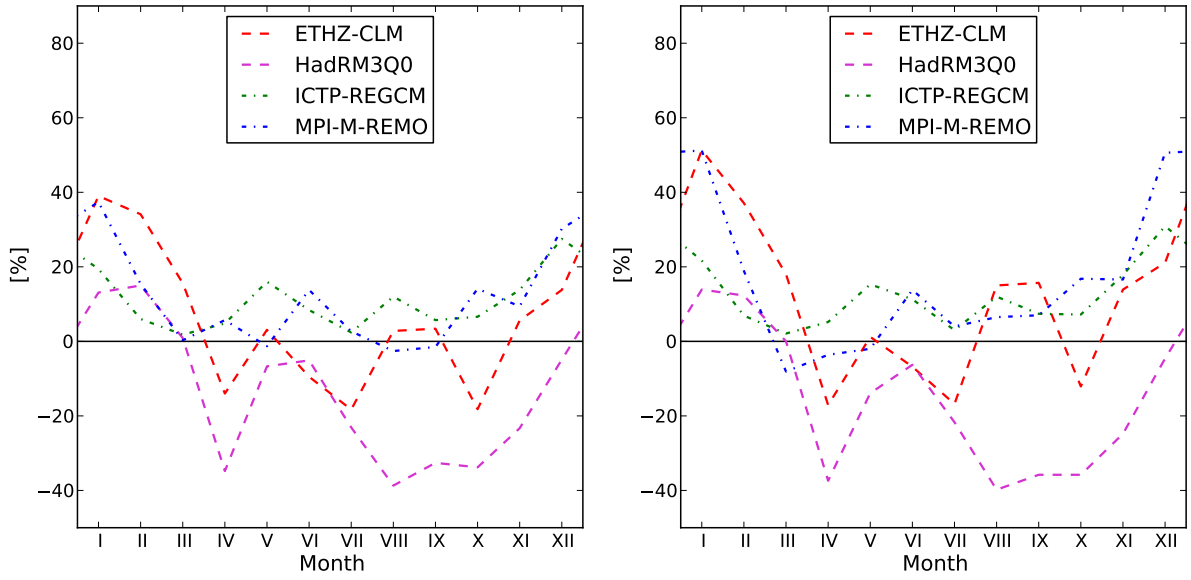


Figure 4.15: Changes in monthly mean discharge at gauge Hadmersleben between 1961-1990 and 2061-2090, modelled with uncorrected (l) and bias corrected (r) climate model data.

### 4.2.6 Common trends in hydrological projections

The evaluation of all modelling runs carried out reveals large discrepancies but also a number of common tendencies. The most stable communality in all runs is the shift of the high flow period from spring to winter, indicated by the considerable increase of winter and decrease of spring discharge simulated with all RCM. There are however differences in magnitude and temporal evolution in the respective modelling runs, seemingly induced by driving GCM. Simulations forced with ETHZ-CLM and HadRM3Q0 data, both downscaling HadCM circulation pattern, tend to project a strong increase of winter discharge during the next three decades and a roughly stable trend until the end of the century. Simulations with input from the ECHAM5/MPI-OM models (ICTP-REGCM and MPI-M-REMO) indicate a smoother but lasting trend. Changes in spring discharge are in general less pronounced and similar in all modelling runs and the entire ensembles indicates a more profound change for the first than he second scenario period There is no common trend in the simulations for summer and autumn in neither scenario period. ECHAM5/MPI-OM RCM forcing leads in general to more consistent results in the first (reduced summer, increased autumn discharge), HadCM forcing in the second (decreasing spring, summer and autumn discharge). The seasonal variability sums up to a slightly increased yearly water supply from the Saale and its tributaries in the first scenario period and to ambiguous results for the second. HadCM based modelling projects decreasing water supply, the ECHAM5/MPI-OM model chains the opposite.

The regional aspect of climate change is not excessively distinct. Simulations at the single gauging stations do deviate in certain aspects, like height and inter-annual variability of changing rates, but are in general rather similar. Only the much more pronounced change of the hydrological regime at station Rudolstadt is striking. Reasons for the remarkable results can be manifold and found in the meteorological forcing as well as in the physiographical properties of the respective catchment. The position of the gauging station, only a few kilometres downstream the large Saale damsystem, the intense water withdrawal during the second half of the 20th century and the difficulties arising from the implicit modelling of the dam management, should be kept in mind, when interpreting these results.

Bias correction does affect hydrological trends stronger than the differences in meteorological forcing suggest. Changes in river discharge are altered seemingly arbitrary, but a slight tendency towards positive alterations, i.e. a stronger climate change signal in case of upward, a weaker in case of downward trends, can be stated. General trends are basically preserved in the first scenario period, but results from corrected and uncorrected RCM forcing deviate more substantially in the second. The sensitivity to bias correction strongly depends on climate model and driving GCM seems to be a bad predictor. Discharge generated with MPI-M-REMO is frequently affected most, ICTP-REGCM often

least. Trends in ETHZ-CLM simulations are usually more sensitive to bias correction in the first scenario period, HadRM3Q0 forced modelling in the second.

# 5 Discussion

### Study Design

The output from four Regional Climate Models (RCM), also used to force the hydrological model mHM, was evaluated against gridded observational data. The choice of exactly these RCM was lead by considerations about the uncertainties within the climate modelling chain and the predominant research practice in Germany. A lack of common sense in choosing appropriate models and representative sample sizes became apparent when examining the literature. Especially studies evaluating climate change impacts in german river basins are mostly based on a small number of climate projections, usually MPI-M-REMO or statistically downscaled data from ECHAM5/MPI-OM or their predecessors, both setup at the Max Planck Institute for Meteorology in Hamburg (e.g. Hattermann et al. (2008), Kropp et al. (2009), Huang et al. (2010)). On a more international scale ensemble strategies became more widespread during the recent years. Graham et al. (2007b) evaluated the climate change signal from 11 RCM nested into one Global Circulation Model (GCM), in a similar study Graham et al. (2007a) expanded the experimental design by including a second GCM. Andersson et al. (2011) and Graham et al. (2011) explicitly assessed uncertainty in streamflow simulations introduced by GCM boundary conditions. The actual choice of RCM, especially in studies focusing on a low number of climate models, seems often to be motivated by 'national' considerations. Not only german scientists prefer climate models developed at german institutions. British impact studies are subsequently often based on one of the HadRM realisations provided by the Met Office Hadley Centre in Exeter (e.g. Kay et al. (2006), Fowler and Kilsby (2007)), Swedish studies usually use projections from the climate model RCA, developed at the Rosby Centre, Norrköping (e.g. Andersson et al. (2011), Kjellström et al. (2011)).

### Data Characteristics

As reported in the literature (e.g. Jacob et al. (2007), Christensen et al. (2008), Kjellström et al. (2011)), all RCM revealed considerably shortcomings in the representation of the study area climate (section 3.1). Although modelled past temperatures fit the observational data reasonably, precipitation is only poorly represented. The RCM clearly overestimate this important climatological variable and two models, ETHZ-CLM and ICTP-REGCM, also misrepresent the monthly variability of precipitation throughout the

year. It turned out that deviations from observational data are mainly a result of the poor representation of low precipitation events and the underestimation of dry days. It could be shown that aggregated monthly values from RCM nested into the same GCM are closer related to each other than to the remaining models. This conclusion does not hold with respect to the cumulative frequency distributions. Smallest inter model deviations are always found between RCM downscaling different GCM boundary conditions.

Despite the need to evaluate climate model output against observational data in order to detect systematic errors in the different RCM variables, a number of problems arise from this proceeding. Especially precipitation measurement, in the context of the poor representation of rainfall in climate models the most important measured quantity, seems to be a challenging task. Instrument and wind errors occur, Marx (2007) pointed to the fact, that even precipitation measurements from devices in immediate vicinity may deviate considerably. The spatial interpolation of the potentially flawed timeseries, usually necessary to bridge the gap between the different data scales, might multiply these inaccuracies. The horizontal resolution of the available gridded observational dataset (4 km) necessarily implies that, even considering the dense monitoring network operated by the German weather service (DWD), a large number of grid cells do not contain any observations. Lenderink (2010) concluded that errors in spatially interpolated observational data may be substantial in areas of a low measurement/grid-cell ratio and that structural RCM biases may in fact be partly induced by an erroneous basis of comparison. Browsing the literature for methods dealing with different horizontal resolutions, map projections and/or coordinate systems, the lack of attention to this import step in the assessment of climate model uncertainty becomes apparent. Again no common practice can be found, Huang et al. (2010) used inverse distance weighting to interpolate climate data to the hydrological model resolution, van Roosmalen et al. (2010) bilinear interpolation, Kunstmann et al. (2004) a combination of different methods, whereas other studies not even refer to the techniques applied (e.g. te Linde et al. (2010), Graham et al. (2011)).

### Bias Correction

Out of the great variety of methods to deal with climate model biases proposed and modified during the recent years, a relatively simple one was chosen. It was shown that the bias correction applied was able to reduce RCM biases of the focused statistical parameter, monthly mean precipitation, to values between 3% and 6% (subsection 3.2). These results are well line with more complex techniques adjusting several parameters of the empirical distribution function (e.g. te Linde et al. (2010), Graham et al. (2011)). It turned out that the procedure does affect the different moments of the empirical cumulative distribution function (CDF), in case of rainfall data a highly asymmetrical one, differently. Especially the high precipitation amounts at the upper end of the CDF are reduced substantially in order to balance the, with this procedure not adjustable, too high number of rain

days. This does imply, that the sensitivity of the impact model to certain moments of the distribution, the corrected data is to force, and possibly unwanted side-effects have to be considered in advance.

The temporal stability of the correction was rather high when evaluating the generated datasets against observation in a later control period. Yearly biases were in fact in two cases lower, in one identical and in only one higher in the 1980-2009 time-slice than in the bias correction period itself. The spread of seasonal biases is higher. While the ECHAM5/MPI-OM driven models ICTP-REGCM and MPI-M-REMO preserved the data characteristics of the correction period fairly well, the HadCM models ETHZ-CLM and HadRM3Q0 deviate more decisively, especially in summer and spring. The inherent model dynamics is able to counteract the correction, here without pushing results out of a reasonable range. The observational data also revealed a certain precipitation dynamics between the two time-slice. It might be worth considering not to fix the correction period to the 30 years of the climate normal defined by the World Meteorological Organisation (WMO) (Arguez and Vose (2011)), rather than using a longer timeseries.

Although a tendency towards much more complicated correction procedures is found in the literature, keeping things simple seems to be a reasonable choice. It is surely possible to transform any given distribution to a certain target function by statistics. The main idea behind any bias correction should be however, to disturb the physical consistency of the climate model output and the simulated dynamics as less as possible by generating an operable dataset.

### Hydrological Modelling

The synthetic discharge timeseries generated with mHM and observational forcing were evaluated against observed discharge at all five gauging stations for the 1961-1990 control period (section 4.1). The usual performance measures used in hydrology indicate reasonable model fits, although the observed discharge is systematically underestimated (between -19% and -17%). The volumetric bias is only at the smallest gauging station Hadmersleben considerably lower (-4%). Reasons for this misrepresentation can be various, but might be a relict of calibration. The objective function used in the parameter optimisation routine is, according to Krause et al. (2005), not very sensitive to systematic errors and more focused to high than to low extremes. Biases may as well result from erroneous meteorological forcing, an inadequate model structure, insufficient representation of the river basin physiography or the not explicitly modelled, large scale water management for industrial and agricultural proposes during the second half of the 20th century.

Forcing the hydrological model with uncorrected RCM output clearly reflects model biases in the 1961-1990 period, which is in accordance to previous studies (e.g. Graham et al. (2007b), te Linde et al. (2010)). Simulated discharge volumes are, with exception of MPI-

M-REMO forcing and the station Hadmersleben, excessively biased. Differences between the sub-catchments exist, timeseries deviations are in general lowest at gauging station Laucha (Unstrut), but never in a reasonable range. The inter-annual variability, i.e. a discharge peak in spring and marked low flow conditions in summer and autumn, is in turn approximated by all RCM driven modelling runs with exception of the ICTP-REGCM simulations. Discharge biases usually exceed the precipitation biases of any respective model with a factor between two and three, climate model errors do obviously multiply along the modelling chain. The direct use of RCM data as forcing of the hydrological model mHM is not advisable, if reasonable streamflow volumes are in the scope of doing so. GCM characteristics is better preserved in the results from ETHZ-CLM and HadRM3Q0 (HadCM) than from ICTP-REGCM or MPI-M-REMO (ECHAM5/MPI-OM). These similarities seem to be systematic, Graham et al. (2007b) reported comparable results from hydrological modelling with different RCM nested in the atmospheric part of the HadCM model.

Synthetic discharge timeseries from bias corrected climate model forcing are in most cases close to observation. The achieved fit does however depend on RCM and river catchment. The modelling results from ICTP-REGCM forcing are generally biased most, and the performance of all runs is rather low at the two smallest gauging stations Rudolstadt and Hadmersleben. The low number of RCM grid cells covering the small sub-catchments makes these simulations especially susceptible to local input data biases. A certain threshold catchment size seems to be necessary to average out remaining model errors on the grid scale. For the study area and the presented model setup, the size of the Unstrut sub-catchment, about 6000 $km^2$ and thus covered by roughly 10 RCM grid cells, seems to be a reasonable choice.

### Climate Projections

Projected climate change and resulting hydrological impacts were evaluated as the differences in longterm means between any of the two timeslices 2011-2040 and 2061-2090, hereafter also named first and second scenario period, and the 1961-1990 control period. All RCM indicate upward trends for yearly mean temperature, annual precipitation sums and 95-percentiles. The span of temperature increases ranges from 0.8° K to 1.8° K for the 2011-2040 and from 2.6° to 3.9° K for the 2061-2090 period (subsection 3.3.1). Temperature increases are not balanced throughout the year, the climate simulations indicate in fact a more profound change for winter and autumn. Trends in precipitation are more unequivocal. The model ensemble indicates stable positive changing rates for autumn and winter rainfall totals and the corresponding 95-percentiles in the first scenario period. The positive trends in the latter statistical parameter are supplemented by increasing spring 95-percentiles in the second scenario period. All models indicate further a lasting positive trend for winter and less significant increases for spring precipitation totals in the end of

the century time-slice (subsection 3.3.2). Rates of projected changes in precipitation are however always lower than inherent model biases, a weak climate change signal following the argumentation of van Roosmalen et al. (2010), similar projections by four different RCM seem anyhow to be a reasonably resilient result.

The characteristics of GCM boundary conditions are well preserved in both model groups and scenario periods, although simulated changes of monthly mean temperatures and their yearly cycles are closer related in the ECHAM5/MPI-OM driven RCM. Seasonal trends in precipitation are also related to driving GCM, but reveal larger differences on the monthly scale. Even RCM nested into the same GCM indicate in cases opposing climate change signals. The applied bias correction does not disturb the simulated dynamics in precipitation. Deviations in projections from uncorrected and corrected data of any respective model are rather marginal and do not exceed two percentage point for any model, season or scenario period.

### Hydrological Projections

Trends in the projections of future discharge vary according to forcing climate model data. The simulations indicate anyhow a shift of the high flow regime from spring into winter in every sub-catchment and an increase of autumn and yearly average discharge for the Saale River in the first scenario period. Climate change signals for the explicitly simulated tributaries Unstrut and Bode are more unequivocal. MPI-M-REMO forcing projects decreasing yearly average streamflow volumes for the former sub-basin, ICTP-REGCM and MPI-M-REMO for the latter. The remaining modelling results each point into the opposite direction. Changes in hydrological are more variable and pronounced in the second scenario period. Yearly mean discharge volumes are projected to raise in all sub-catchments in the ECHAM5/MPI-OM based modelling chains and, with exception of the Bode River and ETHZ-CLM forcing, to decline in the simulations driven with downscaled HadCM circulations fields. The negative spring discharge trend found in the first scenario period is not that clear in the second. The models MPI-M-REMO and especially ICTP-REGCM indicate in fact possible local upward trends. Most timeseries show in turn a stable decrease of summer discharge and the GCM based dichotomy of projected changes in yearly averages is reflected in autumn (section 4.2).

These results agree in general with other studies assessing impacts of climate change on river hydrology in Germany. A clear negative summer discharge trend in the first half of the century, as frequently reported in the literature (e.g. Dankers et al. (2007), Hattermann et al. (2008), Huang et al. (2010)), is however not supported by the simulations made in the present setup. The unanimous results from these and other studies (see chapter 1) are not surprisingly considering the used meteorological forcing, almost exclusively downscaled circulation patterns from ECHAM5/MPI-OM or its predecessor. These findings are well confirmed with the presented modelling results, as the simulations driven by

both ECHAM5/MPI-OM nested regional climate models maintain these conclusion. The HadCM driven RCM do not, a fact pointing to the necessity of including an adequate number of climate models in impact studies. A comparison to the study from Kropp et al. (2009) shows interesting deviations. The authors modelled streamflow at the gauging stations Calbe-Grizehne and Hadmersleben with bias corrected A1B MPI-M-REMO input to the hydrological model SWIM. Stable upward discharge trends throughout the entire and for three different scenario periods are reported. Although these contrary findings, especially noticeable for spring, would need a precise examination, the diverging results might point to the uncertainty introduced by the hydrological model and/or the applied bias correction procedure.

Bias correcting the meteorological forcing of the hydrological model affects the simulation results more than the numerical differences between corrected and uncorrected datasets suggest (section 4.2). There are certain differences in introduced distortion. The underlying GCM boundary conditions are here a bad predictor for hydrological modelling sensitivity. It could be shown that in fact the two ECHAM5/MPI-OM nested RCM delimit the range of deviations from undisturbed model forcing, ICTP-REGCM at the lower, MPI-M-REMO at the upper end. The HadCM based modelling chains are less consistent. Simulating streamflow with bias corrected input from HadRM3Q0 tends to generate changing rates close to uncorrected forcing in the first, ETHZ-CLM in the second scenario period. Changing rates are seemingly arbitrarily altered, only a slight tendency towards increased rates, i.e. a stronger climate change signal in case of positive alteration, a weaker in case of negative one, can be stated. General direction and magnitude of simulated changes are rather well preserved in the first scenario period and for HadRM3Q0 and ICTP-REGCM forcing also in the second.

Correcting RCM data for biases is a common practice in hydrological climate impact modelling. The numerical effects, especially on the projected change signal, are presented in some studies (e.g. van Pelt et al. (2009) or te Linde et al. (2010)), but they are not always addressed explicitly (e.g. Graham et al. (2011) or Andersson et al. (2011)). Considering the wide variety of methods proposed in the literature, these information would be extremely useful to estimate the suitability of the respective technique. Analysing the modelling results from this study the questions may arise, if bias correction is even a necessary step when assessing climate change impacts by hydrological modelling. The answer is twofold. There is evidence that bias correcting climate model data does not change simulated streamflow dynamics substantially within a 50 year period, but that it does, at least in some model combinations, on larger time scale. With the scope of producing reasonable monthly average discharge volumes for the nearer future, the applied correction method in the described setup seems to be an uncritical choice. It might however be more appropriate to simulate streamflow with uncorrected meteorological forcing if a physically consistent and/or longer term climate change signal is more important than

realistic hydrological simulations.

### RCM performance in hydrological modelling

The large biases in the climatological data and their translation into even higher biased streamflow simulations point to the fact, that non of the RCM is suitable to force an hydrological model directly. If necessary the regional climate model MPI-M-REMO would have to be named as the RCM out of the ensembles performing most reasonable. Deviations from observational data between 32% and 52% in yearly averages, with the one solely exception at gauging station Hadmersleben (-3%), are anyhow far from acceptable modelling errors. Bias correcting the meteorological forcing does in turn work in most cases similarly well, although the simulations driven with the HadCM based models, match the inter-annual variability in the 1961-1990 control period more precisely. Major differences exist concerning the distortion of simulated climate change impact by bias correction. From this point of view even the model ICTP-REGCM, in all evaluated parameters biased most, might be an appropriate choice. MPI-M-REMO preserves the original data characteristics worst.

As the complexity of climate models in general and of climate impact modelling in particular, makes reliable statements on the suitability of single RCM for hydrological modelling purposes difficult, no such validation will be done at this point. All illustrated shortcomings in climate model data and deviations in the impact simulations clearly indicate the necessity of the chosen ensemble approach, in order to identify stable trends, outliers and a section of the uncertainty span.

# 6 Conclusions

All available meteorological observations indicate changing climatological conditions for Europe in general (IPCC (2007)) and Germany in particular (Schönwiese et al. (2006)). Scientific research provides evidence that this artificial climate dynamics is already reflected in most environmental sub-systems (IPCC (2007)), not least in the hydrological cycle (Petrow and Merz (2009)). The particular importance of freshwater supply through streams and rivers and the problematic consequences of hydrological extremes in either direction, makes knowledge about possible impacts of a changing climate increasingly important. The impossibility to directly gather information about the future, favoured the development of a large set of scientific tools allowing to assess possible climatological trends under given boundary conditions. Complexity and non-linearity of the underlying natural systems and their error-prone representation in computer-based models does however result in largely deviating future estimates.

In order to compare these differences in four methodological similar Global Circulation Model (GCM) - Regional Climate Model (RCM) combinations and to analyse their translation into simulated hydrological timeseries, a comprehensive climate impact study has been carried out. The relevant climate model output variables were evaluated against spatially interpolated weather station data, biases within the statistical parameters periodical temperature averages, precipitations sums and, as a measure of extreme events, corresponding 95-percentiles were quantified. The analysis of climate model output proved the shortcomings of RCM data reported in the literature. For the area of the Saale watershed, situated in central Germany, in general rather small temperature, but large positive precipitation biases were found. It was shown that non-precipitation days are clearly underrepresented in all RCM timeseries. Deviations between the empirical cumulative distribution functions (CDF) from modelled and gridded observational data are decreasing towards the upper end of the CDF.

The excessive biases in modelled rainfall were accounted for by a simple bias correction procedure, the numerical effects were analysed for a past and two future scenario periods. The applied correction was able to reduce errors in the corrected statistical parameter, longterm averaged monthly precipitation sums, significantly. It was in turn not possible to adjust the entire CDF comparable. Defined as a single multiplication, the general division of the datasets into dry and raining days was not altered, which implicated a

disproportionately reduction of the high precipitation amounts. With respect to the corrected statistical parameter, a reasonable long-term stability of the method was proven. The inherent data dynamics, the projected climate change, was in none of the scenario periods substantially altered.

The recently developed mesoscale hydrological model mHM was calibrated to observational data. Synthetic discharge timeseries were generated for five gauging station covering two of the three largest tributaries of the Saale and the stream itself threefold. All results were evaluated against observation to estimate general modelling performance of RCM forced hydrological simulations on the mesoscale. Changes in river hydrology induced by altered climatic conditions are analysed for stable trends in two scenario periods. Distortions of the climate change signal introduced by bias correction were accounted for by explicitly simulating streamflow with uncorrected and bias corrected climate model forcing.

Hydrological modelling with uncorrected RCM forcing clearly reflected and even multiplied the inherent climate model biases. Relative deviations between observational and modelled streamflow data were considerably larger than the differences between the precipitation timeseries suggest. Bias corrected RCM input to the hydrological model performed in contrast well. Generated streamflow was in most cases close to observation, the general benefit from bias correction in the climate impact model chain could be shown. A clear decrease of modelling performance, obviously dependent on size of the modelling-domain, became apparent for the small sub-catchments. A certain threshold number of RCM grid cells covering the study area, was necessary in order to ensure reasonable hydrological simulations. In the described setup ten RCM grid cells have been an appropriate choice.

The dynamics in RCM data, as well as the output from hydrological modelling, was quantified for two scenario time slices in the first and the second half of the century. All models in the ensemble clearly indicated upward trends for temperature and precipitation. A general warming throughout the entire year is commonly projected, whereas autumn and winter temperatures are likely to increase more substantially. The magnitude, not the direction, of actual changing rates depended on GCM. Trends in precipitation were not comparably unequivocal, simulations point in different directions for spring/summer in the first and summer/autumn in the second scenario period. There is evidence, that winter and autumn rainfall amounts, as well as frequency and/or intensity of extreme events, already increase during the next three decades. Upward trends in winter precipitation totals, in winter and autumn extremes were projected to last throughout the century. All models indicated further a positive climate change signal for spring rainfall activity.

The numerous hydrological simulations only partly confirmed results from similar stud-

ies. Future increase of winter discharge, frequently reported in the literature, was reproduced in the simulations with mHM. A usually also stated clear trend towards decreasing summer streamflow during the first half of the century in turn not. The entire ensemble indicated a slight increase of yearly average discharge for most gauging stations in the first scenario period. Seasonal trends showed a general dichotomy, obviously controlled by underlying GCM. Streamflow data, generated with downscaled ECHAM5/MPI-OM simulations, also used in most available hydrological impact studies for Germany, did in fact indicate a negative trend for summer mean discharge in the 2011-2040 scenario period. Forcing mHM with downscaled HadCM circulation patterns in contrary not. These inconsistencies in general modelling trends were even stronger in the second scenario timeslice. The ECHAM5/MPI-OM based model chains indicated increasing annual discharge volumes, the HadCM nested regional climate models clearly suggested negative trends. The simulations revealed no significant differences in the hydrological climate change signals for the single gauging stations. Either there are none to be expected or, climate model resolution is not appropriate to simulate a differentiated climate on a regional scale considerably smaller than the size as the Study Area.

Modelled changes in river hydrology due to altered climatic conditions were slightly dependent on input data preprocessing. Bias correcting the meteorological forcing affected the hydrological climate change signal seemingly arbitrary, no clear pattern of distortion could be found. Only a weak tendency towards positive alterations, i.e. stronger climate change signals in case of upwards, weaker in case of downward trends, was quantified. A temporal dependency was shown. Deviations in relative changes introduced by bias correction are small in the first scenario period, but more significant in the second. In cases the arithmetic sign of relative seasonal changes was inverted.

An important methodological contribution to the general practice in hydrological climate change impact modelling was made. The outstanding importance of a reasonably large set of regional climate models and the necessity to include more than one driving Global Circulation Model was proven. Neglecting the uncertainty introduced by the latter was marked as a likely source of misinterpretation of changes to be expected. Discrepancies between simulated and observational data confirmed the need for an adequate interfacing strategy in order to link climate model output to hydrological modelling. The quantification of the numerical effects of a bias correction on simulated future discharge dynamics, pointed to the uncertainty introduced by these widely used techniques.

Differences in RCM data and modelling results indicate that explicit and absolute conclusions about future hydrological conditions are not to be drawn from these. Simulating past streamflow with observational meteorological forcing seems to work reasonably well. The computational representation of the climate system is in turn not exact enough to neither reproduce measurements of temperature and precipitation nor observed streamflow

when coupled to an hydrological model. The results from the present study are therefore not to be mistaken as an authoritative forecast, they are however well suited to provide information about possible and in case of the carved commonalities likely, future trends. The span in results might make their usability in the every-day environmental planning and decision-making practice difficult, but does also point to the uncertain nature of predictions. Examining the current climate impact research and the contributions from this study leads to the conclusion, that very likely changes in the hydrological regimes of the Saale and it main tributaries are best addressed with flexible solutions in planning and permission processes.

# Bibliography


AG Boden, editor (1994). *Bodenkundliche Kartieranleitung*. E. Schweizerbart'sche Verlagsbuchhandlung, Stuttgart.

Andersson, L., Samuelsson, P., and Kjellström, E. (2011). Assessment of climate change impact on water resources in the Pungwe River basin. *Tellus*, 63A:138–157.

Arguez, A. and Vose, R. S. (2011). The definition of the standard WMO climate normal: The key to deriving alternative climate normals. *Bulletin of the American Meteorological Society*, 92:699–704.

Bachmann, G., Ehling, B.-C., Eichner, R., and Schwab, M., editors (2008). *Geologie von Sachsen-Anhalt*. Schweizerbart'sche Verlagsbuchhandlung.

Bergström (1995). The HBV model. In Singh, V., editor, *Computer models of Watershed Hydrology*, pages 443–475. Water Resour. Pbl., Colorado, USA.

Beven, K. J., Lamb, R., Quinn, P., and Romanowicz, R. anf Freer, J. (1995). Top-model. In Singh, V., editor, *Computer Models of Watershed Hydrology.*, pages 627–668. Water Resour. Pbl., Colorado, USA.

Blöschl, G., Reszler, C., and Komma, J. (2008). A spatially distributed flash flood forecasting model. *Environmental Modelling Software*, 23 (4):464–478.

Boehm, U., Kuecken, M., Ahrens, W., Block, A., Hauffe, D., and Keuler, K. (2006). CLM - the climate version of LM: brief description and long-term applications. *COSMO Newsletter*, 6:225–235.

Bramer, H., Hendl, M., Marcinek, J., Nitz, B., and Slobodda, S. (1991). *Physische Geographie - Mecklenburg-Vorpommern, Brandenburg, Sachsen-Anhalt, Sachsen, Thüringen.* Herman Haack Verlagsgesellschaft mbH, Gotha.

Bárdossy, A. and Samaniego, L. (2002). Fuzzy rule-based classification of remotely sensed imagery. *IEEE Transactions on Geoscience and Remote Sensing*, 40(2):362–374.

Christensen, J. H., Boberg, F., Christensen, O., and Lucas-Pichler, P. (2008). On the need for bias correction of regional climate change projections of temperature and precipitation. *Geophysical Research Letters*, 35:L20709.

Dankers, R., Christensen, O. B., Feyen, L., Kalas, M., and de Roo, A. (2007). Evaluation of very high-resolution climate model data for simulating flood hazards in the upper danube basin. *Journal of Hydrology*, 347:319–331.

Das, T., Bárdossy, A., Zehe, E., and He, Y. (2008). Comparison of conceptual model performance using different representations of spatial variability. *Journal of Hydrology*, 356:106–118.

Doms, G. (2011). A description of the nonhydrostatic regional COSMO-model part 1: Dynamics and numerics. Technical report, Consortium for Small-Scale Modelling.

Duffie, J. A. and Beckman, W. A. (1980). *Solar engineering of thermal processes*. Wiley, New York.

Flügel, W. A. (1995). Delineating hydrological response units by geographical information system analyses for regional hydrological modelling using PRMS/MMS in the drainage basin of the river Bröl, Germany. *Hydrological Processes*, 9:423–436.

Fowler, H. J. and Kilsby, C. G. (2007). Using regional climate model data to simulate historical and future river flows in northwest England. *Climatic Change*, 80:337–367.

Frühauf, M. and Schwab, M. (2008). *Harz - Landschaftscharakter und Oberflächengestalt*, chapter 5.6.2, pages 410–412. E. Schweizerbart'sche Verlagsbuchhandlung, Stuttgart.

Graham, L. P., Andersson, L., Horan, M., Kunz, R., Lumsden, T., Schulze, R., Warburton, M., Wilk, J., and Yang, W. (2011). Using multiple climate change projections for assessing hydrological response to climate change in the Thukela River basin, South Africa. *Physics and Chemistry of the Earth*, 36:727–735.

Graham, L. P., Andréasson, J., and Carlsson, B. (2007a). Assessing climate change impacts on hydrology from an ensemble of regional climate models, model scales and linking methods – a case study on the Lule River basin. *Climatic Change*, 81:293–307.

Graham, L. P., Hagemann, S., Juan, S., and Bensiton, M. (2007b). On interpreting hydrological change from regional climate models. *Climatic Change*, 81:97–112.

Grell, G. A., Dudhia, J., and Stauffer, D. R. (1994). Description of the fifth generation Penn State/NCAR Mesoscale Model (MM5). Technical report, NCAR.

Gupta, H. V., Sorooshian, S., Hogue, T. S., and Boyle, D. P. (2002). Advances in automatic calibration of watershed models. In *Calibration of Watershed Models. Vol. 6 of Water Science and Application*, pages 9–28. AGU.

Haerter, J. O., Hagemann, S., Moseley, C., and Piani, C. (2011). Climate model bias correction and the role of timescales. *Hydrology and Earth System Science*, 15:1065–1079.

Hanel, M. and Buishand, T. A. (2011). Analysis of precipitation extremes in an ensemble of transient regional climate model simulations for the Rhine basin. *Climate Dynamics*, 36:1135–1153.

Hargreaves, G. H. and Samani, Z. A. (1985). Reference crop evapotranspiration from temperature. *Applied Engineering in Agriculture*, 1:96–99.

Hattermann, F. F., Post, J., Krysanova, V., Conradt, T., and Wechsung, F. (2008). Assessment of water availability in a Central-European river basin (Elbe) under climate change. *Advances in Climate Change Research*, 4:42–50.

Hay, L. E., Wilby, R. L., and Leavesley, G. H. (2000). A comparison of delta change and downscaled GCM scenarios for three mountainous basins in the United States. *Journal of the American Water Resources Association*, 36:387–397.

Hengl, T. (2007). A practical guide to geostatistical mapping of environmental variables. Technical report, European Commission Joint Research Centre Institute for Environment and Sustainability.

Hennigsen, D. and Katzung, G. (2006). *Einführung in die Geologie Deutschlands*. Spektrum Akademischer Verlag, München.

Huang, S., Krysanova, V., Oesterle, H., and Hattermann, F. F. (2010). Simulation of spatiotemporal dynamics of water fluxes in Germany under climate change. *Hydrological Processes*, 24:3289–3306.

Hundecha, Y. Bárdossy, A. (2004). Modeling effect of land use changes on runoff a generation of a river basin through parameter regionalization of a watershed model. *Journal of Hydrology*, 292:281–295.

Internationale Kommission zum Schutz der Elbe, editor (2005). *Die Elbe und ihr Einzugsgebiet - Ein geographisch-hydrologischer und wasserwirtschaftlicher Überblick*. Schlüter, Schönbeck (Elbe). Authors: Simon, M. and Bekele, V. and Maul, C. and Oppermann, R. and Řehák, P.

IPCC (1990). Emission scenarios prepared by the Response Strategies Working Group of the Intergovernmental Panel on Climate Change. Report of the Expert Group on emmission scenarios. Technical report, Intergovernemental Panel on Climate Change.

IPCC (2000). IPCC special report on emission scenarios — summary for policymakers. A special report of the IPCC Working Group III. Intergovernmental Panel on Climate Change. Technical report, Intergovernmental Panel on Climate Change.

IPCC (2007). Climate Change 2007: Impacts, adaptation and vulnerability. Contribution of Working Group II to the Fourth Assessment Report of the Intergovernmental Panel on Climate Change, 2007. Technical report, Intergovernmental Panel on Climate Change.

Jacob, D., Bärring, L., Christensen, O. B., Christensen, J. H., de Castro, M., Déqué, M., Giorgi, F., Hagemann, S., Hirschi, M., Jones, R., Kjellström, E., Lenderink, G., Rockel, B., Sánchez, E., Schär, C., Seneviratne, S. I., Somot, S., van Ulden, A., and van den Hurk, B. (2007). An inter-comparison of regional climate models for europe: model performance in present-day climate. *Climatic Change*, 81:31–52.

Jacob, D., Göttel, H., Kotlarski, S., Lorenz, P., and Sieck, K. (2008). Klimaauswirkungen und Anpassungen in Deutschland - Phase 1: Erstellung regionaler Klimaszenarien für Deutschland. Technical report, Umweltbundesamt.

Jones, R., Noguer, M., Hassell, D., Hudson, D., Wilson, S., Jenkins, G., and Mitchell, J. (2004). Generating high resolution climate change scenarios using PRECIS. Technical report, Met Office Hadley Centre, Exeter, UK.

Kay, A. L., Jones, R. G., and Reynard, N. S. (2006). RCM rainfall for UK flood frequency estimation. II. Climate change results. *Journal of Hydrology*, 318:163–172.

Kirchner, J. W. (2006). Getting the right answers for the right reasons: Linking measurements, analyses, and models to advance the science of hydrology. *Water Resources Research*, 42.

Kjellström, E., Nikulin, G. andHansson, U., Strandberg, G., and Ullerstig, A. (2011). 21st century changes in the european climate: uncertainties derived from an ensemble of regional climate model simulations. *Tellus*, 63A:24–40.

Kottek, M., Grieser, J., Beck, C., Rudolf, B., and Rubel, F. (2006). World map of the Köppen-Geiger climate classification updated. *Meteorologische Zeitschrift*, 15:259–263.

Krause, P., Boyle, D. P., and Bäse, F. (2005). Comparison of different efficiency criteria for hydrological model assessment. *Advances in Geosciences*, 5:89–97.

Kropp, J., Roithmeier, O., Hattermann, F., Rachimow, C., Lüttger, A., Wechsung, F., Lasch, P., Christiansen, E. S., Reyer, C., Suckow, F., Gutsch, M., Holsten, A., Kartschall, T., Wodinski, M., Hauf, Y., Conradt, T., Österle, H., Walther, C., Lissner, T., Lux, N., Tekken, V., Ritchie, S., Kossak, J., Klaus, M., Costa, L., Vetter, T.,

and Klose, M. (2009). "Klimawandel in Sachsen-Anhalt - Verletzlichkeiten gegenüber den Folgen des Klimawandels". Abschlussbericht des Potsdam-Instituts für Klimafolgenforschung (PIK). Technical report, Ministerium für Landwirtschaft und Umwelt Sachsen-Anhalt.

Kumar, R. (2010). *Distributed Hydrologic Model Parameterization: Application in a Mesoscale River Basin*. PhD thesis, Friedrich-Schiller-Universität Jena.

Kumar, R., Samaniego, L., and Attinger, S. (2010). The effects of spatial discretization and model parameterization on the prediction of extreme runoff characteristics. *Journal of Hydrology*, 392:54–69.

Kunstmann, H., Schneider, K., Forkel, R., and Knoche, R. (2004). Impact analysis of climate change for an alpine catchment using high resolution dynamic downscaling of ECHAM4 time slices. *Hydrology and Earth System Science*, 8:1030–1044.

Landesbetrieb für Hochwasserschutz und Wasserwirtschaft Sachsen-Anhalt, editor (2010). *Deutsches Gewässerkundliches Jahrbuch 2007 - Elbgebiet Teil 1, Von der Grenze zur CR bis zur Havelmündung*. Magdeburg.

Leander, R. and Buishand, T. A. (2007). Resampling of regional climate model output for the simulation of extreme river flows. *Journal of Hydrology*, 332:487,496.

Leavesley, G. H., Lichty, R. W., Troutman, B. M., and Saindon, L. G. (1983). Precipitation–runoff modeling system: User's manual,. Technical Report Rep. 83–4238, US Geological Survey Water-Resources Investigations, Denver - Colorado.

Leggett, J., Pepper, W. J., Swart, R. J., Edmonds, J., Meira Filho, L. G., Mintzer, I., and Wang, M. X. Watson, J. (1992). Emissions scenarios for the IPCC: an Update. In *Climate Change 1992: The Supplementary Report to The IPCC Scientific Assessment*, pages 68–95. Cambridge University Press, Cambridge, UK.

Leibniz-Institut für Länderkunde, editor (2003). *Nationalatlas Bundesrepublik Deutschland - Klima, Pflanzen- und Tierwelt*. Spektrum Akademischer Verlag, Heidelberg, Berlin.

Lenderink, G. (2010). Exploring metrics of extreme daily precipitation in a large ensemble of regional climate model simulations. *Climate Research*, 44:151–166.

Liedtke, H. and Marcinek, J., editors (2002). *Physische Geographie Deutschlands*. Justus Perthes Verlag Gotha GmbH, Gotha.

Lindström, G., Johansson, B., Persson, M., Gardelin, M., and Bergström, S. (1997). Development and test of the distributed HBV-96 hydrological model. *Journal of Hydrology*, 201:272–288.

Marx, A. (2007). *Einsatz gekoppelter Modelle und Wetterradar zur Abschätzung von Niederschlagsintensitäten und zur Abflussvorhersage*. PhD thesis, Institute of Hydraulic Engineering, University of Stuttgart.

McGuffie, K. and Henderson-Sellers, A. (2008). *A Climate Modelling Primer*. John Wiley and Sons, Ltd., Hoboken, NJ, 3 edition.

Menzel, L. and Bürger, G. (2002). Climate change scenarios and runoff response in the Mulde catchment (Southern Elbe, Germany). *Journal of Hydrology*, 267:53–64.

Menzel, L., Thieken, A. H., Schwandt, D., and Burger, G. (2006). Impact of climate change on the regional hydrology – scenario-based modelling studies in the German Rhine catchment. *Natural Hazard*, 38:45–61.

Nash, J. E. and Sutcliffe, J. V. (1970). River flow forecasting through conceptual models, 1. A discussion of principles. *Journal of Hydrology*, 10:282–290.

Pal, J. S., Giorgi, F., Bi, X., Elguindi, N., Solmon, F., Gao, X., Rauscher, S. A., Francisco, R., Zakey, A., Winter, J., Ashfaq, M., Syed, F. S., Bell, J. L., Diffenbaugh, N. S., Karmacharya, J., Konaré, A., Martinez, D., Da Rocha, R. P., Sloan, L. C., and Steiner, A. L. (2007). Regional climate modeling for the Developing World: The ICTP regCM3 and regCNET. *Bulletin of the American Meteorological Society*, 9:1395–1409.

Petrow, T. and Merz, B. (2009). Trends in flood magnitude, frequency and seasonality in Germany in the period 1951–2002. *Journal of Hydrology*, 371:129–141.

Pokhrel, P., Gupta, H. V., and Wagener, T. (2008). A spatial regularization approach to parameter estimation for a distributed watershed model. *Water Resources Research*, 44.

Pope, V. D., Gallani, M. L., Rowntree, P. R., and Stratton, R. A. (2000). The impact of new physical parametrizations in the Hadley Centre climate model: HadAM3. *Climate Dynamics*, 16:123–146.

Pälchen, W., editor (2008). *Geologie von Sachsen - Geologischer Bau und Entwicklungsgeschichte*. E. Schweizerbart'sche Verlagsbuchhandlung, Stuttgart.

Rawl, W. (1983). Estimating soil bulk density from particle size analysis and organic matter content. *Soil Science*, 135:123–125.

Roeckner, E., Brokopf, M., Esch, M., Giorgetta, S., Hagemann, S., and Kornblueh, L. (2006). Sensitivity of simulated climate to horizontal and vertical resolution in the ECHAM5 atmosphere model. *Journal of Climate*, 19:3771–3791.

Rothe, P. (2009). *Die Geologie Deutschlands*. Wissenschaftliche Buchgesellschaft, Darmstadt.

Samaniego, L. (2003). *Hydrological Consequences of Land Use/Land Cover Change in Mesoscale Catchments*. PhD thesis, Institute of Hydraulic Engineering, University of Stuttgart.

Samaniego, L., Kumar, R., and Attinger, S. (2010). Multiscale parameter regionalization of a grid-based hydrologic model at the mesoscale. *WATER RESOURCES RESEARCH*, 46.

Schulla, J. and Jasper, K. (2007). Model description waSiM-ETH (Water balance Simulation Model ETH). Technical report, ETH, Zürich.

Schönwiese, C.-D. (2006). *Praktische Statistik für Meteorologen und Geowissenschaftler*. Gebrüder Borntraeger, Berlin, Stuttgart, 4 edition.

Schönwiese, C.-D., Staeger, T., and Trömel, S. (2006). Klimawandel und Extremereignisse in Deutschland. In *Klimastatusbericht 2005*. Deutscher Wetterdienst, Offenbach.

Seidel, G. (2003). *Geologie von Thüringen*. E. Schweizerbart'sche Verlagsbuchhandlung, Stuttgart.

Senatore, A., Mendicino, G., Smiatek, G., and Kunstmann, H. (2011). Regional climate change projections and hydrological impact analysis for a Mediterranean basin in Southern Italy. *Journal of Hydrology*, 399:70–92.

Shabalova, M. V., van Deursen, W. P. A., and Buishand, T. A. (2003). Assessing future discharge of the river rhine using regional climate model integrations and a hydrological model. *Climate Research*, 23:233–246.

Stratton, R. A. (1999). A high resolution amip integration using the hadley centre model hadam2b. *Climate Dynamics*, 15:9–28.

te Linde, A. H., Aerts, J. C. J. H., Bakker, A. M. R., and Kwadijk, J. C. J. (2010). Simulating lowprobability peak discharges for the Rhine basin using resampled climate modeling data. *Water Resources Research*, 46:W03512.

Tolson, B. A. and Shoemaker, C. A. (2007). Dynamically dimensioned search algorithm for computationally efficient watershed model calibration. *Water Resources Research*, 43:WR004723.

van der Linden, P. and Mitchell, J., editors (2009). *ENSEMBLES: Climate Change and its Impacts: Summary of research and results from the ENSEMBLES project.* Met Office Hadley Centre, FitzRoy Road, Exeter EX1 3PB, UK.

van Pelt, S. C., Kabat, P., ter Maat, H., van den Hurk, B. J. J. M., and Weerts, A. H. (2009). Discharge simulations performed with a hydrological model using bias corrected regional climate model input. *Hydrology and Earth System Science*, 13:2387–2397.

van Roosmalen, L., Christensen, J. H., Butts, M. B., Jensen, K. H., and Refsgaard, J. C. (2010). An intercomparison of regional climate model data for hydrological impact studies in Denmark. *Journal of Hydrology*, 380:406–419.

von Storch, H., Güss, S., and Heinmann, M. (1999). *Das Klimasystem und seine Modellierung*. Springer-Verlag, Berlin, Heidelberg.

Wackernagel, H. (1995). *Multivariate Geostatistics*. Springer-Verlag, Berlin, Heidelberg.

Walter, R. (2007). *Geologie von Mitteleuropa*. E. Schweizerbart'sche Verlagsbuchhandlung, Stuttgart.

Webster, R. and Oliver, M. A. (2007). *Geostatistics for environmental scientists*. John Wiley and Sons, Ltd.

Wilby, R. L. and Wigley, T. M. L. (1997). Downscaling general circulation model output: a review of methods and limitations. *Progress in Physical Geography*, 21(4):530–548.

Wilks, D. S. (2006). *Statistical methods in the atmospheric sciences*. Elsevier, Amsterdam, and others, 2 edition.

Yang, W., Andréasson, J., Graham, L. P., Olsson, J., Rosberg, J., and Wetterhall, F. (2010). Distribution-based scaling to improve usability of regional climate model projections for hydrological climate change impacts studies. *Hydrology Research*, 41:211–229.